RV SONNE 241
Cruise Report / Fahrtbericht

Manzanillo, 23.6.2015 – Guayaquil, 24.7.2015

SO241 - MAKS: Magmatism induced carbon escape from marine sediments as a climate driver – Guaymas Basin, Gulf of California

Christian Berndt
GEOMAR Helmholtz Centre for Ocean Research Kiel

With contributions by Christian Hensen, Sina Muff, Jens Karstens, Mark Schmidt, Volker Liebetrau, Rolf Kipfer, Mark Lever, Christoph Böttner, Mechthild Doll, Sudipta Sarkar, and Sonja Geilert

Table of Content / Inhaltsverzeichnis

1. Cruise summary / Zusammenfassung

1.1 German / Deutsch

Auf der Reise SO241 wollten wir die Hypothese testen, dass durch Spreizung verursachter Magmatismus, so viele Ganggesteine in den darüber liegenden Sedimentbecken erzeugen kann, dass die dadurch freigesetzten Kohlenwasserstoffe das Klima verändern können. Das Guaymas Becken im Golf von Kalifornien ist eines der wenigen geologischen Gebiete, in denen heutzutage durch Krustenspreizung hervorgerufener Vulkanismus zur Bildung von Ganggesteinen und damit verbundenen Kohlenstoffaustritten führt. Während der Reise SO241 sammelten wir insgesamt 1100 km 2D-seismische Profile in diesem Becken, um damit die Ausdehnung und das Volumen der vulkanischen Intrusionen sowie das Ausmaß der metamorphen und diagenetischen Überprägung zu bestimmen, die durch das Eindringen der Ganggesteine ausgelöst wurde. Dann wählten wir drei repräsentative Fluidaustrittstellen aus, an denen wir mit Hilfe des TV-Multicorers, des Schwerelotes und des TV-Greifers den Meeresboden beprobten. Aus dem dadurch gewonnenen Kernmaterial lassen sich nun die Art der Kohlenstoffverbindungen und ihr Gesamtvolumen bestimmen. Über authigene Karbonatkrusten können wir konstruieren, wie sich die Fluidaustritte zeitlich verändern. An einem der größten Fluidaustritte führten wir ein Ozeanbodenseismometerexperiment durch, mit dem wir bestimmen werden, wie groß die metamorphe Aureole um die Ganggesteine ist und wie freies Gas im Untergrund verteilt ist. Am nordöstlichen Rand des Guaymas Beckens wurden schon früher Hinweise auf Gashydrate gefunden. Während SO241 konnten wir diese zum ersten Mal beproben und mit den gesammelten seismischen Daten konnte ihre Verbreitung kartiert werden. Es ist davon auszugehen, dass sie eine wichtige Rolle für das gesamte Fluidmigrationssystem spielen. Aus ihrer Tiefenlage werden wir Rückschlüsse auf die Temperaturverteilung im Becken ziehen können. Mit Hilfe der seismischen Daten fanden wir an der Südflanke der nördlichen Spreizungsachse eine bisher unbekannte geologische Struktur: einen großen Hügel, der ausschließlich aus den Ablagerungen schwarzer Raucher zu bestehen scheint und der höchstwahrscheinlich auf rezentes Eindringen von Magma in die obere Kruste zurückführen ist. Diese Struktur untersuchten wir mit einem umfangreichen geologischen, geochemischen, und geophysikalischen Messprogramm. Wir fanden mindestens sieben aktive Schlote und Hinweise, dass die austretenden, methanreichenden Fluide mehrere hundert Meter in die Wassersäule aufsteigen. Diese vorläufigen Resultate unterstützen die Hypothese, dass großräumig auftretender Vulkanismus, z.B. während der Öffnung eines Ozeanbeckens, sich in der Tat auf das Klima auswirken könnte. Zusätzlich zu diesem zentralen Thema des Forschungsprojektes konnten wir auch Hinweise auf eine große untermeerische Hangrutschung finden, die den südlichen Teil des Guaymas Beckens mit bis zu 150 mächtigen Ablagerungen bedeckt hat. Es ist davon auszugehen, dass diese Rutschung einen Tsunami im Golf von Kalifornien ausgelöst hat.

1.2 English / Englisch

SO241 set out to test the hypothesis that rift-related magmatism is able to increase carbon emissions from sedimentary basins to the extent that they can actively force climate. To this end we investigated a study area in the Guaymas Basin in the Gulf of California which is one of very few geological settings where rift-related magmatism presently leads to magmatic intrusions into a sediment basin. During the cruise we collected 1100 km of 2D seismic lines to image the extent and volume of magmatic intrusions as well as the extent of metamorphic overprinting of the surrounding sediments and associated subsurface sediment mobilization. We selected three typical seep sites above magmatic intrusions for detailed geochemical studies using gravity corers, multicorers and TV grab. With these samples we will be able to determine the pore water composition to assess the amount and composition of hydrocarbon compounds that are released from these systems. Detailed ocean bottom seismometer measurements at a seep site in the center of the Guaymas Basin will provide further insights into effects of magmatic intrusions on carbon release and diagenetic

overprinting of the sediments. It will be possible to reconstruct its long-term seepage history from big carbonate blocks that we have collected with a TV-grab. The northeastern margin of the Guaymas Basin is known for the presence of gas hydrates. During the cruise we collected several seismic lines, which show a clear but unusually shallow BSR indicating high heat flow in the region. Using the seismic data we discovered a previously unknown geological structure on the flank of the northern rift segment: a large mound that seems to consist entirely of black smoker deposits. It seems to be the result of a recent intrusion into the underlying sediments and changes the view how such systems function. The structure was investigated with a comprehensive geochemical, geothermal, and video surveying program which revealed at least seven vents that are active simultaneously. These vents inject methane and helium-rich vent fluids several hundred meters up into the water column. These findings suggest that large-scale magmatism, for example during the opening of an ocean basin under the influence of a hot spot, can be an effective way of liberating large amounts of carbon high up into the water column. The data collected during SO241 will allow us to constrain the amount of carbon that can escape into the atmosphere during LIP emplacement and their relevance on a global scale can be assessed. In addition to reaching the main objectives of the project we discovered a large landslide complex that was probably associated with a tsunami.

2. Participants / Teilnehmer

2.1 Principal investigators / Leitende Wissenschaftler

Prof. Dr. Christian Berndt, GEOMAR

Dr. Christian Hensen, GEOMAR

Prof. Dr. Carlos Mortera-Gutierrez, UNAM

2.2 Scientific party / wissenschaftliche Fahrtteilnehmer

Prof. Dr. Christian Berndt	Chief scientist	GEOMAR
Dr. Christian Hensen	Leader geochemistry	GEOMAR
Dr. Mark Schmidt	Water column chemistry	GEOMAR
Prof. Dr. Rolf Kipfer	Isotope geochemistry	EAWAG/ETH
Dr. Volker Liebetrau	Carbonate chemistry	GEOMAR
Dr. Florian Scholz	Sediment chemistry	GEOMAR
Dr. Sonja Geilert	Sediment chemistry	GEOMAR
Annika Fiskal	Sediment chemistry	GEOMAR
Anja Bräunig	Sediment chemistry	GEOMAR
Simon Jost	Sediment chemistry	GEOMAR
Regina Surberg	Chemical Engineer	GEOMAR
Sina Muff	P-Cable	GEOMAR
Dr. Jens Karstens	OBS	GEOMAR
Christoph Böttner	Hydroacoustics	GEOMAR

Prof. Dr. Carlos Mortera-Gutierrez	Geophysics	UNAM
Dr. Sudipta Sarkar	Geophysics	GEOMAR
Dr. Wu-Cheng Chi	Thermal modeling	SINICA
Mechthild Doll	Heat flow	UB
Dr. Mark Lever	Microbiology	ETH
Thomas Evans	Microbiology	UB
Scientific party (ctd.)		
Ruth Behrend	Watch leader	GEOMAR
Manuel Moser	Watch leader	GEOMAR
Theresa Roth	Watch leader	GEOMAR
Diego Aguiar Armando	Watch keeper	UNAM
David Balensiefen	Watch keeper	GEOMAR
Itzel Isunza Manrique	Watch keeper	UNAM
Elisabeth Perez Gonzales	Watch keeper	UNAM
Daniel Perez-Calderon		
Francisco Ponce Nunez	Watch keeper	UNAM
Kristina Popp	Watch keeper	GEOMAR
Bettina Schramm	Watch keeper	GEOMAR
Sandra Valle Hernandez	Watch keeper	UNAM
Daria Sukhanova	Seismic processing	VBPR
Mikhail Vorobev	Seismic processing	VBPR
Gero Wetzel	Electronic engineer	GEOMAR
Torge Matthiessen	Mechanical engineer	GEOMAR
Eduard Fabrizius	Electronic engineer	GEOMAR

2.3 Crew / Mannschaft

Oliver Meyer	Master
Nils Aden	Chief mate
Lars Hoffsommer	2. Mate

Ulrich Büchele	2. Mate
Dieter Hermesmeyer	Chief
Roman Horsel	2. Engineer
Tim Stegmann	2. Engineer
Jörg Leppin	Electronic engineer
Hermann Pregler	System operator
Stefan Meinecke	System operator
Anke Walther	Ship’s doctor
Bernd Renken	Electrician
Thomas Beyer	Electrician
Frank Heibeck	Engine
Robert Suhr	Engine
Andreas Schrapel	Boatswain
Arnold Ernst	A.B.
Hannes Betten	A.B.
Ingo Fricke	A.B.
Oliver Eidem	A.B.
Ralf DeMoliner	A.B.
Reno Ross	A.B.
Sascha Fischer	A.B.
Stefan Koch	A.B.
Frank Tiemann	Cook
Andreas Spieler	2. Cook
Bettina Kaiser	Stewardess
Jan Hoppe	Steward
Luis Royo	Steward
Rene Lemm	Steward
Volker Blohm	Deck’s fitter

3. Narrative of the cruise / Ablauf der Forschungsfahrt

RV SONNE left Manzanillo late in the morning of June 23 after tropical storm Carlos had led to delays in the harbor schedule. We arrived in the study area on the morning of June 25 and ran a first TV-CTD and water column sampling program during the morning. In the afternoon we sampled a seep site with dead mussel beds and small carbonate nodules in the northwestern part of the basin close to Tortuga Island using the video multicorer and the video grab. In the evening we began the hydroacoustic program and at midnight 2D seismic surveying of the entire basin. The seismic system was deployed in the early morning of June 26 and recording started at 05:30.

We continued shooting 2D seismic data in calm conditions until June 29 06:30. Because of the calm seas and the new array configuration with two airguns the quality of the seismic data surpassed all previous surveys that we have conducted with the same system. Already during the survey a first run of data processing was conducted, and the data were used to plan the subsequent coring operations.

On June 29 we started coring using a gravity corer. The very first core already produced exciting results smelling strongly of H2S and containing large nodules of hydrate indicating active methane venting. Throughout the day we collected more sediment cores for pore water analysis and microbiological measurements. In the evening of the 29th we carried out a test of the ocean bottom seismometer (OBS) releasers. Unfortunately two of the releasers did not work properly so we were limited to 11 OBS. During the night to Tuesday we carried out two water sampling and CTD profiles and continued coring with the TV multicorer on June 30 until the evening when we switched to the TV grab which successfully sampled several large carbonate blocks.

On July 1 at midnight we began to deploy the ocean bottom seismometers to image one of the seep sites close to the northern rift axis. The operation was finished in the early morning. Originally we intended to collect 3D seismic data, but due to technical problems of the P-Cable system we were only able to shoot along transects across the OBS without collecting 3D seismic data. Shooting of transects across the OBS continued until 08:00 on the July 2. Then we continued TV multicorer sampling at the same vent site discovering living chemosynthetic ecosystems indicating recent venting. Coring and CTD casts continued throughout the day before deploying the airgun again to shoot more seismic data for the OBS throughout the night.

On July 3 we steamed towards Guaymas to meet the pilot boat that delivered a spare part for the engine. In the early morning we collected one more TV multicorer and water samples on the shelf to determine the shelfal sediment input before getting to the meeting point just outside Guaymas harbor. Arriving in Guaymas we found that the wrong spare was sent, but some material for fixing the cooling system could be purchased. In the afternoon we left for the western termination of the northern rift segment where we discovered water column temperature anomalies indicating active seepage. We continued with water sampling and TV-multicorer deployments. These operations continued throughout July 4. In the evening of July 4 the backup cooling system of the ship was confirmed to support one compressor and we could resume shooting seismic data into the OBS.

During the 5th of July we acquired multibeam and parasound data to fill gaps in our data coverage while repairing the broken cooling system pipe and preparing HyBis for deployment. The first HyBis transect was carried out on the southern flank of the northern rift system across a remarkable sedimentary edifice that was discovered in the 2D seismic data. We found several smokers not dissimilar to those in the southern rift system of the Guaymas Basin and we used the grab to recover a sample of the seafloor. During the second HyBis dive we discovered several additional smokers both active and extinct. Subsequent CTD transects showed that the lower 300 m of the water column are perturbed with elevated temperatures and high methane concentrations.

These operations lasted until 8 am on July 6 when we switched back to TV-multicoring

until the evening. At 21:00 we deployed the 2D streamer to obtain more information on the hydrothermal vent site and the surrounding geology. In the morning of July 7 we collected a sound velocity profile for the multibeam system and sailed back to the slope of Guaymas where we took two 10 m-long gravity cores to determine temporal variations in the oxygen minimum zone. Afterwards we collected another spare part for the ship's cooling system from the pilot station off Guaymas and sailed back to the survey area where we redeployed the 2D seismic system. We acquired three 2D seismic lines until 11:00on the next day.

On July 8 we retrieved the 2D seismic system and released the OBSs. All eleven instruments came up and have recorded data. In the night to July 9 we collected a gravity core to date the age of the black smoker edifice and managed to run a CTD water sampler into one of the hot vents to sample the expelled fluids which worked very well. Afterwards we tried again to get the 3D seismic system to run, which was working until about midnight, but then stopped working. It turned out that the surface water temperature of 30 degree C is too high to cool down the modem near the paravane which interrupted the Ethernet connection. We switched back to 2D seismic which ran successfully for two days until July 11.

On July 11 we took a TV grab at the big cold seep in the central part of the OBS survey collecting carbonate samples that will be used to construct the seepage history in the central part of the basin. Afterwards we took two gravity cores in the hydrothermally altered sediments around the black smoker. Throughout the night we ran two heat-flow transects in the same area and continued with gravity coring until the next day.

In the evening of July 12 we continued 2D seismic surveying at the edges of the basin. This lasted until July 14. On the 14th we collected two TV multicorers, ran a CTD across the vent site, retrieved our ADCP lander and took one TV grab lander before we ran another heat flow profile throughout the vent region.

The work program ended on July 15. In the morning we took a gravitycorer at the central seep site before setting sail for Guayaquil at noon.

4. Aims of the Cruise / Zielsetzung der Forschungsfahrt

The major goal of this cruise was to test the hypothesis, that magmatic intrusions into marine sediments can induce the release of sufficient amounts of organic carbon to change climate (Svensen et al., 2004). For this purpose we have addressed the following questions.

First of all, we have tried to constrain the mass of carbon, which is buried in the sediments of the Guaymas Basin, and hence may be released by magmatic intrusions and heating/melting of sediments (Lizarralde et al. 2010). Lizarralde et al. (2010) used DSDP results for estimating the number of sills. Those data, however, indicate major variations in the upper sediment column (1-4 wt.%; DSDP sites 478, 481; Curray and Moore, 1982; Simoneit und Lonsdale, 1982). We have attempted to improve these estimates by systematic coring.

The second objective was to constrain the volume of sills that recently intruded into the Guaymas Basin. To this end we have conducted high-resolution 2D and 3D seismic surveys and ocean bottom seismometer experiments. These data will also be used to estimate the volume of the metamorphic aureole around the sill intrusions which is the carbon source for the hydrothermal vent fluids. While Svensen et al. (2004) used a simple approach to estimate the amount of methane released from around the magmatic aureole, we will use a more comprehensive, thermal-geochemical approach, which will consider 3D-heat distribution around a sill and kinetic laws for the thermal cracking of organic compounds (Berner et al., 1995). This will allow us to approach the time lag between the intrusion of magma and the discharge of hydrothermal fluids at the seafloor, and hence constrain the results of Lizarralde et al. (2010).

A factor that has not been considered to date is which fraction of the carbon released by heating will actually arrive at the seafloor. Only rapid migration of methane enriched fluids, which would bypass sedimentary filters, would eventually have the chance to reach the

atmosphere and become relevant in terms of climate change. Slow advection would enhance biogeochemical processes like AOM, which effectively “filters” methane by oxidation to CO2 and conversion to bicarbonate, which, in turn, favours the formation of authigenic carbonates as a final sink for mobilized carbon. In order to provide reliable estimates of the mass of carbon reaching the seafloor and being released into the water column it is essential to determine the concentration of dissolved and free gas in pore waters and in the bottom water. We will address this aspect of our study by a detailed study on active systems that has not been done before (e.g. Svensen et al., 2004; Lizarralde et al. (2010). Specifically, pore water geochemical investigations addressing the calculation of fluid advection rates and the release of methane into the water column have not been addressed at all. The suggested pore water geochemical investigations, specifically the application of various isotopic tracers (e.g. δ18O, δD,δ13C, δ7Li, 87Sr/86Sr on pore fluids and δ13C, δD, C1-C12 on hydrocarbon gases and CO2) will help elucidate this question and help to develop a consistent model of fluid formation and circulation.

Overall, we have conducted an extensive research program addressing (i) the precise localization and characterization of fluid vents using hydroacoustic and seismic methods, (ii) the calculation of fluid advection rates at active vents, (iii) the origin of fluids and gases by isotope-geochemical and biomarker analyses (testing the hypothesis of Chan et al., 1994; open hydrothermal system), (iv) plume detection and surveys in order to quantify the carbon output from sediments, and the variability of fluid discharge over time by dating of authigenic carbonates. Detailed surveys of the vent fields enabled us to quantify the amount of carbon stored in authigenic carbonates. This, in turn, will provide us with an estimate of the fraction of carbon, which was released in the subsurface, but did not reach the water column, and hence is removed from biogeochemical cycles for a longer period of time and cannot affect climate.

Our investigations will provide an updated estimate of the mass of carbon that can be released from sediments upon magmatic intrusions and specifically to calculate the amount of carbon recently arriving at the seafloor and emitting into bottom water.

5. Setting of the working area / Beschreibung des Arbeitsgebiets

The Guaymas Basin is an about 100 km wide area of the Gulf of California which has formed by rifting that started 12-15 Mio. years ago between the Lower Californian Peninsula (Baja California) and the Mexican mainland (Stock and Lee, 1994). The basin comprises two rift segments separated by a transform fault. Opening of the basin to form an ocean basin is thought to have occurred about 6 Mio. years ago (Lizarralde et al., 2007). Multichannel seismic lines acquired in 2002 on FS Maurice Ewing show magmatic sills, which intruded for about 50 km to the northwest and for 40 km to the southeast of the rift axis (Lizarralde et al., 2010). Whereas the northwestern intrusions are marked by a strong, inconsistent reflector in biogenic sediments, the southeastern intrusions are characterized are cusped and have intruded into a mixture of biogenic and terrigenous sediments. Association of these reflectors with intrusions is suggested from drilling results of DSDP sites 481 and 477 in which igneous sill rocks were encountered. It is further confirmed by typical syn-magmatic deformation structures and indications for hydrothermal activity that are often observed in conjunction with magmatic intrusions (Hansen et al., 2005; Svensen et al., 2004). Below the intrusion-associated reflectors further sedimentary reflectors can be observed (Lizarralde et al., 2010), however, their amplitudes are much lower due to the high impedance contrast and 3-dimensional scattering of the rough sill surfaces, making them more difficult to observe. From the thickness of sediments overlying the sills and known local sedimentation rates, the maximum age of the intrusions may be inferred. Published sedimentation rates in the Guaymas Basin are about 1 km/Mio. years (Schrader, 1982). With a sediment thickness of 200-400 m, this gives a maximum age of about 400,000 years, but the intrusions are probably much younger.

Magma intruding into sediments with a high organic carbon content alters the sediments and promotes release of carbon as methane and carbon dioxide (Seewald et al., 1990;

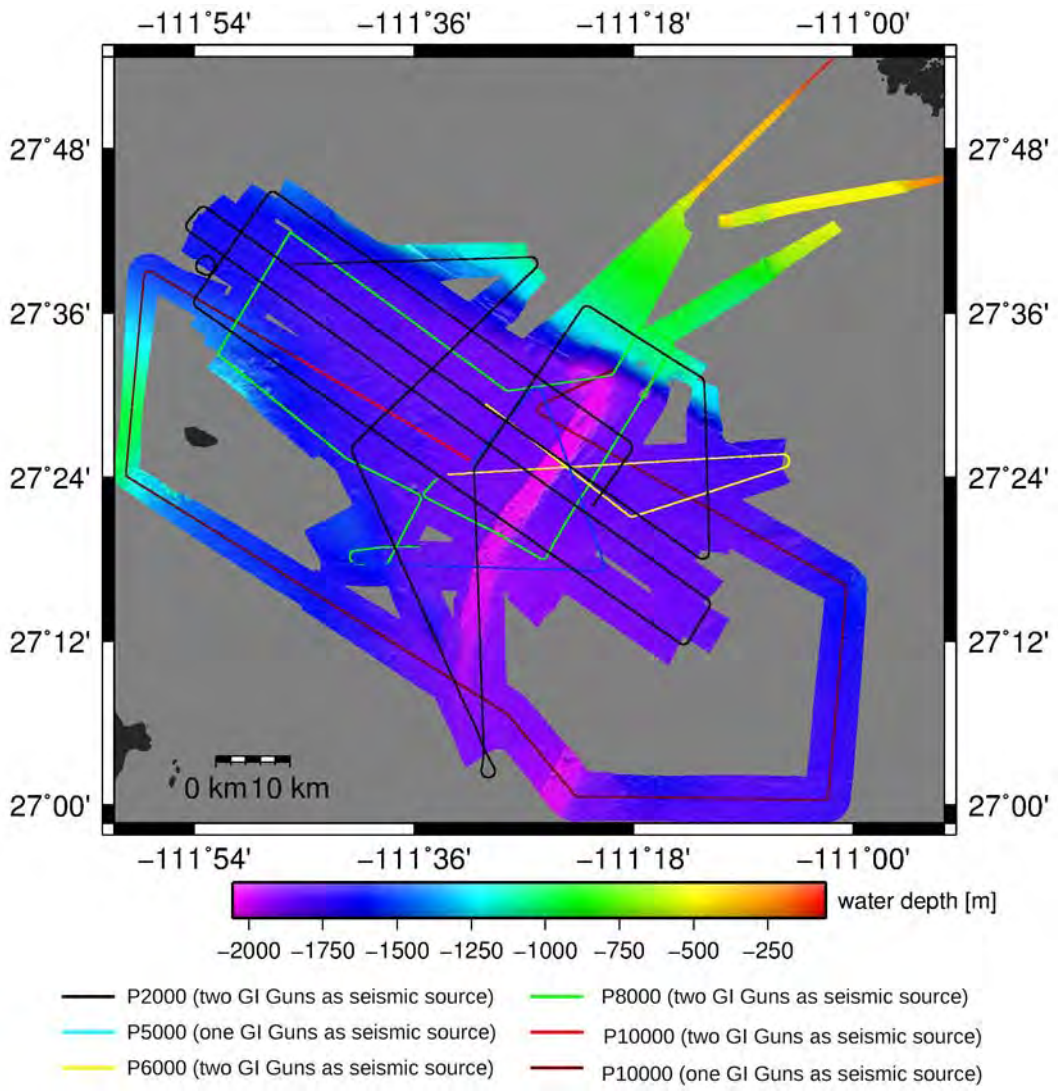

Fig. 6.1.1: Local bathymetry acquired during Cruise SO241 and 2D survey lines.

Svensen et al., 2003). These alteration processes have also been studied in the Guaymas Basin (Lonsdale and Becker, 1985; Simoneit and Lonsdale, 1982; Thornton and Seyfried Jr., 1987). The DSDP drill cores of Leg 64 showed that around the sills pore water was squeezed out, porosity decreased and calcareous and silicious microfossils were not present as they had apparently been dissolved (Galimov and Simoneit, 1982). Isotope-geochemical results of Chan et al. (1994) for sediments and hydrothermal fluids of DSDP Leg 64 (site 477) also show that the high temperatures generally cause dissolution of lithium (and probably other volatile elements) from sediments. However, there are no significant accumulations of lithium in the “vent fluids” and also no isotope fractionation compared to ridge basalts. This led Chan et al. (1994) to formulate the hypothesis that the Guaymas Basin is an open hydrothermal system with a constant supply of seawater as it is known from spreading axes not covered by sediments. Possibly the most interesting geochemical observation at the Guaymas fluid escape zones was the discovery of petroleum (Simoneit and Lonsdale, 1982) which directly showed the occurrence of thermal cracking of organic sediment contents. As long-chained petroleum components only constitute a small part of hydrocarbons produced during petroleum genesis, it is possible to infer that also large amounts of methane and maybe even carbon dioxide must have been produced in the course of magmatic intrusions. During a seafloor survey in 2009 a number of fluid escape sites were found, located above still warm magmatic intrusions (Lizarralde et al. 2010).

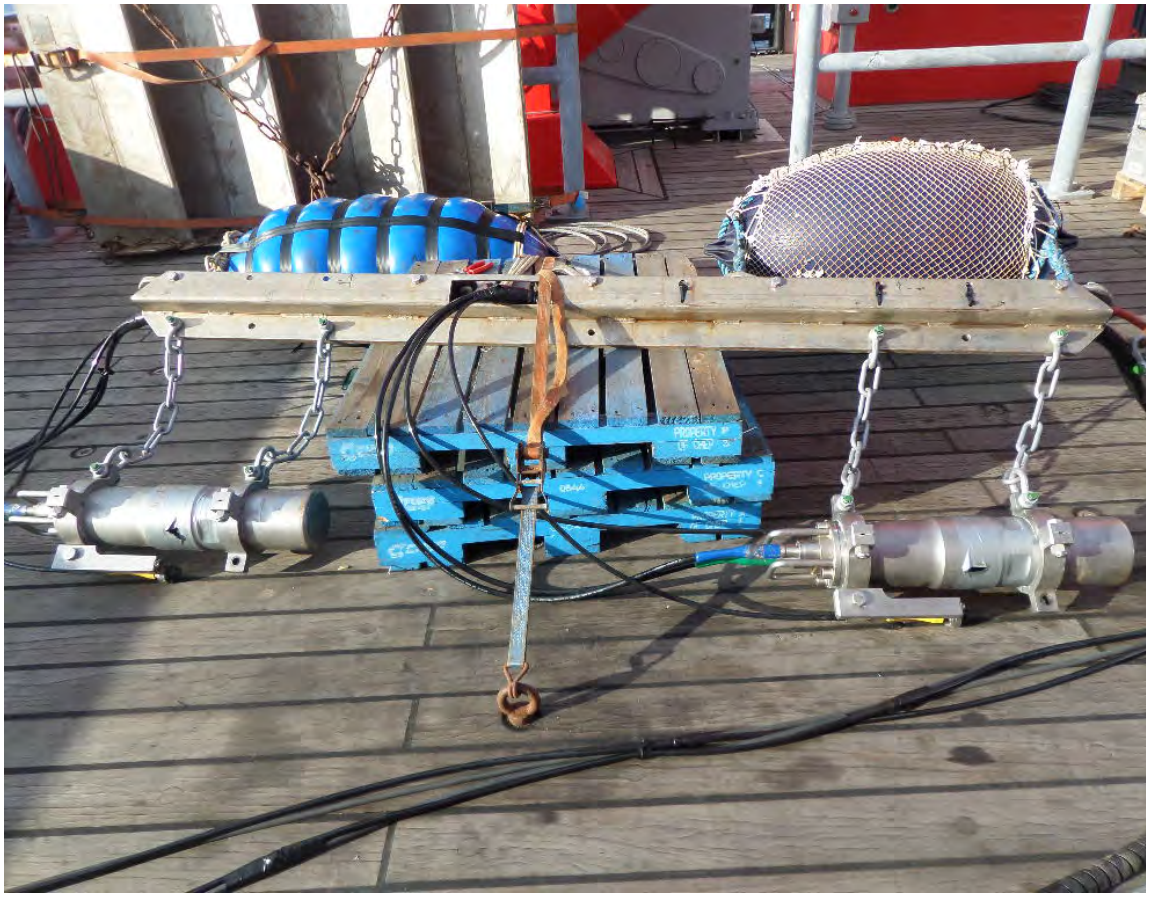

Fig. 6.1.2: Two standard GI-Guns (105/105 in^3) in harmonic mode were operated as seismic source during SO241.

Temperature measurements showed an increase in bottom water temperatures of 0.005 to 0.05 °C which is not explained by oceanography. Also, methane concentrations measured at 100 m above the seafloor significantly exceed background values (1.2 to 2500 nMol/kg). Photos from the seafloor show benthic ecosystems that are typical for warm vents (Vesicomyide mussels, Vestimentifera tube worms, bacterial mats and crusts of authigenic carbonate).

6. Work details and first results / Beschreibung der Arbeiten im Detail einschließlich erster Ergebnisse

6.1 2D reflection seismic imaging

6.1.1 Method and experiment setup

The aim of the seismic survey was to map the spatial extent of the sill intrusions and investigate the sediment-basalt interface as well as the internal sediment structures in the survey area of the Guaymas Basin. During the cruise an array of two 105/105 in^3 GI-Gun's was fired as seismic source for the seismic lines. Due to technical problems of the vessel's cooling system some lines had to be acquired with a single GI-Gun configuration. Data were recorded with GeoEel digital streamer segments. Fig. 6.1.1 gives an overview over the seismic 2D lines during Cruise SO241.

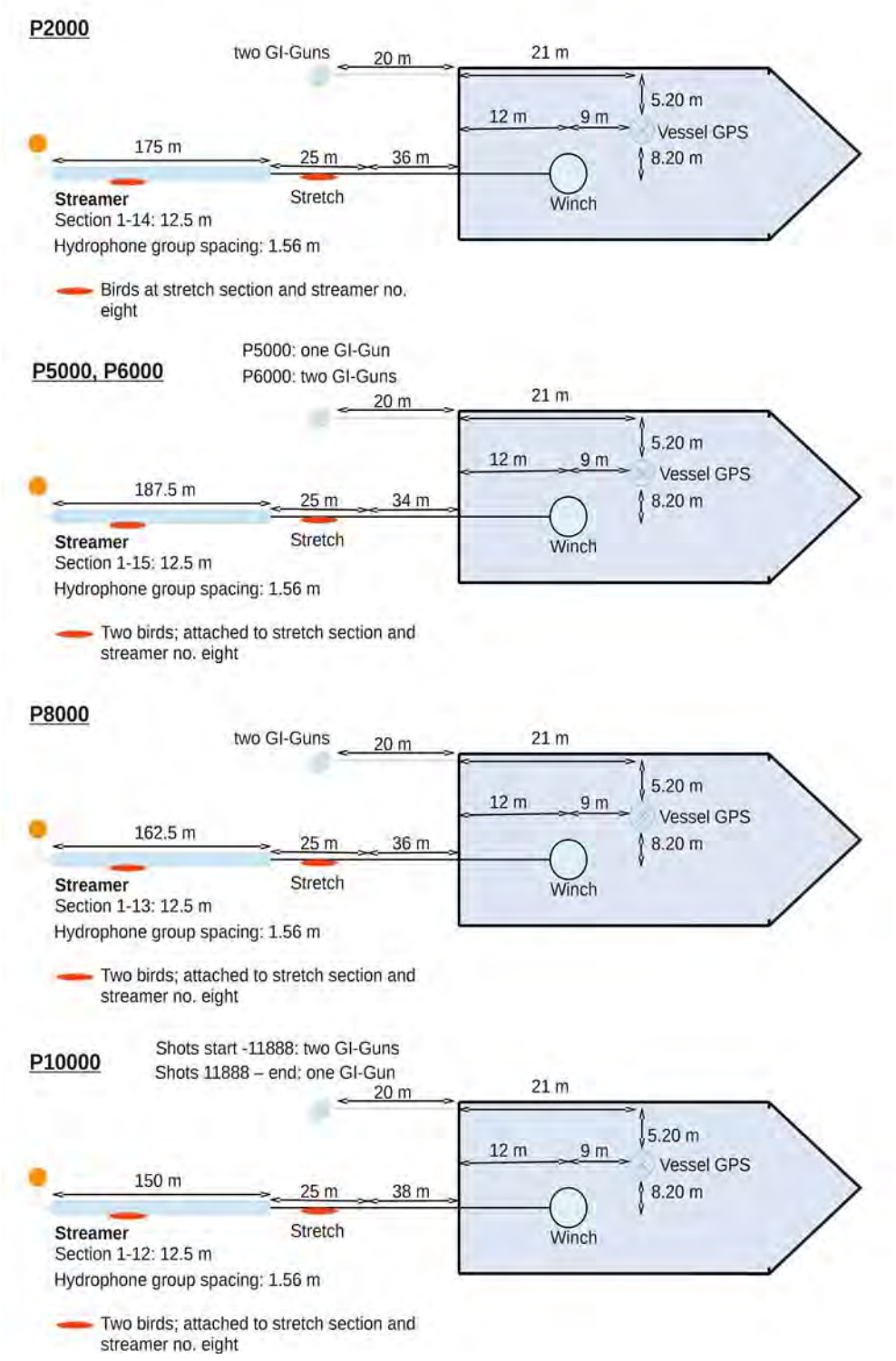

Fig. 6.1.3: Deck geometries, streamer configuration and gun setting during Cruise SO241.

Seismic sources

During this cruise two standard GI-Guns in harmonic mode were operated as seismic source. Both guns were connected to a stringer with the GI-Guns hanging on two chains about 70 cm beneath. An elongated buoy, which stabilized the guns in a horizontal position at a water depth of ~2 m, was connected to the stringer by two rope loops (Fig. 6.1.2). Each

Fig. 6.1.4: GeoEel streamer segments of 12.5 m length were connected to build up the 2D streamer system.

gun had a volume of 210 in^3, separated in 105 in^3 for the generator and 105 in^3 for the injector chamber. A gun hydrophone, which is located inside the air bubble, is supposed to provide both, the time break and the shape of the near-field signal for permanent monitoring and direct quality control of the source signal. Due to display problems in the Longshot controller the release of the injector pulse was triggered with a delay of 63 ms in manual mode with respect to the generator signal. This value was adjusted to the approximated source depth of 2 m and a gun pressure of 3000 psi (210 bar). The shooting interval was adjusted to 7 seconds, resulting in a shot point distance of 12.25 - 17.50 m in a range of approximately 3.5 – 5 knots. The frequency range of the two-GI-Gun-array is 15 - 500 Hz. The gun array operated very reliably until an O-ring failed and the last line was shot with only one airgun.

Streamer system

Different configurations in digital streamer length (Geometrics GeoEel streamer segments) were used for recording the seismic signal. Deck geometries, streamer configuration and seismic gun setting for the 2D surveys are illustrated in Fig. 6.1.3. The surveys P2000, P5000, P6000, P8000, and P10000 have varying streamer length from 150 m to 187.5 m. Each streamer configuration consisted of a tow cable, one vibro stretch section of 25 m length behind the tow cable and 12 to 14 active sections (each 12.5 m) attached behind the stretch zone. P2000 was recorded with 112 channels, P5000 and P6000 with 120 channels, P8000 with 104 and P10000 with 96 channels. The tow cable had a length of 34 – 38 m behind the vessel's stern. Each active section contained 8 channels with a hydrophone group spacing of 1.56 m. One AD digitizer module belonged to each active section. These AD digitizer modules are small Linux computers. Communication between the AD digitizer modules and the recording system in the lab was transmitted via TCP/IP. A

repeater was located between the deck cable and the tow cable (Lead-In). The SPSU managed the power supply and communication between the recording system and the AD digitizer modules. Two birds controlled and monitored the streamer depth. They were attached to the stretch zone and the 8th streamer segment. A small buoy was connected to the tail swivel of the 2D streamer (Fig. 6.1.4).

Bird Controller

Two Oyo Geospace Bird Remote Units (RUs) were deployed on the streamer. The locations of the birds are listed in Fig. CC. The RUs have adjustable wings. A bird controller in the seismic lab controlled the RUs. Controller and RUs communicate via communication coils nested within the streamer. A twisted pair wire within the deck cable connects controller and coils. Designated streamer depth was 2 m in accordance with good weather conditions and low swell noise. The RUs thus forced the streamer to the chosen depth by adjusting the wing angles accordingly. The birds were deployed at the beginning of a survey but no scanning of the birds was carried out during the survey because bird scans caused false triggers. However, the birds worked very reliably and kept the streamer at the designated depth.

Data acquisition systems

Data were recorded with acquisition software provided by Geometrics. The analogue signal was digitized with 2 kHz. The seismic data were recorded as multiplexed SEG-D. Recording length was 6 seconds. One file with all channels within the streamer configuration was generated per shot. The corresponding Shotlog reports shot number and time information contained in the RMC string. The acquisition PC allowed online quality control by displaying shot gathers, a noise window, and the frequency spectrum of each shot. The cycle time of the shots were displayed as well. The software also allows online NMO-Correction and stacking of data for displaying stacked sections. The vessel's GPS was simultaneously logged in RMC string and logged time and position information.

Trigger unit

A long shot was used as gun controller. The injector was triggered with a delay of 63 ms in manual mode. The arming point for the gun was set to 20 ms. From seismic data analyses we determined a total delay of 38 ms for survey P2000 and P6000, 26 ms for P5000 and 40 ms for P8000 and P10000 between triggering and real shooting time. No direct quality control of the source signal was carried out.

Processing

On-board processing included geometry calculations, delay calculations and source and receiver depth control. A ghost effect in the seismic data could not be detected (Fig. 6.1.5). The source-receiver locations were then binned on a grid with 1.5625 m by 1.5625 m cells. Different filter tests were applied and the frequency spectra plotted (Fig. 6.1.6). Seismic traces were balanced and filtered (bandpass corner frequencies 20, 45, 250, 40 Hz) before an NMO correction (with a constant velocity of 1492.30 m/s calculated from CTD measurements) and stacking were applied. The stack was migrated with a 2D Stolt algorithm (1500 m/s constant velocity model).

During SO241 all 2D seismic data were processed twice. First with the flow outlined above and secondly by colleagues from Deco Geophysical who used RadExPro to compare the data processing routines. During this flow we have tested the processing parameters for the various processes on the first line. We have found that the following processing flow works best: After data input we assigned the geometry based on the measured length of streamer and lay out of the air gun array. The SEG-D data contain the shot time in the trace headers. We received a file with the GPS positions measured at the stern of the vessel. After matching the shot and GPS coordinates by time we used the marine geometry input module in RadEx. To assign CDPs we used crooked line binning to bin the data with a bin size of 3.25 meters. When we had loaded the data we applied a bandpass filter, amplitude correction for spherical divergence, static corrections and TFD noise attenuation (to suppress

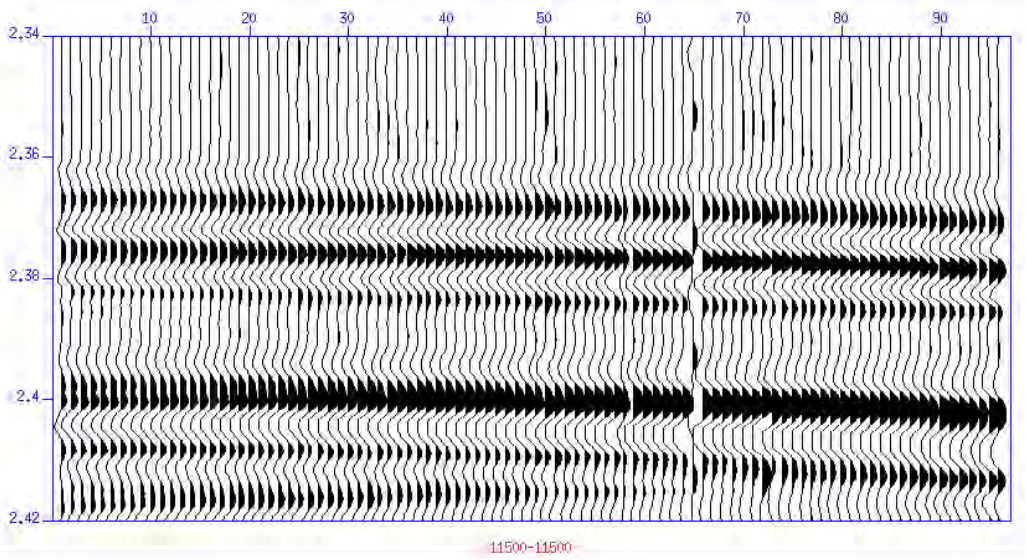

Fig. 6.1.5: Plotting of the seafloor signal for one shot and 96 channels in survey P10000. A separation of the seafloor signal is not observed.

frequency dependent noise). For the bandpass filter we used a low-cut ramp at 25-50 Hz and a high-cut ramp at 225-350 Hz. Furthermore, a static shift of 42 ms was applied which was determined from the difference between the seafloor arrival and the first seafloor multiple. Before stacking the CDP traces we applied a NMO correction with a constant velocity of 1.5 km/s and stretch muting to 30 %. We then ran a postack time migration. We have used the Stolt F-K Migration procedure in RadEx with a constant velocity 1480 m/s.

6.1.2 Initial results

Preliminary onboard seismic interpretation reveals several interesting features associated with interactions between sills and sedimentary cover, fluid migration and entrapment. Different types of igneous intrusions were identified, such as saucer-shaped intrusives, layer-parallel sills and clusters of strong positive polarity reflections, which probably represent short sill segments (Fig. 6.1.7). Sills are mostly associated with an overlying chaotic and deformed (folded) facies indicating contact metamorphism and deformation associated with emplacement of the intrusives. Some intrusives also reveal a similar underlying contact metamorphic aureole. Intrusions occur at variable depths and the thickness of metamorhic aureoles varies. A systematic study of the geometry of the intrusives, spatial distribution and nature of alteration of the surrounding strata will be carried out to determine the volume of sediments that are affected by igneous intrusions and determine the ways in which carbon has been transported.

A gas hydrate bottom simulating reflector (BSR) was traced out in the seismic data (Fig. 6.1.8). The presence of hydrates was already known from parts of the study area, such as the transform margin adjacent to the Guaymas Basin. Our result indicates that the BSR bearing area is more extensive than previously found. A clear cross-cutting BSR is not discernable in the basin floor, because it would follow the stratification. However, the hydrate samples that we collected in this area clearly show that the area is hydrate prone and that it is likely that some of the high amplitude reflections in this area represent the BSR. Additionally, heat flow and conductivity measurements carried out during the survey will help to understand whether P, T conditions are conducive for hydrate stability in deeper parts of the basin.

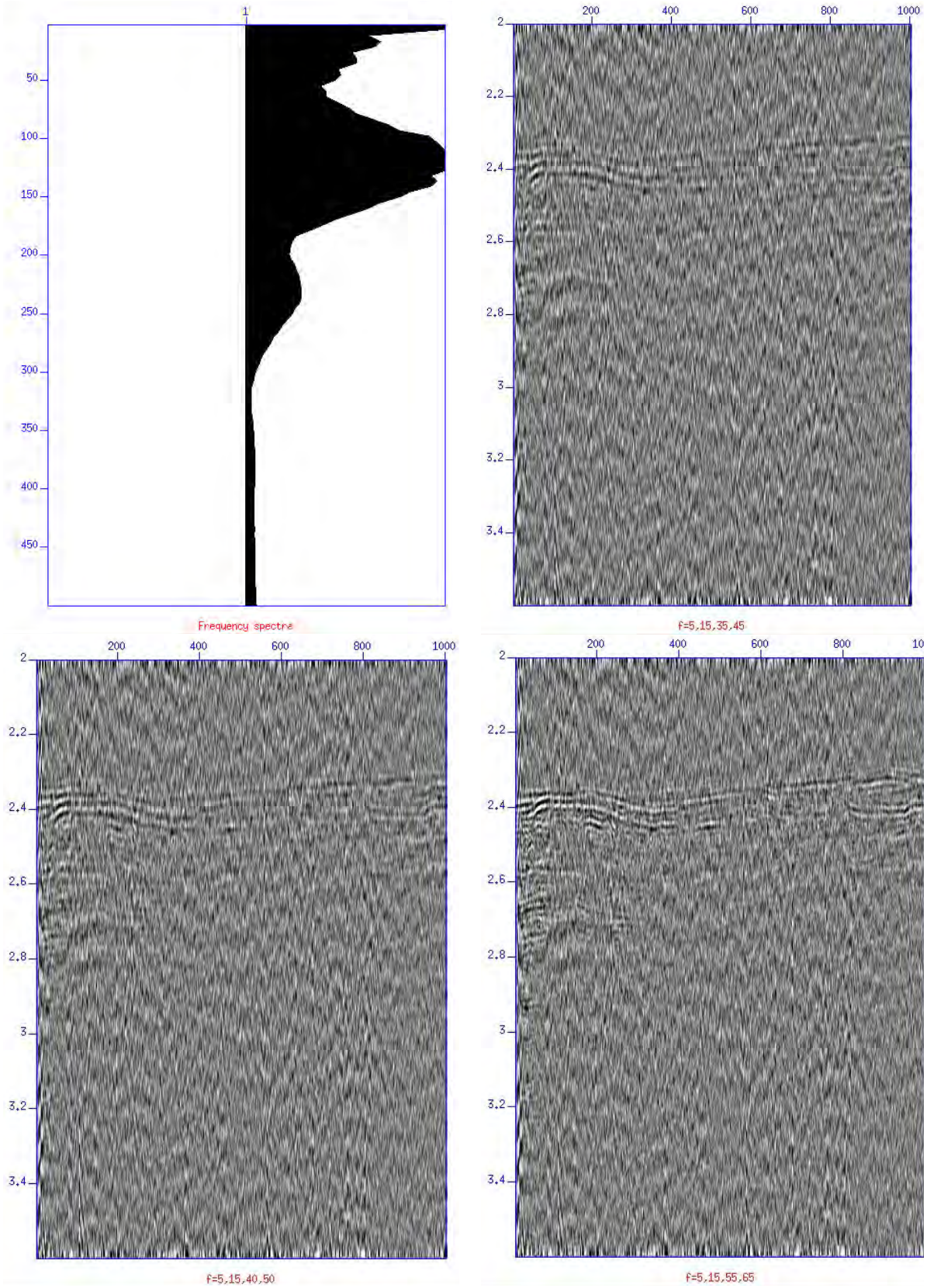

Fig. 6.1.6: Frequency spectra and low-cut frequency tests.

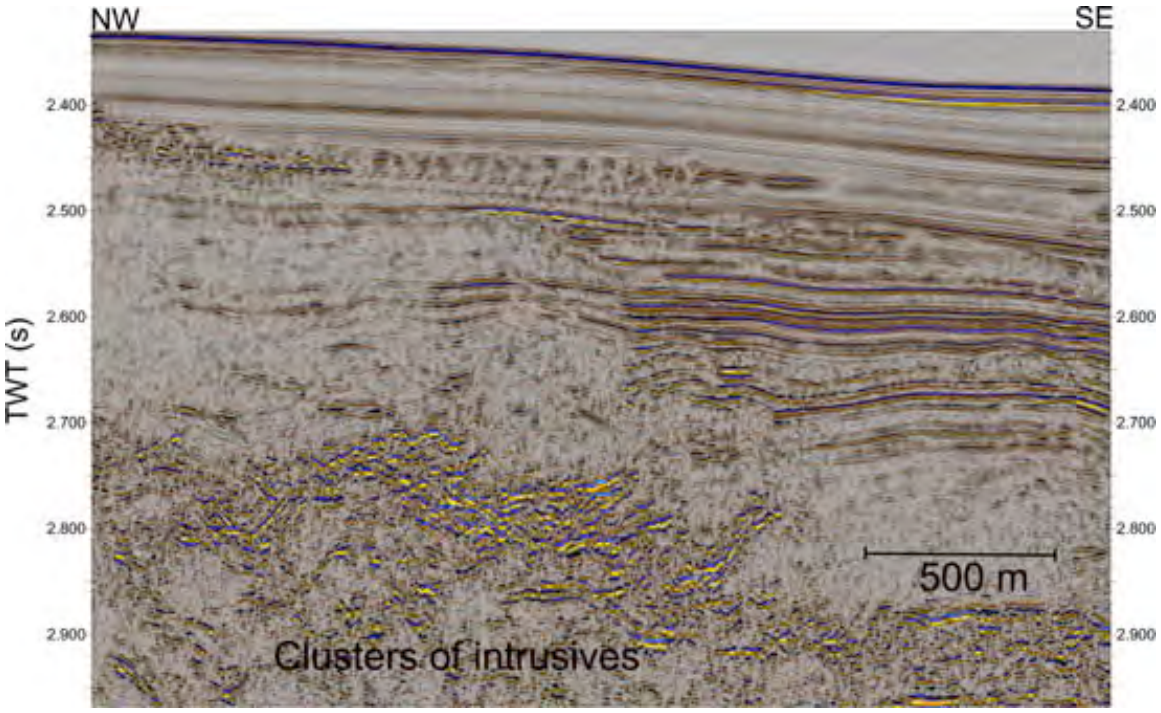

Fig.6.1.7: Typical seismic facies related to magmatic intrusions, contact metamorphism, and hemipelagic sedimentation, central part of the Guaymas Basin north of the rift axis.

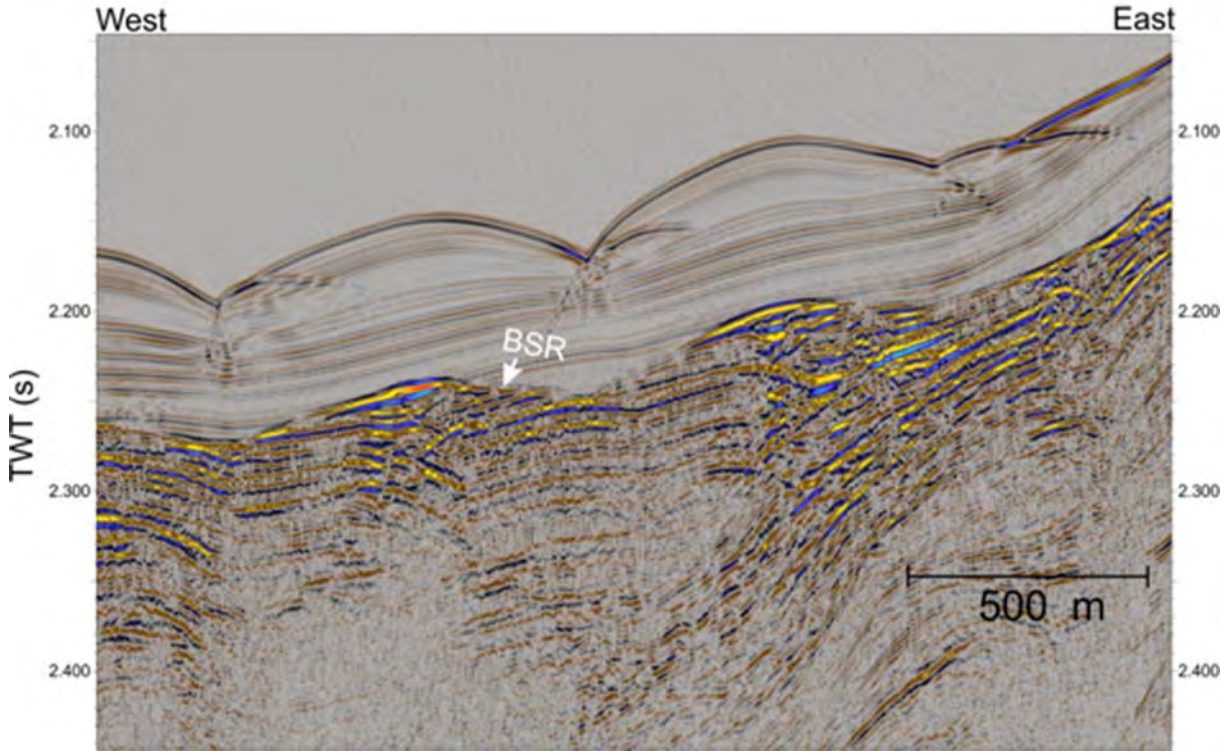

Fig. 6.1.8: Bottom Simulating Reflector (BSR) caused by free gas that is trapped underneath gas hydrates. Note, the negative seismic polarity and the cross-cutting relationship. The sediment waves are the same as shown in figure 6.4.2.

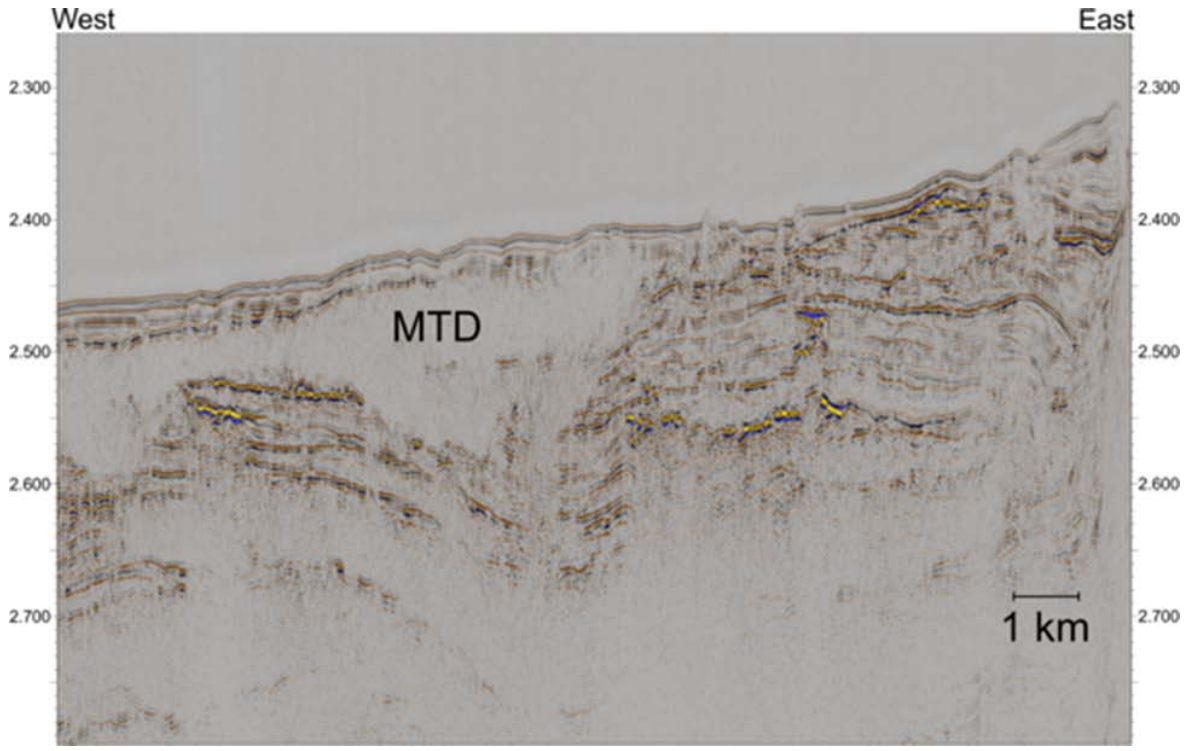

Fig. 6.1.9. A thick mass transport deposit in the central part of the Guaymas Basin south of the northern spreading axis.

Several small and large mass transport deposits (MTD) are identified southeast of the northern axial graben. They appear as transparent regions in the seismic data. The largest MTD (Fig. 6.1.9) covers approximately 1440 sq. km and extends from the distal Yaqui Fan to the southern half of the northern axial graben. The sedimentary environment in the northwestern Guaymas Basin is mostly dominated by sedimentary drifts indicating the influence of bottom water current. The seismic data will be analyzed further to get an understanding on variations in depositional environment in relation to different tectonic regimes, such as regions undergoing extension and transform margin.

6.2 Ocean bottom seismology

6.2.1 Method and experiment setup

The OBS consists of four floats connected to a frame, which carries a three-component seismometer, a hydrophone and a data recorder cased in a high-pressure tube (Fig. 6.2.1.). The sensors are connected to the recording unit, which continuously records the signals of the sensors. The systems itself floats at the sea surface, so in order to deploy it at the ocean bottom a weight is mounted to the frame with a releaser. The releaser has an acoustic communication unit, which can be addressed from the ship in order to disconnect the weight after the experiment. The OBS will then ascend to the surface and can be recovered. A flashlight, a radio transmitter and a flag are attached to the frame in order to facilitate sighting the OBS. While the OBS continuously records seismic signals an additional data logger on board records the shot times.

Fig. 6.2.1: Ocean-bottom seismometers used during deployment

The data recorders have to be programmed before the deployment of the system. The sample rate of the OBS recorders was set to 500 Hz, while the time logger recorded at a sample rate of 1000 Hz. The gain of the input channels was set to 15 for the three geophone components and 7 for the hydrophone. The recorder was equipped with four 2 GB flash cards. The exact recording parameter for the deployments can be found in Appendix C (OBS protocols). The recording units were synchronized with a GPS signal before as well as after the recording period in order to correct the drift of the logger's internal clock.

The OBS experiment focused on the Central Vent Site close to the northern rift graben and included eleven OBS, which were deployed on July the 1st 2015 (Fig. 6.2.1). Nine OBS formed an array of three profiles consisting of three instruments, whereas the central profile was covering the seep site. Two additional OBS extended the central profile towards the east. The OBS experiment was designed to complement the 3D reflection seismic experiment, which could not be conducted due to technical problems. Therefore, we decided to acquire additional 2D seismic reflection data and profiles dedicated to the OBS profile (Fig. 6.2.2 and 6.2.3). All eleven OBS were recovered on July the 8th and all instruments have recorded data. No instrument showed an error message during synchronization. There were notable amounts of condensation water in 5 of the pressure tubes, which may be attributed to high humidity inside the wet lab. The OBS recorded between 1.4 and 1.6 GB and no flash card showed any problems. All data have been copied and converted to SEG-Y on board.

6.2.2 Initial results

A first quick quality control showed promising data (Fig. 6.2.4). The shots are clearly visible on all 4 components. Detailed processing will be carried out after the cruise. During the period of the OBS experiment, Mexican broadband seismometer stations have recorded 31 earthquakes with magnitudes between 3.3 and 4.2 in the study area (Fig. 6.2.2 and 6.2.3). These earthquakes may be attributed to tectonic activity along the northern and the southern rift as well as transform faults, which confine the northern margin of the Guaymas Basin. The OBS data may be helpful for relocating these earthquakes and to constrain tectonic parameters of the ongoing rift processes.

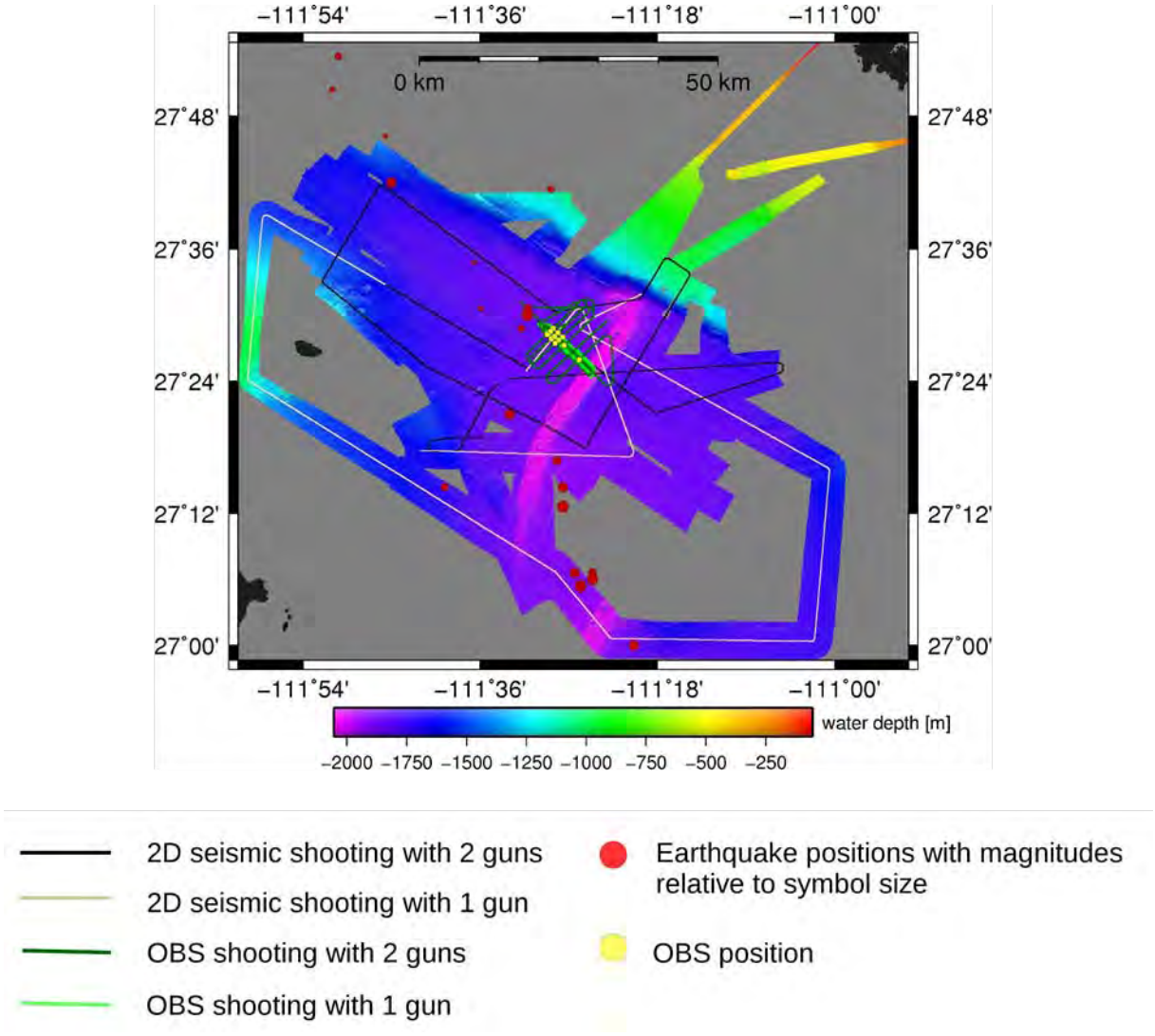

Fig. 6.2.2: Overview map of OBS locations, seismic profiles and local earthquakes during OBS deployment in the Guaymas Basin

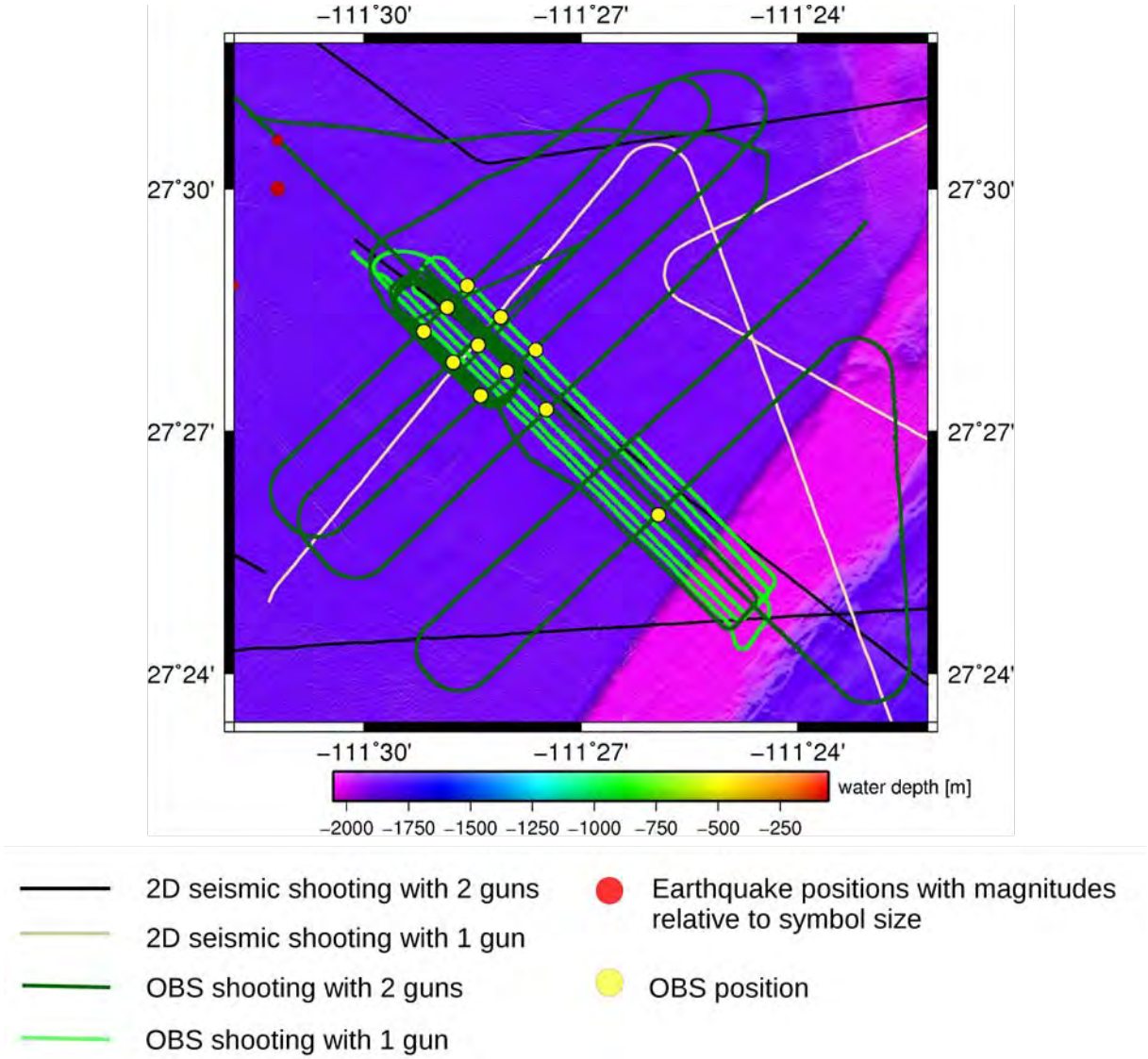

Fig 6.2.3: Detailed map of the OBS area

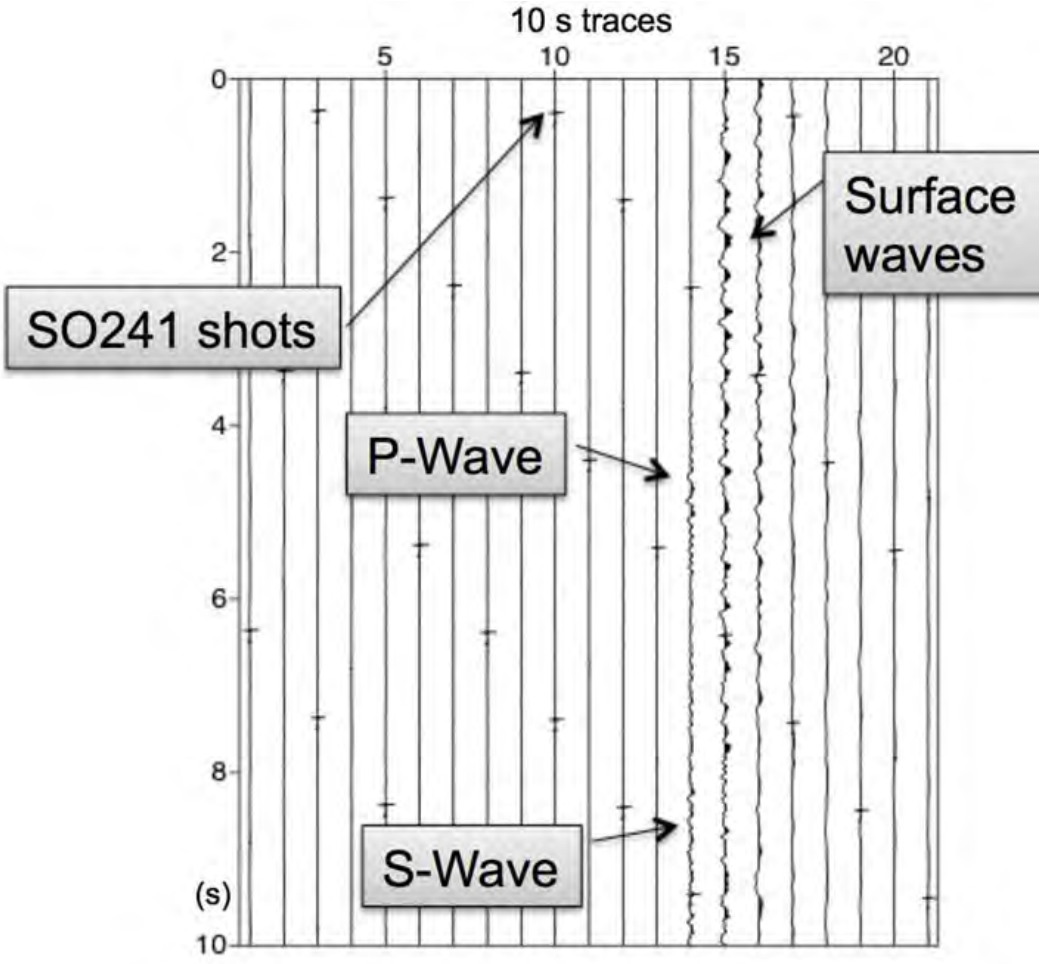

Fig. 6.2.4: OBS recording showing the airgun shots and the different arrivals of an earthquake.

6.3 Multi-beam bathymetry

6.3.1 Method and experiment setup

During Cruise SO241 the hull-mounted Kongsberg Simrad system EM122 was used for bathymetric mapping continuously while we were in the Guaymas Basin study area (Fig. 6.3.1). The EM122 system allows accurate bathymetric mapping up to full ocean depth. Basic components of the system are two linear transducer arrays in a Mills cross configuration with separate units for transmitting and receiving. The nominal sonar frequency is 12 kHz with an angular coverage sector of up to 150° and 864 beams per ping. The emission angle is up to 150° wide across track, and 0.5° along track direction. The reception is obtained by beam forming of 864 beams, with widths of 0.5° across track and 1° along track. Thus, the actual footprint of a single beam has a dimension of 0.5° by 1°. The achievable swath width on a flat bottom will normally be up to six times the water depth dependent on the character of the seafloor and the selected opening angle. The angular coverage sector and beam pointing angles may be set to vary automatically with depth according to achievable coverage. This maximizes the number of usable beams. In areas where we collected a dense net of PARASOUND or 3D seismic profiles with a profile distance of less than 100 m, the swath width was manually reduced in order to increase data density and quality. The beam spacing is normally equidistant, but equiangular is also available. For depth measurements, 864 isolated depth values were obtained perpendicular to the track for each ping. The depth is calculated by using beam forming and beam steering. Beam forming uses the 2-way-travel-time and the beam angle known for each beam to send out the swath from the transducer. Beam steering takes into account the ray bending due to refraction in the water column by sound speed variations and sets the receiver in the right direction. The accuracy of the depth measurements depends on weather conditions and

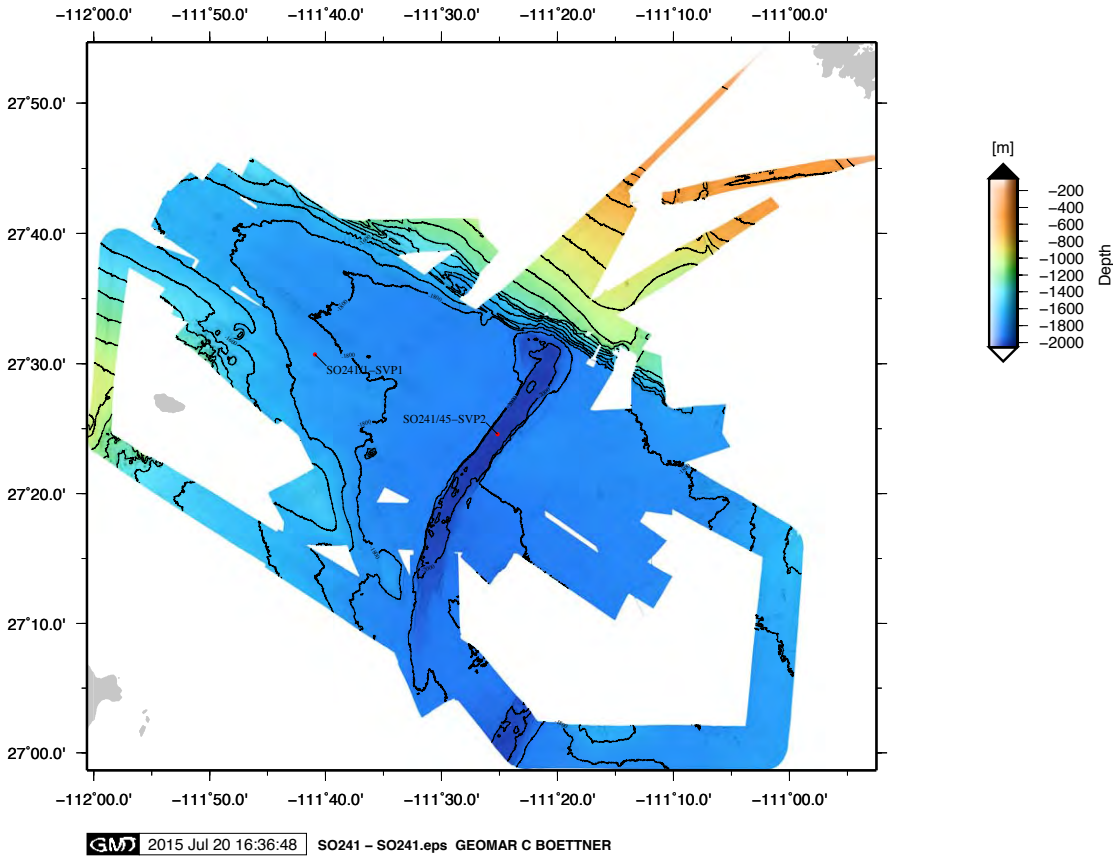

Fig. 6.3.1: Bathymetry collected during cruise SO241. The data were acquired with the Kongsberg Simrad system EM122. The locations of sound-velocity profiles (SVPs) are shown as red dots.

survey speed. Survey speed was variable ranging from 3 - 4.5 kn during the 2D seismic and P-cable surveys to 8 kn during dedicated bathymetry profiles. A roll calibration was carried out but no error could be determined. VCTDs for collecting an accurate sound velocity profile were taken at several sites. A combination of amplitude (for the central beams) and phase (slant beams) is used to provide measurement accuracy practically independent of the beam pointing angle. Beside the depth values, the EM122 provides also backscatter values and pseudo-sidescan images. These images were of high value to verify possible seep sights, which correspond with a high attendance of carbonate crusts and therefore a high backscatter value.

In general the system worked reliably and only minor data gaps exist due to the start and end points of the 2D seismic lines. However, the outer beams exceeding 60° show a time variant flapping which may limit the usable swath width. On-board processing was not able to correct this error fully.

Furthermore the EM122 seems to emit too high-density inner beams, even though the pinging mode was set to SHALLOW and the marine mammal protection was switched on to reduce the intensity by -20 db. After three day of survey we set the angle of the transducer to 5° along direction to reduce the scattered energy. But still the EM122 did not refuse to penetrate into the subsurface. In order to characterise high backscatter areas the EM122 results were compared to PARASOUND profiles. In one case we could estimate the depth of the anomaly of amplitude to 8-10 m depth. This made the inner beams unusable or at least offered a low S/N-ratio. The resulting seafloor showed a wide range of depth values.

Multi-beam data were processed on board using the MB-System© software package for data cleaning, gridding and display. Roll corrections were of no need. The density of

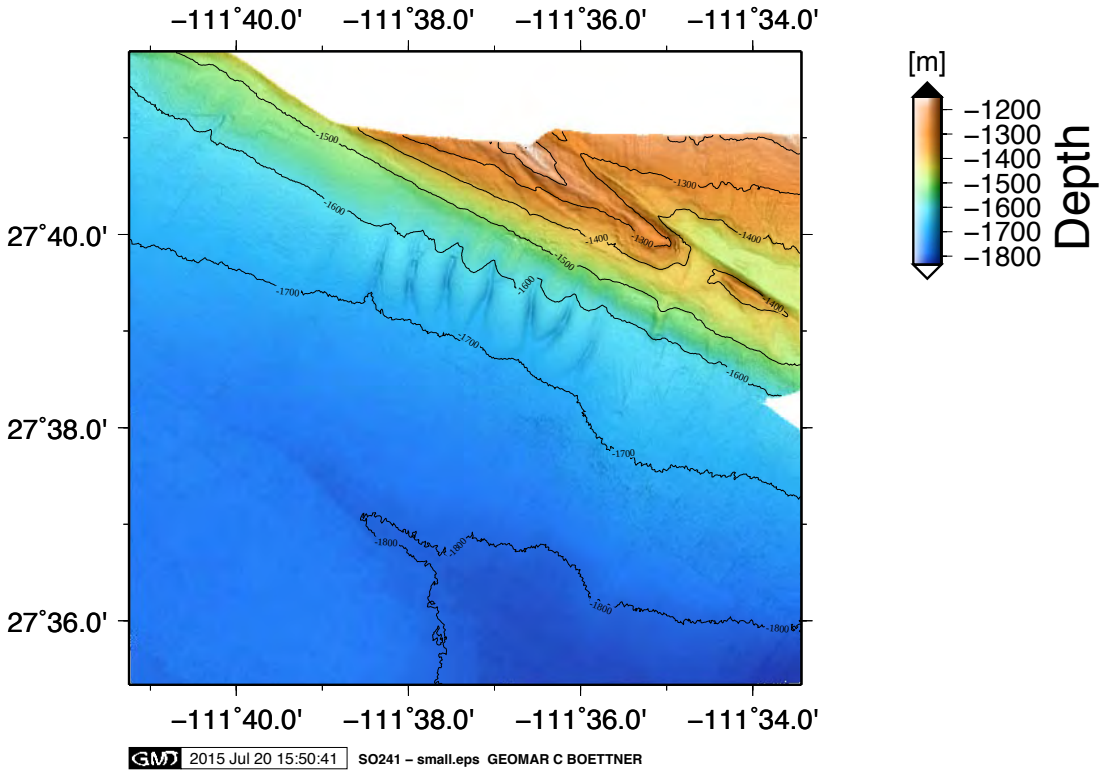

Fig. 6.3.2: Example for the EM122 bathymetric data showing contourites close to the northern boundary of the Guaymas Basin.

sounding allowed gridding the dedicated bathymetry profiles to a 20-25 metres grid size, while the bathymetric data obtained during the surveys around the black smokers allowed gridding at 8 metres grid spacing. The overall bathymetry has been gridded using the median filter scheme, a spline interpolation of two cells and a thin plate spline interpolation with a value of two. The data around the black smokers have been gridded using a Gaussian weighted mean, a spline interpolation of one cell and no thin plate spline interpolation.

The QPS Fledermaus© software package (FMGT, DMAGIC, FLEDERMAUS, FMMidWater) was used for data cleaning, editing, backscatter calculation, mosaic producing and water column imaging. Unfortunately the EM710 could not be run during PARASOUND acquisition due to interference of both systems.

Sound velocity profiles

Reliable depth measurements require a correct sound velocity profile. Sound velocity profiles were collected at the beginning and in the middle of the cruise (PLOT). Sound velocity corrections are automatically applied to bathymetry data in the Simrad operation software (SIS). Unfortunately, the original sound velocity profile obtained on June 26, 2015 was erroneous below 1761 meters water depth due to a lower velocity gradient in the deep water of the Guaymas Basin. This could be corrected by using a sound velocity profile, which was acquired inside the rift graben, which offers the highest depth values.

6.3.2 Initial results

The overall data quality is sufficient to track and identify several sedimentary and tectonic processes. The bathymetry offers a large variety of possibilities to reconstruct the Guaymas Basin history. Seep sights, black smokers, volcanic features and the rift graben are given in a resolution of 10-25 m. This example shows sediment waves at the slope of the continental margin located at the edge of the Guaymas Basin (Fig. 6.3.2).

6.4 PARASOUND sediment echosounder

6.4.1 Method and experiment setup

The hull-mounted parametric sub-bottom profiler PARASOUND DS3 (Atlas Hydrographic) was operated on a 24-hour schedule for flare imaging and to provide high-resolution information on the uppermost 50-100 m of sediment. PARASOUND DS3 works as a narrow beam sediment echo sounder, providing primary frequencies of 18 (PHF) and adjustable 18.5 – 28 kHz, thus generating parametric secondary frequencies in the range of 0.5 – 10 kHz (SLF) and 36.5 – 48 kHz (SHF) respectively. The secondary frequencies develop through nonlinear acoustic interaction of the primary waves at high signal amplitudes. This interaction occurs in the emission cone of the high-frequency primary signals which is limited to an aperture angle of 4° for the PARASOUND DS3. This narrow aperture angles is achieved by using an array of 128 transducers on a rectangular plate of approximately 1 m² surface area. Therefore the footprint size is 7% of the water depth and vertical and lateral resolution is significantly improved compared to conventional 3.5 kHz echo sounder systems. The PARASOUND DS3 is an improvement of the former PARASOUND DS2 (Atlas Elektronik) and is installed on RV SONNE since 2014. The system provides features like recording of the 18 kHz primary signal and both secondary frequencies, continuous recording of the whole water column, beam steering, different types of source signals (continuous wave, chirp, barker coded) and signal shaping. Digitization takes place at 96 kHz to provide sufficient sampling rates for the high secondary frequency. A down-mixing algorithm in the frequency domain is used to reduce the amount of data and allow data distribution over Ethernet.

For the standard operation a parametric frequency of 4 kHz and a sinusoidal source wavelet of 2 periods were chosen to provide a good balance between signal penetration and vertical resolution. The 18 kHz signal was also recorded permanently. If the system was mainly used for flare imaging, it was operated in a single pulse mode.

Unfortunately technical problems, which could only partly be solved during the cruise, resulted in frequent loss of data due to software malfunctioning. The system was rebooted many times and the Atlas Hydrographic support was asked for help and did a remote maintenance, but still frequent program crashes (at least twice a week) occurred until the end of the cruise. However, these data gaps rarely exceeded some minutes and the overall data quality is very good.

All raw data were stored in the ASD data format (Atlas Hydrographic), which contains the data of the full water column of each ping as well as the full set of system parameters. Additionally a 400 m-long reception window centred on the seafloor was recorded in the compressed PS3 data format after mixing the signal back to a final sampling rate of 24 kHz. This format is in wide usage in the PARASOUND user community and the limited reception window provides a detailed view on the subbottom structures.

All data were converted to SEG-Y format during the cruise using the software package ps32sgy (Hanno Keil, Uni Bremen). The software allows generation of one SEG-Y file for longer time periods. If seismic data were collected simultaneously, one SEG-Y file was created for the length of each seismic profile. In all other cases 1h-long pieces were generated (e.g. during transit, long seismic lines). All data were loaded to the seismic interpretation software HIS Kingdom. This approach allowed us to obtain a first impression of sea floor morphology variations, sediment coverage, sedimentation patterns along the ship's track and imaging of the shallow BSR. In addition the exact locations of the seep sights could be determined, which was important for selecting locations for the TV-GRAB, TV-MUC, sediment coring, and water sampling.

6.5 Pore-water geochemistry

6.5.1 Method and experiment setup

To obtain enable an updated estimate of the mass of carbon that can be released from sediments upon magmatic intrusions and specifically to calculate the amount of carbon

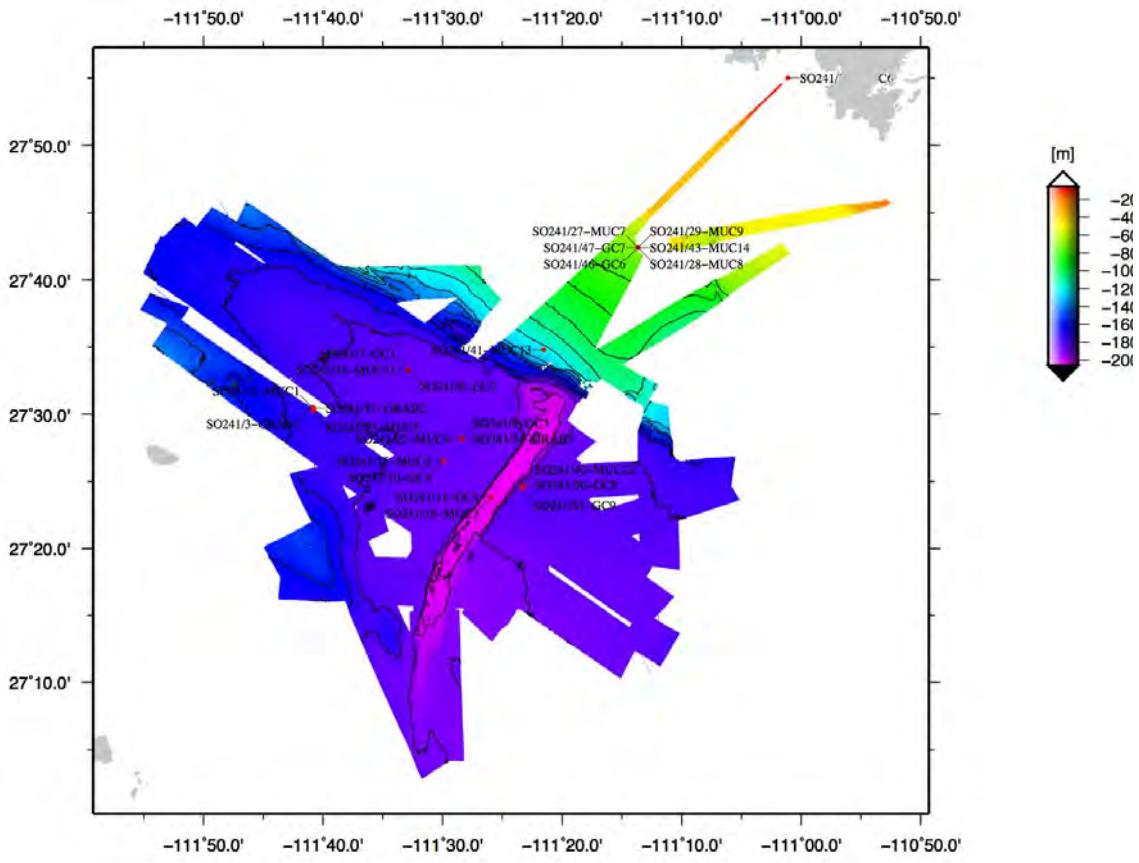

Fig. 6.5.1: Coring stations during SO241.

recently arriving at the seafloor and emitting into bottom water. For this purpose, sediment cores were taken (by means of a multicorer and a gravity corer) from active vent and seep locations as well as reference sites constraining the normal diagenetic background and impact of lateral terrigeneous input.

After retrieval all cores were immediately transferred into a cooling lab (4°C) and processed within 1-2 hours. Supernatant bottom water of the multicorer-cores was sampled and filtered for subsequent analyses. For all measurements and sub-samples of redox-sensitive parameters (e.g. Fe, trace metals) one core was cut in a glove bag using argon gas as protection atmosphere at maximum resolution of 1 cm; pore-water separation was performed using a cooled centrifuge. Subsequently, the pore water samples were filtered (0.2 nm cellulose-acetate filters) under argon atmosphere. Gravity cores were cut lengthwise after recovery. On the working halves sample intervals of 10 to 50 cm were taken for pressure filtration and centrifugation. Syringe samples for detection of volatile hydrocarbon gases were taken on deck from every cut segment surface. Sediment samples equal to about 3 ml material were transferred into 20 ml septum vials containing 9 ml of a concentrated NaCl-solution. Each sample depth for pore water squeezing was additionally sampled for (1) the calculation of sediment density and (2) for determination of redox-sensitive elements. Porosity sub-samples were filled into pre-weighed plastic vials and redox-samples were kept in specific gas-tight containers under argon atmosphere for subsequent analyses in the home laboratory. For pressure filtration Teflon- and PE-squeezers were used. The squeezers were operated with argon at a pressure gradually increasing up to 2.5 bar MUC and 5 bar (GC), respectively. Depending on the porosity and compressibility of the sediments, up to 20 ml of pore water were received from each sample. The pore water was filtered through 0.2 µm regenerated cellulose acetate membrane filters.

Pore water analyses of the following parameters were carried out: ammonia, phosphate,

silicate, alkalinity, hydrogen sulfide, and chloride as well as ferrous iron, nitrate, and nitrite for MUCs (Tab. 6.5.1). The analytical techniques used on board to determine the various dissolved constituents are listed in Table 1. Modifications of some methods were necessary for samples with high sulfide concentrations. Ferrous iron, phosphate, ammonium, hydrogen sulfide and silicate were measured photometrically using standard methods described by Grasshoff et al. (1997). Samples of the sediment pore water for total alkalinity measurements were analyzed by titration of 0.1-1 ml of pore water according to Ivanenkov and Lyakhin (1978). Titration was finished until a stable pink color occurred. During titration the sample was degassed by continuously bubbling argon to remove the generated CO_2 or H_2S. The acid was standardized using an IAPSO seawater solution. Chloride was determined by titration with $AgNO_3$ standardized against IAPSO seawater. The method for hydrogen sulfide determination according to Grasshoff et al. (1997) has been adapted for pore water concentrations of S2- up to mM amounts. For reliable and reproducible results, an aliquot of pore water was diluted with appropriate amounts of oxygen-free artificial seawater; the sulfide was fixed by immediate addition of zinc acetate gelatin solution immediately after pore water recovery. After dilution, the sulfide concentration in the sample should be less than 50 µmol L^{-1}. For the analysis of iron concentrations sub-samples of 1 ml were taken within the glove bag and immediately complexed with 20 µl of Ferrozin and afterwards determined photometrically.

Table 6.5.1: Techniques used for pore water analyses.

Parameter	Method	Detection limit	analytical error (accuracy)
Fe^{2+}	Photometer	1 µmol/l	5 µmol/l
HS^-	Photometer	1 µmol/l	3 µmol/l
NH_4^+	Photometer	2 µmol/l	5 µmol/l
PO_4^{3-}	Photometer	1 µmol/l	5 µmol/l
SiO_4^{4-}	Photometer	1 µmol/l	5 µmol/l
NO_3^-, NO_2^-	Photometer	1 µmol/l	1 µmol/l
Cl^-	Titration		5 mmol/l
Alkalinity	Titration		0.1 meq/l

Acidified sub-samples (35µl suprapure HCl + 3 ml sample) were prepared for ICP analyses of major ions (K, Li, B, Mg, Ca, Sr, Mn, Br, and I) and trace elements. DOC, DIC, $d^{13}C$ of DIC will be determined on selected sub-samples in the shore-based laboratories.

6.5.2 Initial results

In total, we processed samples from 13 MUC and 11 GC deployments. In addition, samples from a HyBis grab were analyzed. An overview of the coring locations is presented in Table 6.5.2 and Figure 6.5.1 Below, we present characteristic examples of pore water profiles from different working areas: (1) smoker vents, (2) cold seeps (e.g. Ring, North, Central), (3) slope and basin (input and reference).

Slope and basin sediments

A number of MUC and GC cores were taken along a depth transect from the shelf into the basin to characterize the sedimentary input and constrain normal diagenetic processes. In principle, the continental margin is characterized by high sedimentation rates of organic-rich material. For illustration, MUC 09 and GC 07 located in the central part of the oxygen minimum zone (OMZ) at roughly 660 m water depth are presented in Figures 6.5.2 and 6.5.3. All measured parameters show indications for strong suboxic to anoxic diagenesis.

Table 6.5.2: List of core locations. Latitude and longitude are ship positions.

Station N°	Latitude (S)	Longitude (W)	Area	Water Depth	*Recovery*	*Remarks*
SO241-02, MUC01	27°30.558	111°40.922	Ring-Seep	1725	20 cm	
SO241-07, GC01	27°33.301	111°32.882	North-Seep	1845	300 cm	
SO241-07, GC02	27°33.301	111°32.885	North-Seep	1842	300 cm	squeeze core
SO241-09, GC03	27°28.138	111°28.420	Central-Seep	1837	476 cm	overpenetration
SO241-10, GC04	27°26.531	111°29.928	Basin-Reference	1847	500 cm	overpenetration, squeeze core
SO241-14, GC05	27°23.864	111°25.940	Graben	2038	484 cm	overpenetration
SO241-15, MUC02	27°26.925	111°29.926	Basin-Reference	1845	35 cm	
SO241-16, MUC03	27°23.815	111°25.935	Graben	2041	35 cm	
SO241-22, MUC04	27° 28.165	111° 28,347	Central-Seep	1839	30 cm	
SO241-23, MUC05	27° 30.282	111° 40.770	Ring-Seep	1726	27 cm	
SO241-26, MUC06	27° 55.013	111° 1.127'	Shelf	39	30 cm	
SO241-29, MUC07	27° 42.415	111° 13.654	Slope, OMZ	662	-	overpenetration, no sample
SO241-29, MUC08	27° 42.413	111° 13.656	Slope, OMZ	665	-	overpenetration, no sample
SO241-29, MUC09	27° 42.410	111° 13.656	Slope, OMZ	665	50 cm	partly overpenetration
SO241-32, MUC10	27°17.741	111°30.671	Graben	2000	-	video track, no sample
SO241-33, MUC11	27° 33.301	111° 32.883	North-Seep	1855	25 cm	
SO241-37, HyBis1	27° 24.761	111° 23.229	Smoker-Vent	1852	30 cm	grab samples
SO241-40, MUC12	27° 24.698	111° 23.254	Smoker-Vent	1852	32 cm	
SO241-41, MUC13	27° 34.800	111° 21.537	Slope, blw. OMZ	1221	40 cm	
SO241-43, MUC14	27° 42.409	111° 13.656	Slope, OMZ	664	50 cm	microb., no PW
SO241-46, GC06	27° 42.412	111° 13.651	Slope, OMZ	664	1000 cm	microb., overpenetration
SO241-47, GC07	27° 42.412	111° 13.649	Slope, OMZ	671	766 cm	rhizon sampling
SO241-50, GC08	27°24.715	111°23.228	N-Smoker-Vent	1852	-	no penetration
SO241-51, GC09	27° 24.472	111° 23.377	S-Smoker-Vents	1840	487 cm	
SO241-58, GC10	27° 24.487	111° 23.377	S-Smoker-Vents	1845	498 cm	slightly overpenetrated
SO241-59, GC11	27° 24.471	111° 23.370	S-Smoker-Vents	1840	500 cm	overpenetration, squeeze core
SO241-62, GC13	27° 28.193	111° 28.365	Central-Seep	1838	483 cm	overpenetration
SO241-65, MUC15	27° 24.342	111° 22.970	SE off Smokers	1846	35 cm	
SO241-66, MUC16	27° 24.577	111° 23.265	Smoker-Vent	1842	25 cm	
SO241-71, GC14	27° 28.187	111° 28.380	Central-Seep	1839		no penetration
SO241-72, GC15	27° 28.193	111° 28.387	Central-Seep	1837	72 cm	

Most intriguing are high concentrations of dissolved ferrous iron at shallow subsurface depths, likely inducing high benthic Fe-fluxes at the sediment water interface and Fe-sulfide precipitation below. Almost constant values for dissolved silica of about 800 µM are indicative for intense dissolution of diatom frustules accumulating in the sediment. A local maximum of H_2S at about 400 cm indicates the zone of anaerobic oxidation of methane (AOM) and defines the methanogenic zone below. Interestingly, alkalinity values increase below the AOM and reach very high values of about 70 meq L^{-1}. Such high alkalinities are typically reached in areas, where intense sub-seafloor silicate weathering prevails (Wallmann et al., 2008). Expected low levels of chemical weathering under arid conditions on land support this hypothesis as the deposition of immature terrigeneous material is a prerequisite for sub-seafloor weathering (Scholz et al., 2013).

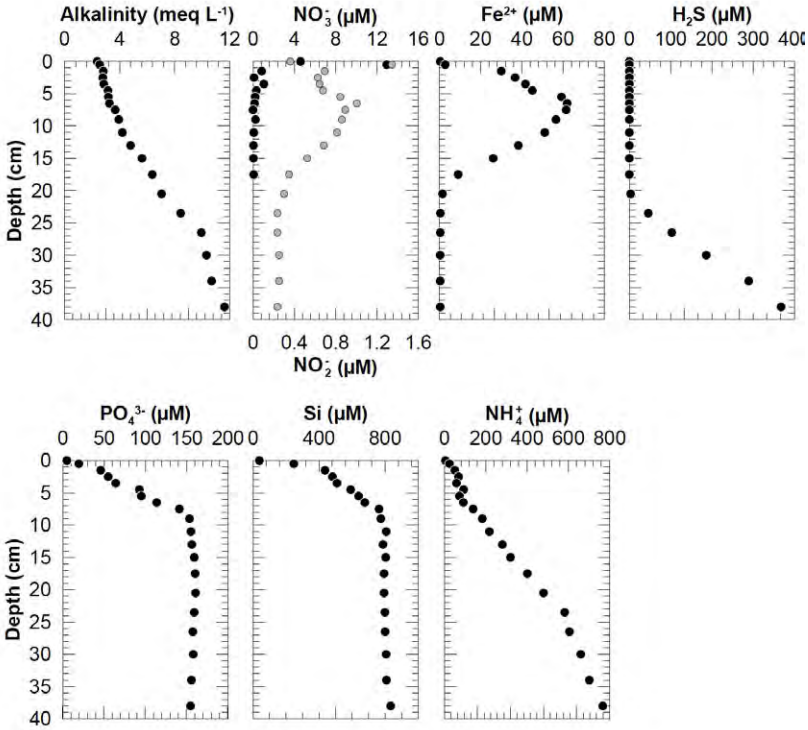

Fig 6.5.2: Pore water profiles of MUC 09, located about 660 m water depth on the continental slope.

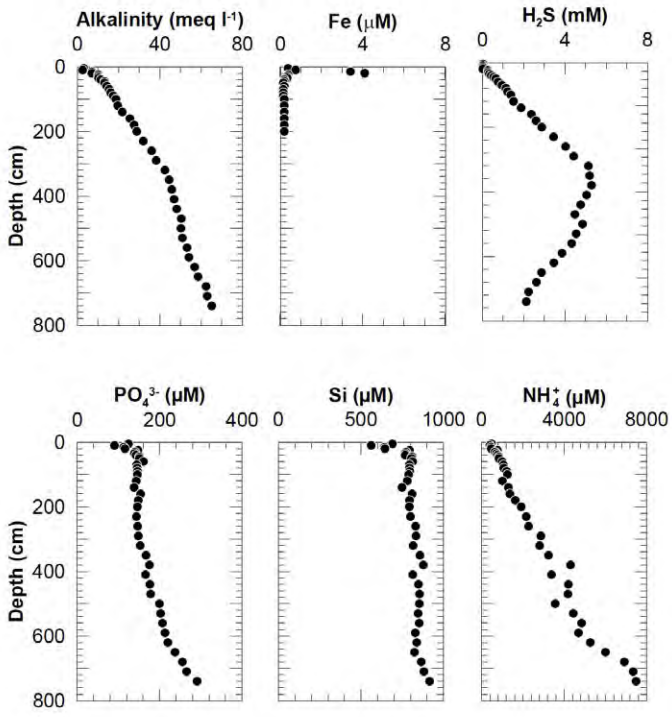

Fig. 6.5.3: Pore water profiles of GC 07, located about 660 m water depth on the continental slope.

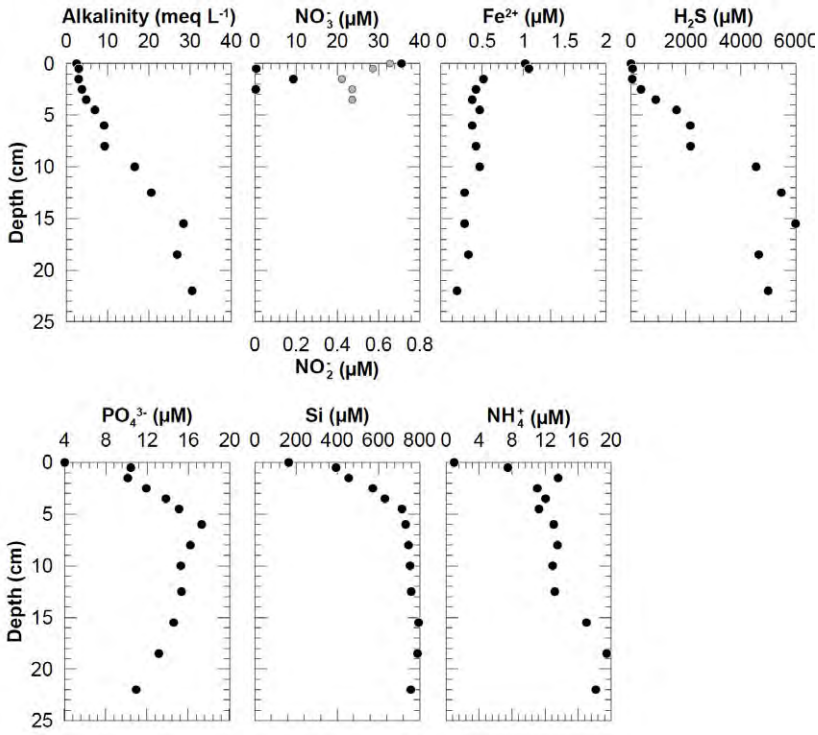

Fig. 6.5.4: Pore water profiles of MUC 11 from the central part of the Northern Seep location.

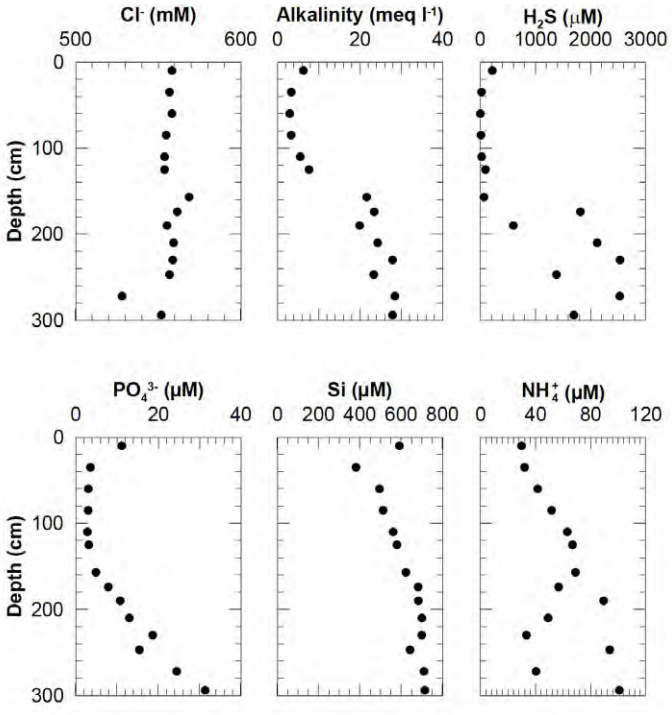

Fig. 6.5.5: Pore water profiles of GC 01 from the central part of the Northern Seep location.

Cold seeps

A number of previously discovered seep locations, named Ring Seep, Northern Seep, and Central Seep were extensively studied. These sites are characterized by prominent blanked zones in the seismic record reaching up to the sediment surface, which have been interpreted as resulting from sediment mobilization above sill intrusions (Lizarralde et al., 2011; Karstens and Berndt, 2015). Advection of methane-enriched fluids could be proven at all sampled seep locations. Video observations showed typical chemosynthetic seep fauna as vesicomid bivalves, tubeworms, and bacterial mats in association with authigenic carbonates. Pore water peaks of alkalinity and H_2S at shallow subsurface depths clearly reflect the location of the AOM (MUC 04, 05,11; GC 01, 15; Figs. 6.5.4, 6.5.5). The much shallower location of the AOM is a function of advection velocities of CH_4-rich fluids. This concept has been validated for various cold seep and mud volcano sites (e.g. Luff & Wallmann, 2003; Hensen et al., 2007; Karaca et al. 2014). Si enrichments in the pore water are at the same level as observed at the slope stations, indicating that dissolution of diatom skeletons is occurring at the same intensity. Other nutrients (PO_4, NH_4) are comparatively depleted indicating that the composition of the advecting fluid is strongly different from that of surface sediments.

Smoker Vents

At the Smoker Vent sites, sediment sampling was only possible at some distance to the active smoker pipes, where sufficient sediment cover exists. In the close vicinity of the smokers sampling attempts failed, because sediments consist mostly of rock pieces of broken smoker pipes. Below, pore water profiles of MUC 12 and GC 09 are shown (Fig. 6.5.5 and 6.5.6). MUC 09 was deployed about 50 m south of the northernmost and most prominent smoker hill. The sediments consist mostly of fine-grained, likely Fe-rich material, which has probably been accumulated from precipitates of cooled and neutralized, low pH smoker fluids. With regard to the pore water composition, the most conspicuous observation is the strong enrichment in dissolved Fe. The most likely reason for the high Fe-level is re-dissolution of Fe-rich minerals in the sediments. Almost constant alkalinity values suggest that advection of CO_2 –rich, acidic fluids helps to maintain high Fe concentrations in pore water. Advection of CO_2-enriched fluids is in line with water column investigations (cf. section 6.7). Evidence from GC coring supports this hypothesis. GC 09 is from the southern tip of the mound structure. On deck, a temperature anomaly of >50 °C was detected at the base of the core and the temperature gradient measured by thermistors attached to the core is about 10 °C m^{-1} (cf. section 6.9). The sediments at the base consist of the same type of black, metal-rich sediments and are overlain by a mixture of hemipelagic sediments and intercalated layers of hydrothermal deposits (cf. section 6.6.2). The sediment transition also marks a pronounced difference in pore water composition. Below, alkalinity returns to nearly bottom water concentrations and PO_4 and NH_4 are relatively enriched, suggesting percolation of a distinct, hot, CO_2-rich fluid. Nevertheless, nutrient concentrations are much lower than compared to hot (>300 °C) smoker fluids sampled during Alvin dives in southern branch of the Guaymas spreading centre (Von Damm et al., 1985). The AOM zone is indicated by a slight increase in alkalinity accompanied by a peak in H_2S. H_2S concentrations are extremely low in this Fe-dominated system.

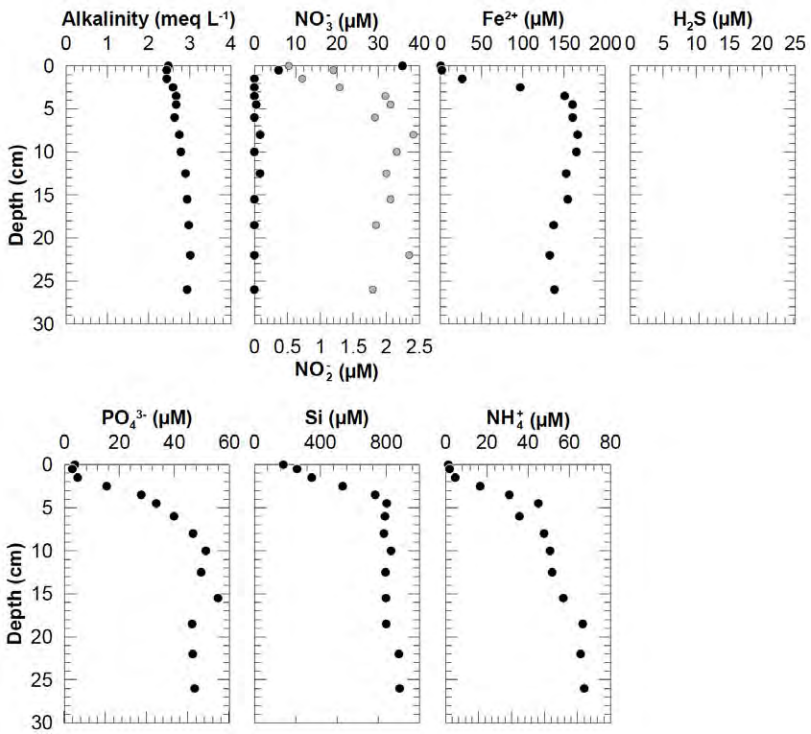

Fig. 6.5.5: Pore water profiles of MUC 12, located about 50 m south of the northern smoker hill.

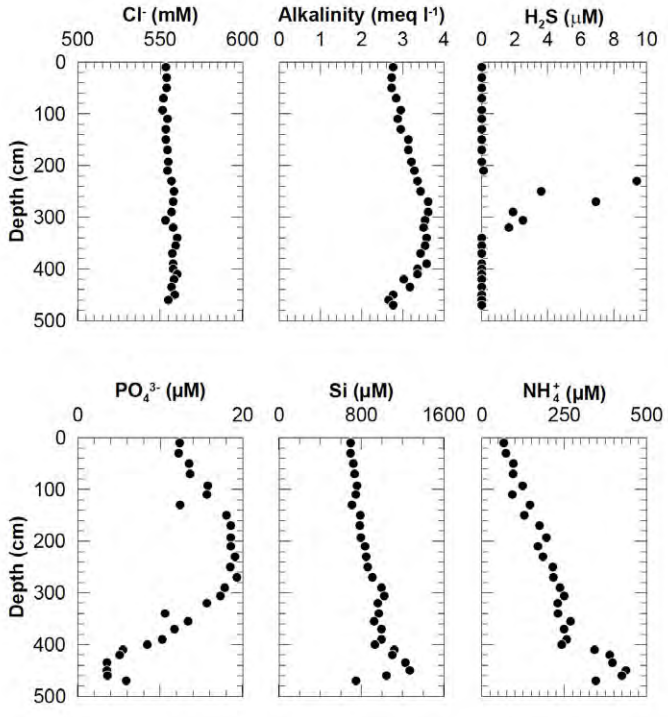

Fig. 6.5.6: Pore water profiles of GC 09, located south of the southern smoker hill.

6.5.3 Geochemical surface exploration

Isotope (geochemical) signatures of hydrocarbons analysed in interstitial waters of the upper sediment structure (DSDP drill cores) have proven the exceptional hot hydrocarbon kitchen in the Guaymas Basin. The concept if isotope geochemistry of adsorbed hydrocarbons in surface sediment also indicate deep subsurface magma intrusions will be tested on sediment and porewater samples which were recovered during a RV SONNE cruise SO241 (rift and transform axes in the Guaymas Basin). The study aims at indicating deep alteration processes mirrored in surface sediments that are related to magma intrusions or the percolation of hydrothermal fluids. The major goal is to develop an isotope geochemical fingerprint of adsorbed hydrocarbons in 0-6 m deep surface sediments, to calculate respective vitrinite maturation based on existing δ^{13}C-equations and to correlate it to other organic and inorganic (isotope) tracers in sediments and pore fluids (e.g. according to Faber et al., 2015). The final challenge is to define the extent of alteration as a function of geological control parameters such as fluid temperatures, fluid advection velocities, deeper sediment strata, tectonic features (rift axis, transform faults) and magmatic intrusions.

10-20 g of wet sediment sampled from selected sediment depths (Tab. 6.5.3), were stored and shipped to the land laboratory at 4°C. The clay-silt fraction of the sediments will be separated from coarse material by wet sieving and adsorbed hydrocarbons will be extracted by an acid-vacuum extraction procedure at GEOMAR (according to Schmitt and Thiessen, 2003). Concentrations of hydrocarbons (C1-C6) will be determined by gas chromatography and δ^{13}C-signatures of methane, ethane, and propane will be analyzeda by cf-GC combustion-isotope ratio mass spectrometry.

Data modelling and interpretation e.g. calculation of maturity of organic source rocks will be performed with empiric δ^{13}C-C2-C3 plots (i.e. according to Faber et al., 2015). The (isotope) geochemical data of adsorbed hydrocarbons will be compared with porewater hydrocarbon signatures and maturity trends, mixtures (biogenic, thermogenic), secondary diagenetic processes will be discussed. All gas-geochemical data will be spatially analyzed by ArcGIS program and compared with data from other disciplines (geophysics, biogeochemistry). The interdisciplinary data evaluation mainly aims to investigate correlations of (isotope) signatures of adsorbed hydrocarbons with magmatic intrusions (heat-effected sediment) in the subsurface.

Table 6.5.3: Sediment samples taken for isotope geochemical analyses of adsorbed hydrocarbons.

Cruise	Station	Device	Device ID	Depth_[cm]
SO241	7	GC	1	27-30
SO241	7	GC	1	88-90
SO241	7	GC	1	168-170
SO241	7	GC	1	281-284
SO241	9	GC	3	33-36
SO241	9	GC	3	99-102
SO241	9	GC	3	141-144
SO241	9	GC	3	236-239
SO241	9	GC	3	336-339
SO241	9	GC	3	406-409
SO241	14	GC	5	23-26
SO241	14	GC	5	118-121
SO241	14	GC	5	235-238
SO241	14	GC	5	247-250
SO241	14	GC	5	275-278

SO241	14	GC	5	344-347
SO241	14	GC	5	444-447
SO241	51	GC	9	75-78
SO241	51	GC	9	157-160
SO241	51	GC	9	216-219
SO241	51	GC	9	345-348
SO241	51	GC	9	424-427
SO241	58	GC	10	30-33
SO241	58	GC	10	80-83
SO241	58	GC	10	182-185
SO241	58	GC	10	281-284
SO241	58	GC	10	376-379
SO241	58	GC	10	476-479
SO241	59	GC	11	325
SO241	59	GC	11	375
SO241	59	GC	11	425
SO241	59	GC	11	475
SO241	62	GC	13	53-56
SO241	62	GC	13	148-151
SO241	62	GC	13	248-251
SO241	62	GC	13	353-356
SO241	62	GC	13	422-425
SO241	62	GC	13	466-469
SO241	72	GC	15	20
SO241	65	MUC		29-32
SO241	40	MUC		15
SO241	40	MUC		30
SO241	40	MUC		32-33
SO241	41	MUC		33-36
SO241	33	MUC		Bottom
SO241	33	MUC		Bottom
SO241	56	TV_GRAB		0-30
SO241	56	TV_GRAB		0-30
SO241	37	Hybis	1	0-20

6.6. Carbonate Geochemistry and VGHG based seafloor sampling

Authigenic carbonates of seep environments in the Guaymas Basin are expected to provide robust stationary geochemical archives for the reconstruction of changes in fluid emanation dynamics and composition in high spatial and temporal resolution as already shown for its northeastern transform margin (Paull et al., 2007) and central American seep sites (Liebetrau et al., 2014). In order to recover suitable sample material from the seafloor, potentially reflecting seep activity of several thousands of years, two sampling techniques were applied on cruise SO241.

1) Precisely targeted deployments of a video guided hydraulic grab system (VGHG) were conducted in accord to prior bathymetric, backscatter and visual seafloor observations, the

latter by video guided multi-corer (TV-MUC). This technique allows especially the recovery of surface exposed successions of potentially focused seepage driven carbonate precipitates in meter scale sizes. In addition this system was successfully applied to sample hard-substrates combined with surface sediments and bacterial mats from the active hydrothermal vent site discovered on this cruise (s. chapter 6.10 for details).

2) Sediment profiles provided by gravity corer (GC) deployments (s. chapter 6.5 pore water geochemistry for details) were co-sampled for authigenic carbonates and remnants of seep related faunal communities in order to support stratigraphical approaches on the reconstruction of seepage systematics.

6.6.1. Video Guided Hydraulic Grab System (VGHG)

This kind of deep sea grab technique (Fig. 6.6.1), made out of approx. 2 t of steel, was originally designed to dig into soft sediments and very successful used for the recovery of Fe-Mn-concretions and gas hydrates from the seafloor. The tool used on SO241 is characterized by a penetration depth of usually 0.5 to 1 m, a sample volume of around 1 m^3 and a deployment depth of up to 6000 m.

Fig. 6.6.1: The GEOMAR video guided hydraulic grab (VGHG).

The integrated online video system allows a detailed search for suitable targets and sampling documentation by a straight vertical seafloor observation through the open jaws of the grab. Due to the fact of a closing pressure of around 5 t of the actual system hosted by GEOMAR, provided by the integrated battery-driven hydraulic system, the jaws could hold and recover samples even larger than the volume of the closed grab. The optimized design of a less vertical extension at a wider foot print and individual jaw closure hydraulics supports sampling on slope positions, even tolerating slight tilt.

The successful deployment on large rock samples or detailed structured seafloor surfaces depends strongly on the coordination of ship positioning, winch control and the timing of jaw closure. A final challenge is getting the recovered sample on deck when its weight is almost doubled by leaving the water column. During SO241 the required team work effort was provided in a very convincing manner from all contributing sides.

In principle, this technique provides well documented, unique large samples for detailed profile studies through the uppermost hard-substrate bearing sediments.

Based on this material ex-situ vertical profiles enable the high resolution sub-sampling and reconstruction of potentially late stage carbonate formation sequences and detailed insights into growth structures and calcification processes within one sample. Therefore, this approach provides an important extension of gravity and multi coring techniques towards undestroyed surface samples from core penetration resistant environments.

Furthermore, the well targeted recovery of big bolder and blocks including the surrounding sediment provides the option to sample habitats in there functional context for combined geobiological studies by retrieving typical seafloor faunal communities at only minor impact on the whole ecosystem, especially when compared to biological and geological dredge techniques.

The sediment surface samples are not as undisturbed as provided by box-coring, but an important additional option for sedimentologists and biologists by being more selective and targeted due to the video control and documentation. Already by the potential sample size and weight the video guided grab provides an important addition and partially an alternative to ROV (remote operating vehicle) and submersible sampling approaches.

6.6.2. VGHG and Carbonate sampling results

As shown by the example in Fig. 6.6.2 the VGHG-system was deployed successfully on cruise SO241. The details of deployments are implemented in the station list (Appendix B) and the recovered samples (see table 6.6.1) are still under investigation for biology, geochemistry, isotope geochemistry and chronology.

Fig. 6.6.2: The VGHG system after successful deployment on RV SONNE (station 17, VGHG-2). The incomplete closure reflects the blocking carbonate load.

During the MAKS cruise SO241 5 VGHG deployments were conducted and resulted in 4 sample sets (tab. 6.6.1) of different size from 3 locations (“ring” (2x), “central” and “smoker”). Additionally the co-sampling of GC and MUC cores (tab. 6.6.2) provided important stratigraphically documented successions of authigenic carbonates and seep fauna remnants.

Table 6.6.1: VGHG based sampling

Station no.	VGHG no.	Site	Lat. "N"	Long. "W"	Depth	Remarks / Storage
3	1	“ring”	27° 30,538'	111° 40,900'	1721	mainly sediment of a dead clam field with minor amounts of authigenic carbonates as coating, cement between shell fragments and concretions within the sediment / cumulative blue box, 3 bags, 18 sub-samples
17	2	“ring”	27° 30,280'	111° 40,746'	1752	porous carbonate blocks from steep SE slope of ring structure / 2 large pieces on 1 palette & 1 blue box with fragments
63	3	“central”	27° 28,183'	111° 28,388'	1836	failed
56	4	“central”	27° 28,181'	111° 28,379'	1843	porous carbonate extracted from high tube worm abundance area / succession of three block fragments, largest on palette others in blue box, 1 bag of fragile shell fragments in cumulative blue box
69	5	“smoker”	27° 24,749'	111° 23,224'	1830	hard-substrate out of black smoker precipitate material with bacterial mat coverage and adjacent sediment from active hydrothermal vent site / 1 pack of broken block in HyBis sample blue box on VGHG-4 palette

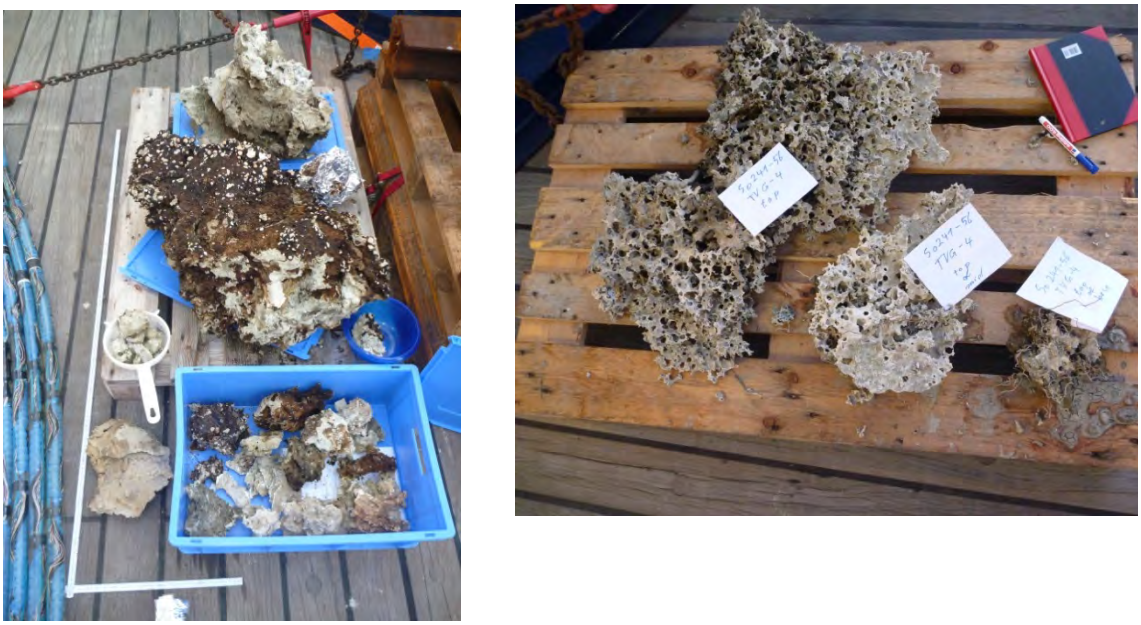

Fig: 6.6.3: Authigenic carbonates recovered at the “ring” (SO241-17, VGHG-2, left) and the “central” seep site (SO241-56, VGHG-4, right) of the Guaymas Basin. Originally the three blocks (VGHG-4) formed one which is broken apart on board during cleaning from sediment (succession from left to right follows from top to bottom).

Fig. 6.6.4 Block recovered from hydrothermal vent site (So241-69, VGHG-69) showing whitish remnants of microbial mats, which were mainly washed away during transfer through the water column. Small parts of the originally fluffy mat cover could be saved and frozen for further biochemical investigation and identification. On the right the internal layering of hydrothermal precipitates became visible after cracking the whole block into two parts.

Table 6.6.2: Co-sampling for authigenic carbonates on GC and MUC station (s. chapter 6.5 pore water geochemistry for deployment details).

Station no.	Tool & Deployment no.	Site	Remarks / storage
7	GC-1	"north"	stratigraphic sampling 1 -6 / 1 bag in cumulative box
9	GC-3	"central"	stratigraphic sampling 1 -7 / 1 bag in cumulative box
62	GC-13	"central"	stratigraphic sampling 1 -9 / 1 bag in cumulative box
72	GC-15	"central"	stratigraphic sampling 1 -4 / 1 bag in cumulative box
22	MUC-4	"central"	1 piece, 1 bag, MUC-bag, cumulative box
23	MUC-5	"ring"	x pieces in stratigraphic order from Radon sampling core & 1 piece from base of pore water core / 1 bag, MUC-bag, cumulative box
33	MUC-11	"north"	1 piece from base of pore water core / 1 bag, MUC-bag, cumulative box
40	MUC-12	"smoker"	1 piece / 1 bag, MUC-bag, cumulative box

6.6.3 Radon (^{222}Rn) measurements extending the water column and pore water chemistry program

On board SO241 ^{222}Rn water column (CTD) and multi-corer (MUC) based pore water profiles were performed in order to study gas transport through marine sediments of different marine settings into the water column. The goal of the study is the determination of advection and diffusion rates in cold seep, non-seep and hydrothermal vent site settings.

^{222}Rn is a member of the ^{238}U decay chain and directly produced by the decay of ^{226}Ra in the marine sediments. Because ^{238}U is enriched in sediments its production is depth dependent and increases as a function of the sedimentary height below the water column. ^{222}Rn is an excellent tracer in order to determine diffusion and advection rates because as a radioactive rare gas it is chemically inert and decays away with a half-life of about 3.5 days (l=0.0001374 1/min). Thus the time dependent transport of ^{222}Rn can be observed as a function of time and sediment depth directly on board of a ship while performing liquid-scintillation-alpha counting (Purkl and Eisenhauer, 2004). The results from ^{222}Rn depth profile measurements can then be compared and applied to other gases of interest (e.g. CH_4, He) supplied from the sediments and advecting fluids to the water column. An important aspect for the interpretation is the determination of the amount of excess ^{222}Rn at time of sampling by re-measuring the extracted samples after several weeks again. This defines the amount of the parent isotope ^{226}Ra, a typically reactive divalent cation.

6.6.4 Radon (^{222}Rn) method

For ^{222}Rn measurements sea water (SW) column samples are typically retrieved from CTD deployments (s. chapter 6.7. water column chemistry for details) and sediments for pore water (PW) profiles from TV-MUC cores (see chapter 6.5 pore water geochemistry for details). An additional and important option to fill the sampling gap at the sediment / water column interface is the bottom water (BW) enclosed in the MUC tubes above the sediment. SW samples typically vary between 1 and of 1.5 l samples and the Rn is extracted directly by adding 20 ml of an organic scintillation cocktail which is after robust shaking extracted and measured. The applied method follows in generally Purkl and Eisenhauer (2004). Usually these low concentration measurements require 6 hrs. of counting time in a liquid scintillation counter. For pore water measurements typically 40 ml of raw sediment is extracted close to the top, at the middle and close to the bottom of a MUC core, often covering a coarse profile length between 25 and 50 cm. The scintillation cocktail is usually directly added on top of the wet sediment to avoid any Rn loss during the later phase separation by centrifuging. PW and scintillator are extracted from the sediment, vigorously shaked to transfer the Rn from the PW into the scintillation cocktail, and later on separated from each other. Alternatively pre-extracted pore water could be layered underneath 10 ml of scintillation cocktail directly in a measurement vial to extract the radon and measure it several times to observe the decay of excess ^{222}Rn directly.

6.6.5 Preliminary Radon (^{222}Rn) results

The most striking success of the Radon approach was the measurement of 12 dpm/l in a water sample taken above an active hydrothermal vent. This value is more than 20 times higher as the typical SW value in the Guaymas Basin. If this is due to a large amount of excess ^{222}Rn or rather a consequence of a fluid enrichment in dissolved ^{226}Ra will be answered after returning the samples to Kiel. However, this result seems to be no artifact because other samples only some meters more distal from the vent showed the same trend. This SW result is therefore significant and a comparison with other dissolved gases like methane (CH_4) and Helium (He) and with the general water chemistry (divalent cation concentration and isotope signature, e.g. ^{87}Sr/^{86}Sr) is of highest priority to extrapolate and identify the fluid source.

Another important observation is the elevation of Rn concentrations in the water column above the so-called “ring seep” site. Possibly this cold seep system evolved above and drains a former hydrothermal vent. Interestingly the Rn pore water profiles of both sites, “ring” and “smoker” show strong similarities and the highest values of 0.65 and 0.95 dpm/g, respectively, when compared to all other PW analyses on this cruise (from 0.05 to 0.35 dpm/g).

All these results are preliminary and await further data reduction procedures like decay correction and extraction yield normalization. Nevertheless, the actual numbers are rather underestimating and provide already a base for comparison of the different settings.

6.7. Water chemistry

Main objective of water column investigations conducted during SO241 cruise is to localize cold and hot fluids venting from the seafloor in the working area. The fluid and gas release at pre-selected sites (by means of seismic reflection-, sidescan, and multibeam data) will be quantified (carbon release), and gas and fluid origin will be determined by (isotope) geochemical methods. The aim is to determine the variation of crustal, mantle and sedimentary input to the venting fluids and to characterize secondary diagenetic processes. The distribution of venting fluids in the water column and characterization of water mass transport will help to validate the proposed concept if high subsea carbon release at transform-type ridge segments (like in the Guaymas Basin) could play a major role in releasing greenhouse gases to the atmosphere at relatively short time scales.

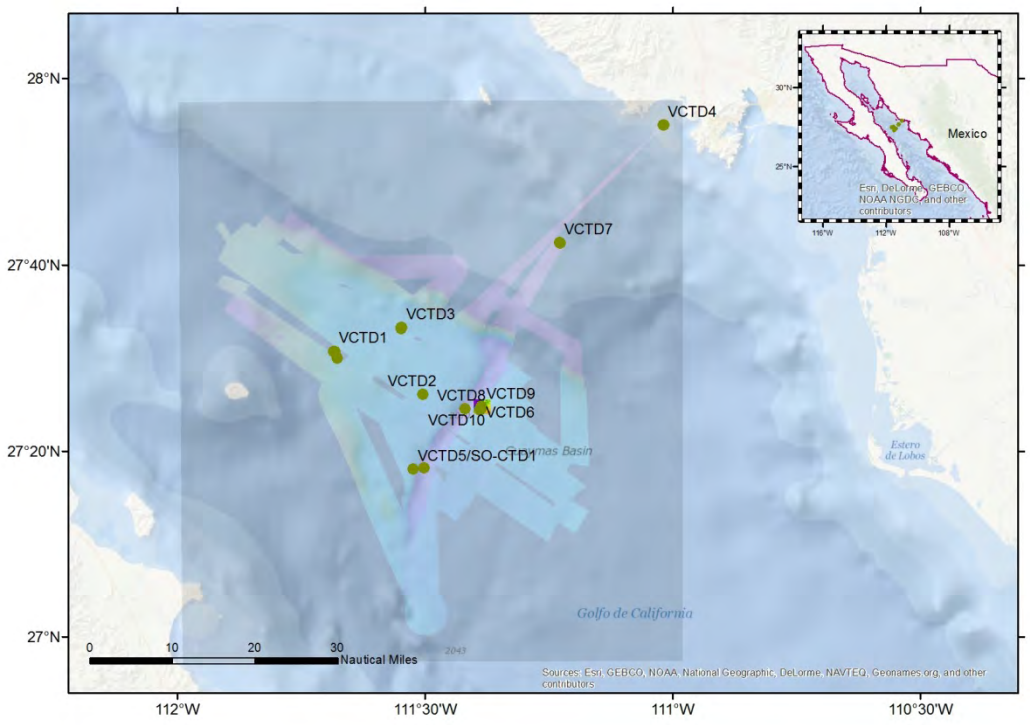

Fig. 6.7: Overview map of SO241 sampling area. Water sampling hydrocasts and towed Video-CTDs (VCTD) are marked by green dots.

6.7.1 Methods

Video-CTD Water Sampler

A newly designed video guided Water Sampler Rosette System (**VCTD**; Fig. 6.7.1) was used to study water column chemistry and oceanographic parameters in the working area. The system was operated instead of the ship-owned CTD-Water Sampler, and was attached to a ship's coaxial cable (cable length ~8500 m, cable diameter = 11 mm). The sampling device was used in a towed mode (vessel speed ~ 0.3-0.5 kns) and in station keeping hydro-cast mode. Water depths were controlled by pressure readings, by altitude sensor (<50m distance to bottom), or by online video observations near the seafloor (1-2 m above seafloor).

The digital video system and modem technology (Sea and Sun Technology) used during the first four CTD stations is described in details elsewhere (Linke et al., 2015). Highest data transfer rates of 184 kbps (downstream) and 713 kbps (upstream), respectively, could be reached by using the combination with the ship's 8500 m coaxial cable. However, due to weak stability of data transfer rates it was decided to use the VCTD system attached to the mobile GEOMAR winch (MW25, 4500m coaxial/fiber optics cable). Unfortunately this attempt failed due to the strong interference of the winch motor with the data transfer process. Thus all subsequent CTD stations were powered and recorded by using the ship's SBE11 deck unit (without using online video data storage or transfer).

SBE9plus CTD

The SBE 9plus underwater unit was equipped with 2 pressure sensors, 2 temperature sensors, 2 oxygen sensors and 2 conductivity sensors. CTD data monitoring and recording was performed with SEASAVE software (Version 4.21). CTD data were recorded with 24 Hz.

Fig. 6.7.1: Water sampler (11x10 L Niskin bottles) rosette, including Seabird SBE9plus CTD, SBE O2 sensors, Wetlab fluorescence and turbidity sensor, altimeter, Kongsberg-CONTROS HydroC™-CO2 and HydroCplus-CH4 sensors.

Sip's GPS position data (NMEA string) was logged parallel to the CTD and Video data. Five analogue channels at the SBE underwater unit were used for external sensors (Altimeter, HydroC-CO2-, HydroCplus-CH4-, and Wetlab Fluorescence/turbidity sensor). Analogue sensor readings monitored online were used as indicators for sampling decisions. Hydro-casts and hydrographic data from towed CTDs were processed by using SBE software SBE7.23.1. Usually data files of 5 minute bins and bottle files were created from raw data files and exported to ASCII. CTD data is combined with HydroC-sensor measurements. All data sets are correlated with their NMEA (UTC) time stamps.

HydroC™-CO2 sensor

The HydroC-CO2 (CO2-0412-005) sensor, equipped with pumped (Seabird SBE5T) sensor head, was integrated into the video-CTD device to monitor hydrothermal CO2 seepage (Fig. 6.7.2). Technical specifications of the sensor are given in table A. The measured data is stored internally on SD card, however, the sensors reading is also monitored onboard by using one analogue 0-5V channel of the SBE9plus.The HydroCTM-

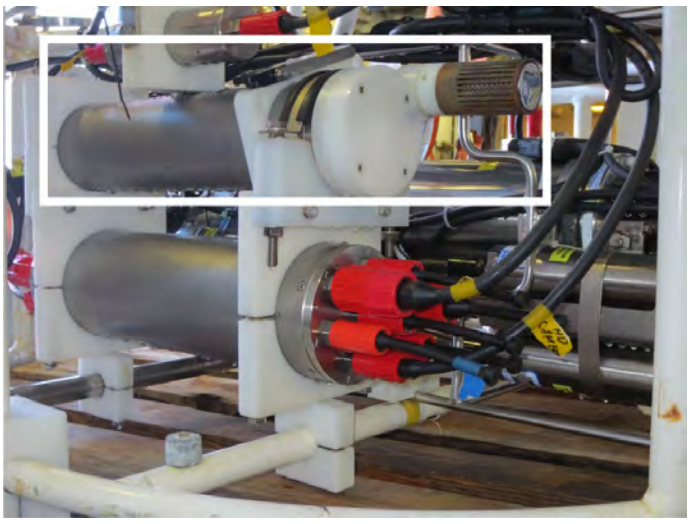

HydroC-CO2 sensor specifications:

- Measuring range 0-6000 µatm
- Resolution 1 µatm
- Operational depth 4000 m

Figure 6.7.2 HydroC-CO2 sensor (marked by white rectangle mounted in the Video CTD.

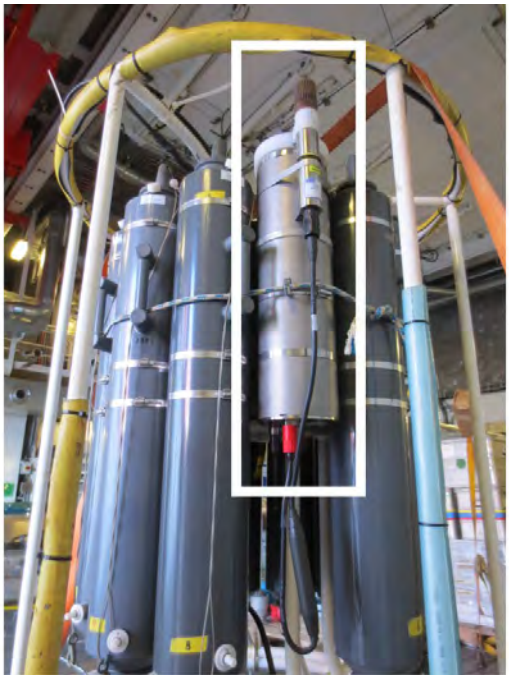

HydroCplus-CH4 sensor specifications:

Measuring range	0-40000 µatm
Resolution	0.01 µatm
Detection limit	<1 µatm
Operational depth	3000 m

Fig. 6.7.3: HydroCplus-CH4 sensor (marked by white rectangle) is mounted to the Video CTD Rosette frame instead of Niskin bottle 7.

CO2 is powered by an external NiMH-power unit (16V, >10h at ~16°C). Further details of the system are given in Schmidt et al., 2015.

HydroCplus-CH4 sensor

The HydroCplus-CH4 (CH4P-0115-001) sensor, equipped with pumped (Seabird) sensor head, integrated into the Niskin-CTD Rosette by replacing one Niskin bottle by the HydroCplus-sensor (Fig. 6.7.3). Technical specifications of the sensor are given below. The measured data is stored internally on SD card, however, the sensors reading is also monitored onboard by using one analogue 0-5V channel of the SBE9plus. The HydroCplus-CH4 is powered by an external battery pack (32V, >10h at ~16°C). Further details of the system are given in Schmidt et al., 2013.

ADCP measurements

The ship-based downward looking 38 kHz ADCP (RDI; ~1600 m long range) and a LANDER-mounted upward looking 300 kHz ADCP (RDI; 100 m range; Fig. 6.7.4) were used to monitor current velocities and current directions in the water column of the sampling area. WinADCP software was used for onboard evaluation of ADCP data derived from LANDER based measurements. Additional pressure and temperature data was recorded by an autonomous TP-logger (RBR) which was also attached to the LANDER.

6.7.2 Initial results

10 VCTD stations have been conducted in total during SO241 cruise. Three hydro-casts have been performed for seawater sampling in areas “Shelf”, “Slope”, and “Graben” (Tab. 6.7.1). An additional hydro-cast was conducted without water sampling in area “Graben” for sound velocity determination (Stat. 45). Six towed VCTDs were used to monitor and sample fluid/gas release from active cold and hot seep sites in areas “Ring”, Central”, North”, and “Smoker” (Tab. 6.7.7). A few CTD and sensor data examples are described below.

Fig. 6.7.4: ADCP LANDER deployment from starboard side of RV SONNE (free falling deployment).

Table 6.7.1: Video-CTD (VCTD) stations performed during SO241 cruise.

Station	date	time (UTC)	Area	Gear ID	Latitude	Longitude	Action	Comment
SO241/1	25.06.2015	12:15	Ring	VCTD1	27° 30,781' N	111° 41,062' W	station start	11 Nibo during upcast; ***1,3, 4, 5, 6***
		13:28			27° 30,728' N	111° 40,932' W	bottom view	
		13:30			27° 30,716' N	111° 40,915' W	profile start	
		15:15			27° 30,063' N	111° 40,658' W	profile end	
		15:52			27° 30,069' N	111° 40,654' W	station end	
SO241/12	30.06.2015	0:48	Central	VCTD2	27° 26,160' N	111° 30,263' W	station start	11 Nibo during upcast; ***1,3, 4, 6***
		2:08			27° 26,133' N	111° 30,268' W	Bottom view	
		3:19			27° 26,149' N	111° 30,271' W	station end	
SO241/13	30.06.2015	4:23	North	VCTD3	27° 33,344' N	111° 32,871' W	station start	Bottom contact during down cast; 11 Nibo during towed CTD; ***1***
		6:10			27° 33,328' N	111° 32,874' W	bottom view	
		6:24			27° 33,348' N	111° 32,885' W	profile start	
		11:01			27° 33,281' N	111° 32,874' W	station end	
SO241/25	03.07.2015	13:21	Shelf	VCTD4	27° 55,012' N	111° 1,157' W	station start	11 Nibo during upcast; ***1, 3, 4, 5***
		14:09			27° 55,021' N	111° 01,108' W	bottom view	
		14:22			27° 55,013' N	111° 1,126' W	station end	
SO241/31	04.07.2015	7:12	Graben	VCTD5/SO-CTD1	27° 18,121' N	111° 31,463' W	station start	24 Nibo during upcast; ***1, 4, 5, 7***
		11:25			27° 18,233' N	111° 30,144' W	Bottom view	
		12:32			27° 18,233' N	111° 30,148' W	station end	
SO241/39	06.07.2015	8:52	Smoker	VCTD6	27° 24,763' N	111° 23,232' W	station start	11 Nibo during towed CTD; ***1,3, 4, 5, 6, 7***
		10:28			27° 24,768' N	111° 23,229' W	bottom view	
		12:14			27° 24,544' N	111° 23,339' W	station end	
SO241/42	06.07.2015	20:36	Slope	VCTD7	27° 42,438' N	111° 13,733' W	station start	11 Nibo during upcast; ***1, 2, 3, 4***
		21:01			27° 42,411' N	111° 13,663' W	bottom view	
		21:30			27° 42,409' N	111° 13,655' W	station end	
SO241/45	07.07.2015	14:15	Graben	VCTD8	27° 24,577' N	111° 25,184' W	station start	no sampling; SV profile

		15:15			27° 24,580' N	111° 25,164' W	bottom view	
		16:25			27° 24,578' N	111° 25,166' W	station end	
SO241/52	09.07.2015	7:11	Smoker	VCTD9	27° 24,753' N	111° 23,165' W	station start	11 Nibo during towed CTD; ***1, 2, 3, 4, 5, 7***
		8:30			27° 24,750' N	111° 23,240' W	bottom view	
		11:16			27° 24,731' N	111° 23,234' W	station end	
SO241/67	14.07.2015	19:30	Smoker	VCTD10	27° 24,842' N	111° 23,181' W	station start	11 Nibo during towed CTD; ***1, 4, 5***
		23:49			27° 24,439' N	111° 23,381' W	station end	

1 marked stations have been sampled for trace gas measurements (methane-propane, δ^{13}C-methane-propane)

2 marked stations have been sampled for DIC, δ^{13}C-DIC measurements

3 marked stations have been sampled for nutrient and inorganic element determinations

4 marked stations have been measured/sampled for Radon/Radium determinations

5 marked stations have been measured by onboard Membrane Inlet Mass Spectrometry

6 marked stations have been measured with Winckler O2-titration

7 marked stations have been sampled for 3He/4He ratio determinations

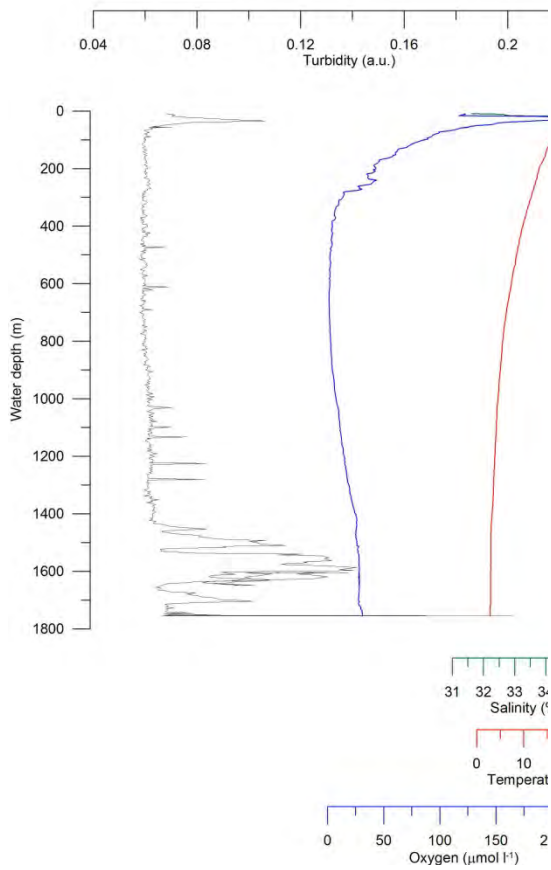

Fig. 6.7.5: Hydrocast VCTD10 showing temperature, salinity, oxygen and turbidity data above "Smoker" area.

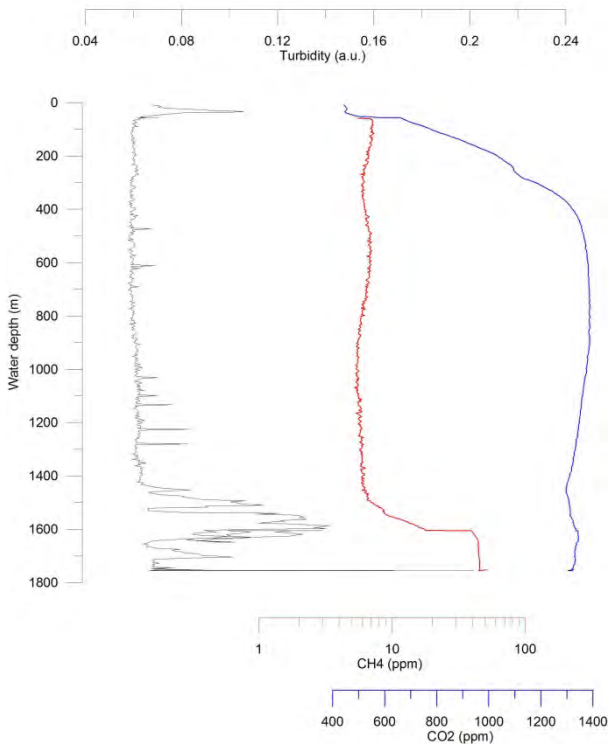

Fig. 6.7.6: Hydrocast VCTD10 showing turbidity, CO2, and methane data (VCTD10).

Water column chemistry

General characteristics of the water column

Warm surface water of about 29.5°C (35.1 ‰ salinity) is mixed down to about 20°C within the upper 50 m in the central working area. The oxygen concentration (225 µmol/l) peaks between 20-40 m below sea level (mbsl). Below this depth progressing oxygen depletion is ending with a thick oxygen minimum zone (1.5 – 3 µmol/l) between 450 and 800 mbsl (Fig. 6.7.5). Oxygen depletion is accompanied by pCO2 increase from about 405 ppm to about 1380 ppm (Fig. 6.7.6).

A well-mixed deep water layer (~1400-1800) is indicated by homogeneous temperature (3.0-2.9°C), salinity (34.54-34.60), and high backscatter (turbidity) values (Fig. 6.7.5).

The methane background (~6 ppm) is generally low down to 1400 mbsl, whereas the mixed deep water layer shows enrichment of ~50 ppm CH_4 (Fig. 6.7.6).

Hydrothermal vent area

The water column of the hydrothermal active (black) smoker area explored during SO241 cruise was investigated in detail with towed CTD-tracks. First indications of hydrothermal venting were monitored by strong increase in turbidity and methane in the hydrothermal plume when approaching the smoker area. High temperature anomalies and high CO2 concentrations could be measured 5-10 m above the venting smokers (Fig. 6.7.7).

First rough estimates based on temperature mixing calculations indicated an end member fluid mixing factor of about 1:15 with seawater. Measured methane concentrations exceeded background concentrations by a factor of more than 10.000.

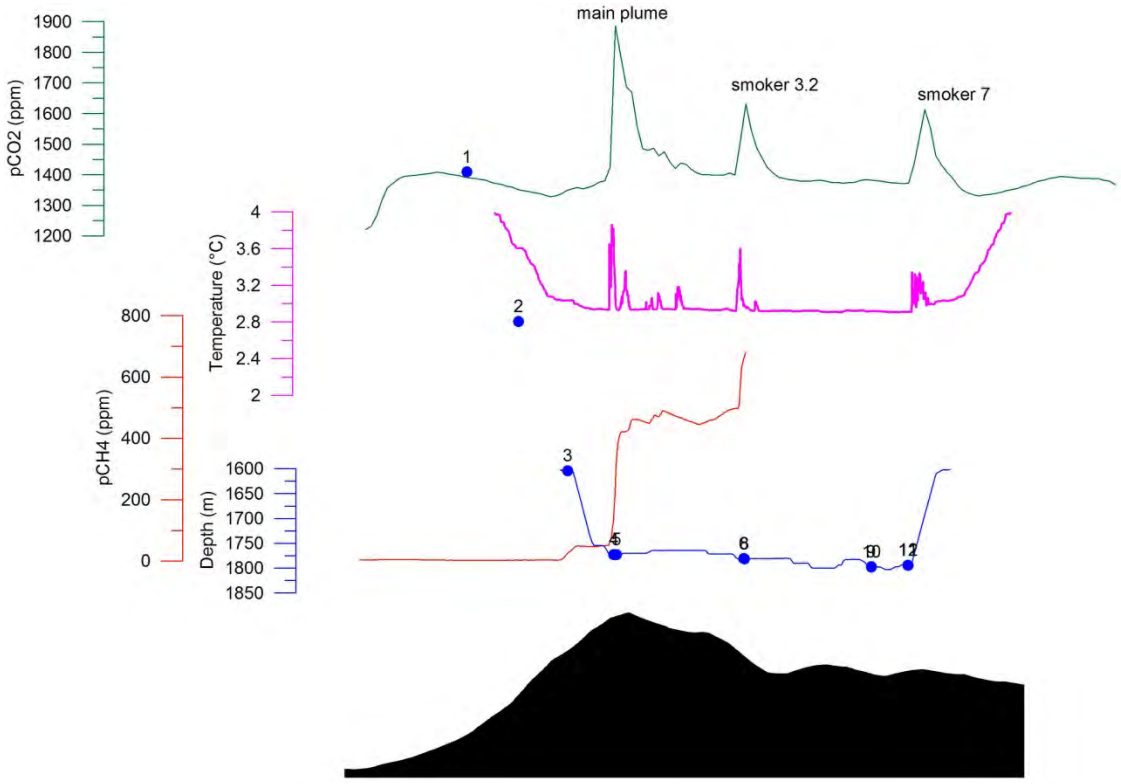

Fig. 6.7.7: Temperature, CO2, CH4 anomalies above the smoker area (Towed VCTD6, Tab. X). Black hill side shape corresponds to bathymetric heights at the site. Blue (labeled) dots mark the Niskin bottles sampling time and depth

Deep currents at "Smoker" site

The ADCP LANDER deployment started in free fall-mode on July 11th (7:25 pm UTC) in area "Smoker". The LANDER was placed about 500 m southeast of the smoker chain at a water depth of about 1850 m. Current velocity and direction was determined with ping rate of 1/300s up to 100m into the overlying water mass. LANDER recovery took place at July 15th at 1am.

Preliminary data evaluation of the upward looking ADCP indicates a weak deep water current regime (1750-1850 m, velocities ~0.05 – 0.15 ms-1). The current direction is tidally driven and is changing from NNW to SSE with maximum pressure differences of about 1 dbar measured at the seafloor.

Continuous monitoring of the water column with 38 kHz ADCP was conducted between June 26th and July 15th with a ping rate of 1/180s. Navigation data (i.e. pitch and roll, ship's heading) still has to be considered for precise current determination. Therefore a high resolution (ping rate 1/1s) ADCP transect was conducted for 12 hours starting on July the 20th and 1pm. Data evaluation and post-processing will be conducted after the cruise.

6.8 Isotope noble gas geochemistry

Currently available techniques to determine (noble) gases in terrestrial fluids, e.g. water, brines, oil, gases, etc., are laboratory-based, expensive and allow only a very limited number of samples to be analysed. Such methods are often not adequate to resolve the gas dynamics on the relevant scales in space and time as only a few samples can be processed and results are not available in real-time. These facts prevent the powerful concepts of

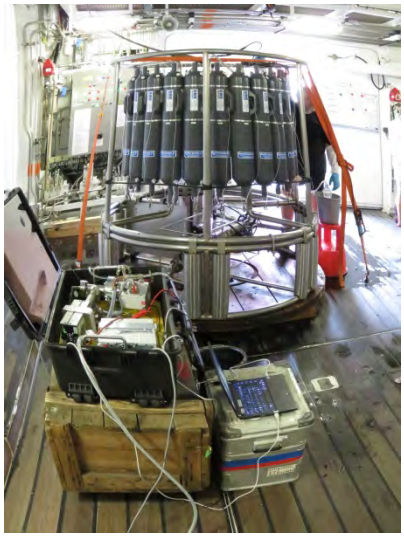

Fig.6.8.1: Left panel. Portable GE-MIMS (black case (< 100l), 40kg, < 40 W) connected to a Niskin-bottle of a CTD probe.

Right panel. Squeezing bulk sediments into copper-tubes for subsequent noble gas analysis in the pore water.

terrestrial noble gas geochemistry to be applied more wildly in environmental science, (tracer) hydrology and oceanography.

6.8.1 Method and experiment setup

To overcome these technical limitations we recently developed a membrane inlet mass spectrometric system operating at gas / water equilibrium (GE-MIMS) which enables the concentrations of dissolved He, Ar, (Kr,) N_2, O_2, CH_4 and CO_2 to be measured quasi-continuously in natural waters under field conditions on site (Mächler et al., 2012 and 2014; Kipfer and Ruedi Ruessel et al., 2015).

This method was originally developed to analyse air / water partitioning in porous media and to study aeration of groundwater. We adopted such GE-MIMS for the dissolved gas analysis in water taken by common Niskin-bottles of CTD-probes. The water flux from the Niskin-bottles trough the membrane contactors was reduced to less than 1l/min. Under these conditions dissolved gas concentrations can be determined within about 15 minutes from a single 10-l Niskin-bottle as soon as the CTD probe is retrieved and back on the ship. As the membrane contactor reverses atmospheric air / water partitioning (at the ocean air interface) the system can easily and simply be calibrated with ambient (free) air.

Such a tailored system (Fig. 6.7.2) was installed and successfully operated - to our knowledge for the first time ever in oceanography - on the MAKS expedition on the RV SONNE. During the cruise more 110 gas analyses were carried out and the dissolved gas concentrations in ~ 30 water samples retrieved by CTD-Niskin-bottles were determined.

6.8.2 Initial results

Helium concentrations in the bottom water of areas showing signs of active fluid emission ('hot vents' / 'black smokers') or passive (fluid) seeping ('cold seeps') exceed the atmospheric equilibrium concentration calculated for the given temperature and salinity of the surrounding water. In contrast shallow and coastal waters have He concentrations very close the atmospheric equilibrium. In the proximity of sites of on-going fluid emission elevated He concentration spread out up to 200 - 300m vertically into the water column producing a bottom water layer being enriched in He. Remarkably this diffuse He-enriched bottom water is present at 'hot vents' as well as at 'cold seeps' indicating the He is not only released at active vent sites, but is also (diffusively) emanating at cold seep sites.

Near the black smokers He is strongly enriched (20x) whereby the largest concentrations are observed in samples showing the highest temperature and lowest light transmission. In 'vent' samples enriched He and CO_2 concentrations are positively correlated. In the most enriched samples even CH_4 concentrations correlate with He concentrations. This pattern

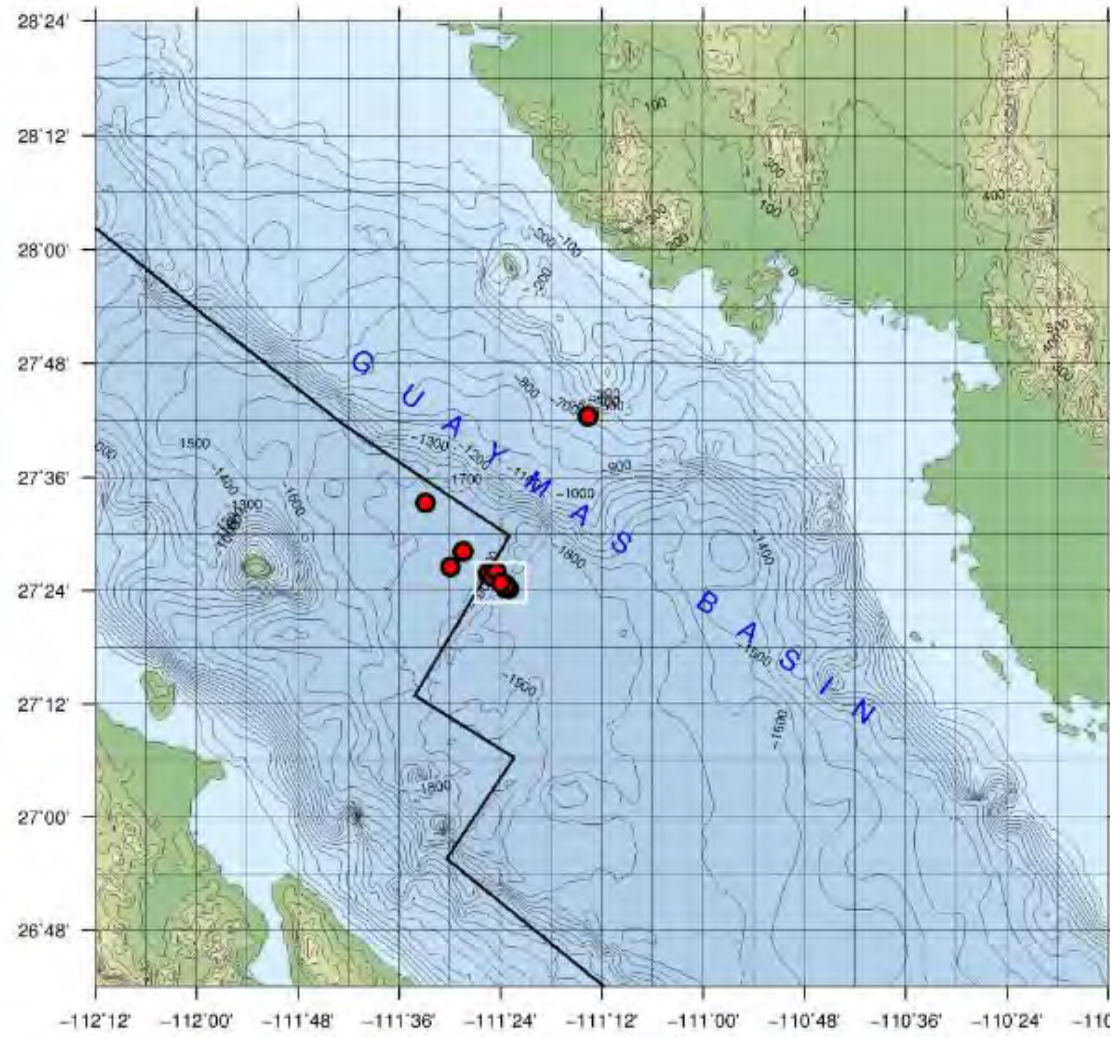

Fig. 6.9.1: Overview of the Guaymas Basin and the locations of measured temperature gradient sites.

makes the case that the fluids emitted by the smokers contain gases (He, CO_2) from deep (magmatic) source being associated with the depleted oceanic mantel. High CH_4 concentrations found in water samples from the open water column not being affected by fluid emission occur in concert with low CO_2 and air-equilibrated He concentrations.

He, CO_2 and CH_4 concentrations in the open water of northern Guaymas Basin can tentatively be understood in terms of mixing of three components: air-equilibrated ocean water, a 'sedimentary' component in coastal waters being enriched in (biogenic) CH_4 and by a 'mantle' component present at the vent and seep sites being enriched in He, CO_2 and CH_4.

Noble gas analysis (He, Ne, Ar, Kr, Xe concentrations, $^3He/^4He$, $^{36}Ar/^{40}Ar$, etc.) of water sampled in conventional copper tubes and in the pore water of sediments will complete the noble gas survey in the Guaymas Basin. In August 2015 Sonja Geilert will present preliminary results of this noble gas survey at the Goldschmidt conference in Prague, CZ.

6.9 Heat flow measurements

The determination of geothermal heat flow is a valuable tool to characterize the pattern of thermal energy distribution. For heat flow density determination, information about the undisturbed temperature gradient is essential as well as the thermal conductivity of the respective material. Heat flow data published in the global heat flow database show some very high heat flow values in this area. Some heat flow measurements exist for the Guaymas Basin, mainly collected by Fisher and Becker (1991). During SO241 22 successful temperature measurements in the seabed were carried out, which will be helpful to better characterize the thermal structure of the Guaymas Basin (see Fig. 6.9.1).

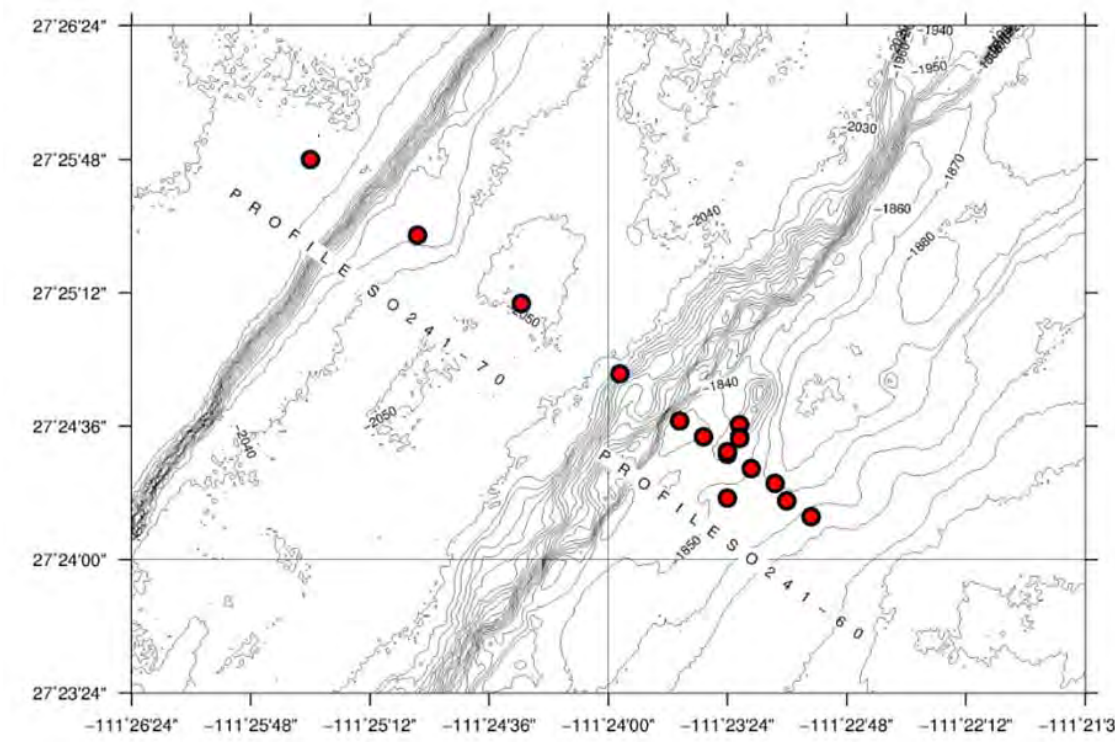

Fig. 6.9.2: Map shows the LIRmeter heat flow transects crosscuts the rift axis. The used bathymetry was created on SO241.

6.9.1 Method and experiment setup

The temperature gradient was measured using a temperature gradient lance (LIRmeter, see Fig. 6.9.2) onto which miniaturized temperature data logger (MTL) were mounted. The temperature range of the loggers is -4°C up to 55°C. Two loggers were tuned to measures temperatures up to 125°C, which was very helpful to get some detailed temperature information in places with strongly elevated heat flow. The loggers have a resolution of approximately 0.001 K and an accuracy of approximately 0.1 K. They were deployed with CTD Profile SO241-1 and CTD Profile SO241-45 during this cruise for calibration.

For thermal conductivity measurements, the DECAGON DEVICES thermal properties meter KD2 Pro is employed with the 6 cm single Needle. The instrument is rated at 5% accuracy in conductivity. Additionally, the MTLs were attached on a gravity corer. Thermal conductivity k was measured on core material, sampled at or close to the depth of the measured temperature positions using the KD2 Pro Needle Probe Instrument.

For temperature measurements, five to six MTLs were mounted onto the 5m long gravity core and the temperature lance. An additional logger for bottom water analyzes and references were attached at the top of the gravity core. All loggers were used for monitoring variations in temperature in time and space. The relative depth positions on the instrument varied between 0.8 m (temperature lance transects) up to 1.50 m (SO241-46 and SO241-47) spacing. For gravity core Sites the spacing between the sensors was mostly 0.9 m.

Two LIRmeter transects were carried out within a distance of 6 km across the rift axis and the venting ridges (see Fig.6.9.2). The transit was run in pogo style with the instrument approximately 200 m above ground. Visual inspections of the vent ridges by HyBis and TV Multicorer (TV-MUC) showed steep flanks and sparsely sedimented rocky areas, which were avoided in order not to damage the gravity core or temperature lance.

Two MTLs were also mounted onto a liner of the TV-MUC to measure the temperature in a sediment depth of approximately 10 and 40 cm. The results give information about the temperature gradients in the uppermost sediment layers. Data reduction and processing of measured time series was done using WinTemp and Matlab. Thermal conductivity could be measured on 6 gravity core sites resulting in good and representative estimates. If there

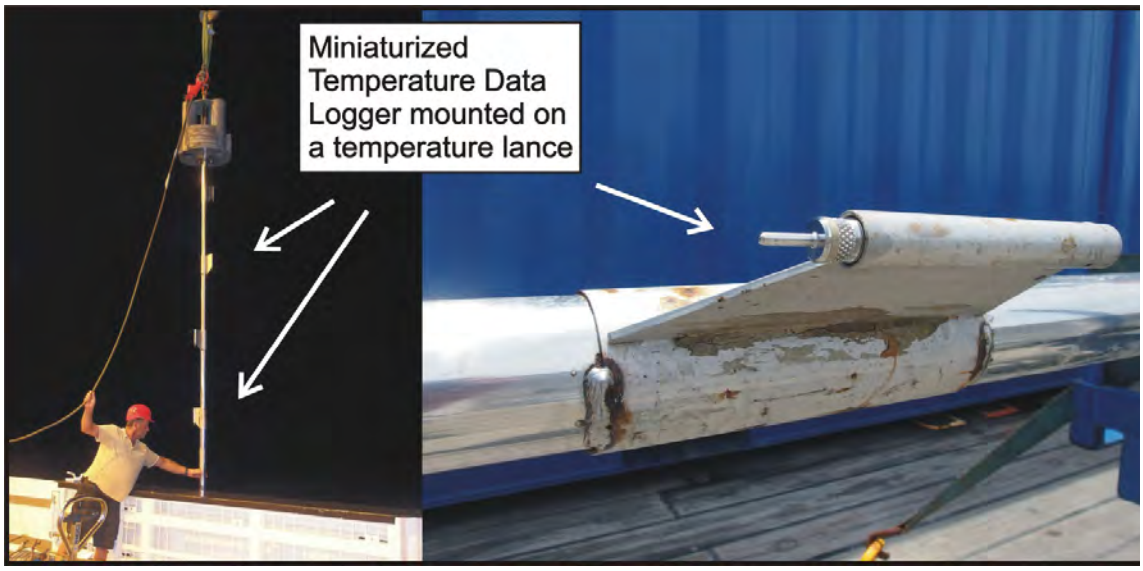

Fig. 6.9.3 Left: The 5 m temperature lance immediately after recovery with five mounted MTLs. Right: MTL in clamp mounted on the temperature lance.

were no thermal conductivity measurements on core samples available, the determined heat flow was carried out with a constant thermal conductivity of 1.

6.9.2 Initial results

A number of 27 heat flow sites were attempted on 13 different stations. 22 of them yielded temperature gradients of good or very good quality and are often constant and linear. The lowest measured temperature gradient is 0.127 °C/m and the highest measured temperature gradient is 15.109 °C/m. All heat flow stations are summarized in Table 6.9.1. In those cases where the penetration failed, hard ground was the reason for poor or no penetration. The lowest measured heat flow is 35.1 mW/m² and the highest measured heat flow is 15067.1 mW/m². The variability of low and high heat flow in the study area is mainly due to the heterogeneity of the sampled sites, ranging from a normal continental slope regime to sill-affected seep locations and hydrothermal vents.

Fig. 6.9.4 shows the analyzed temperature gradient, thermal conductivity and heat flow for the gravity core site SO241-7 (northern seep site). In this location the low heat flow of 35.1 mW/m² is strongly affected through the low thermal conductivity of less than 0.5 W/mK in around 2.5 m sediment depth. This result is different to sample sites SO241-47 (Fig 6.9.5) and SO241-51(Fig 7.9.6).The gravity core sample site at SO241-47 was dropped into the continental slope. The result at this site shows low temperature gradients of 0.127 °C/m, relatively low thermal conductivities of 0.607 W/mK and low heat flow of 79.6 mW/m².

No corrections for slope activities like turbidites or landslides as well as terrain effects have been conducted yet. Site SO241-51 shows high values in temperature gradient, a constant thermal conductivity of 0.687 W/mK and a high heat flow of 7667.4 mW/m². This high temperature and heat flow values result from the closely located black smoker vent site in this area. The Fig. 6.9.4 to 6.9.6 are examples for measured high as well as low and linear temperature gradients, different thermal conductivities and calculated heat flow.

Evaluating the temperature data of the MTLs deployment on the TV-MUC and HyBis brought additional information regarding plume detection in the water body and bottom water temperatures above the seabed. Temperature loggers were mounted during 9 TV_MUC deployments which are shown in Table 6.9.2. During one HyBis dive a temperature anomaly of +11,7 °C could be detected where the HyBis passed vent locations.

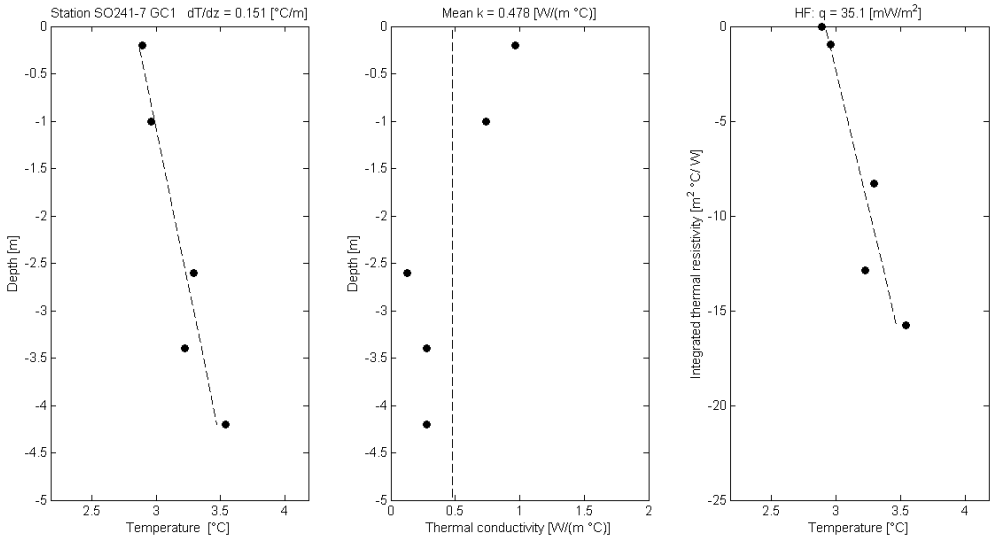

Fig. 6.9.4: Data Plot of SO241-7. The horizontal axis is relative temperature, the vertical axis depth relative to the instrument.

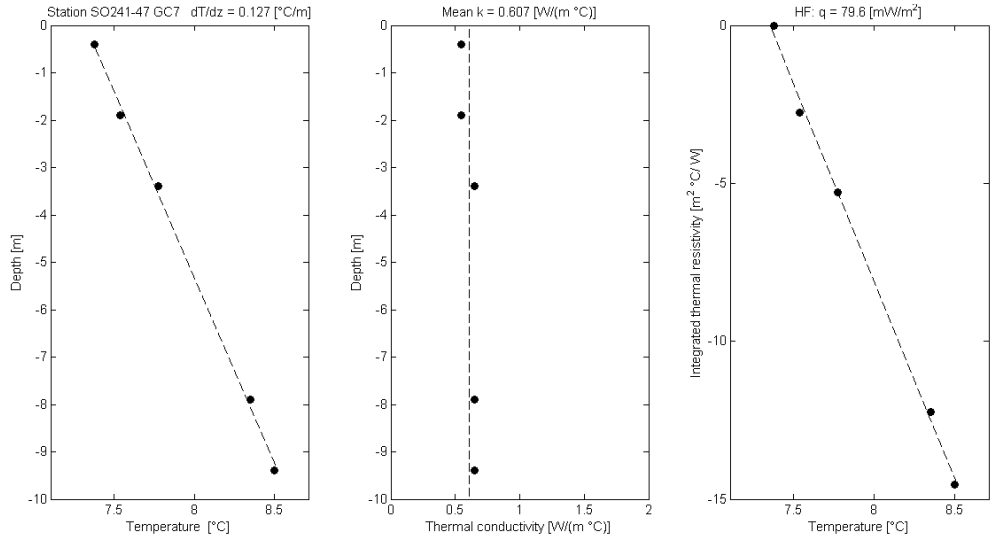

Fig. 6.9.5: Data Plot of SO241-47. The horizontal axis is relative temperature, the vertical axis depth relative to the instrument.

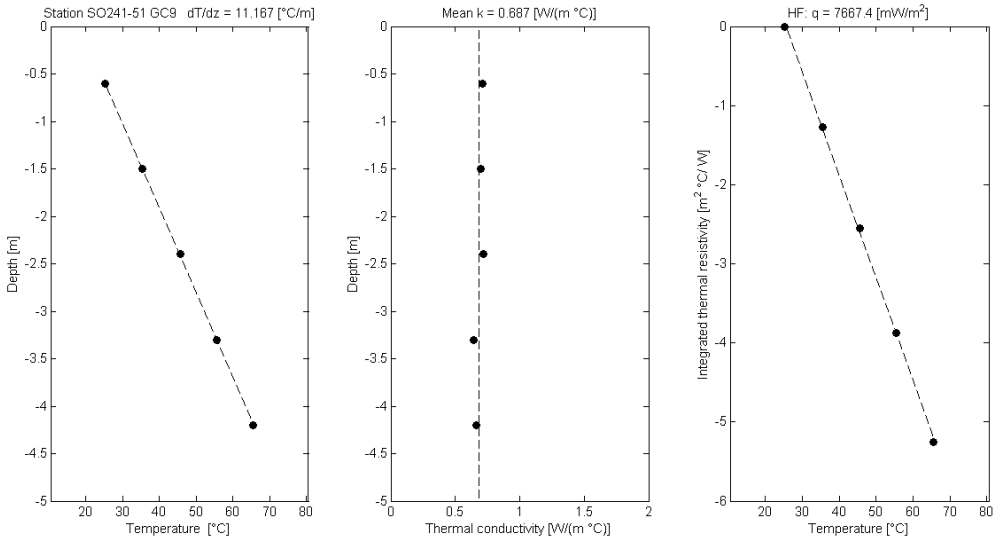

Fig. 6.9.6: Data Plot of SO241-51. The horizontal axis is relative temperature, the vertical axis depth relative to the instrument.

Table 6.9.1: List of heat flow stations on SO241, used Posidonia Coordinates for SO241-60 and SO241-70, all other Coordinates are ship based.

Station	Penetration	Instrument	Latitude	Longitude	Water Depth [m]
SO241-07	Pen 01	Gravety Core	27° 33,301'	111° 32,882'	1845
SO241-09	Pen 01	Gravety Core	27° 28,139'	111° 28,421'	1837
SO241-10	Pen 01	Gravety Core	27° 26,531'	111° 29,928'	1846
SO241-46	Pen 01	Gravety Core	27° 42,412'	111° 13,651'	666
SO241-47	Pen 01	Gravety Core	27° 42,413'	111° 13,649'	669
SO241-50	Pen 01	Gravety Core	27° 24,715'	111° 23,228'	1847
SO241-51	Pen 01	Gravety Core	27° 24,472'	111° 23,377'	1840
SO241-58	Pen 01	Gravety Core	27° 24,487'	111° 23,377'	1837
SO241-60	Pen 01	HF-Lance	27° 24.623'	111° 23.626'	1834
	Pen 02	HF-Lance	27° 24.554'	111° 23.512'	1840
	Pen 03	HF-Lance	27° 24.273'	111° 23.396'	1840
	Pen 04	HF-Lance	27° 24.408'	111° 23.288'	1849
	Pen 05	HF-Lance	27° 24.341'	111° 23.177'	1852
	Pen 06	HF-Lance	27° 24.265'	111° 23.082'	1844
	Pen 07	HF-Lance	27° 24.193'	111° 22.956'	1834
	Pen 08	HF-Lance	27° 24.605'	111° 23.317'	1837
	Pen 09	HF-Lance	27° 24.552'	111° 23.347'	1834
	Pen 10	HF-Lance	27° 24.522'	111° 23.360'	1835
	Pen 11	HF-Lance	27° 24.543'	111° 23.351'	1837
	Pen 12	HF-Lance	27° 24.804'	111° 23.210'	1813
SO241-62	Pen 01	Gravety Core	27° 28,193'	111° 28,365'	1838
SO241-70	Pen 01	HF-Lance	27° 25.802'	111° 25.486'	1870
	Pen 02	HF-Lance	27° 25.460'	111° 24.946'	2019
	Pen 03	HF-Lance	27° 25.955'	111° 24.493'	2046
	Pen 04	HF-Lance	27° 24.837'	111° 23.951	2025
SO241-71	Pen 01	Gravety Core	27° 28,187'	111° 28,380'	1838
SO241-72 a-d	Pen 01	Gravety Core	27° 28,178'	111° 28,396'	1838

Table 6.9.2: List of used MTL with TV-MUC and HyBis.

Station	Instrument	Latitude	Longitude	Water Depth [m]	Logger - Sediment Depth [m]
SO241-2	Multicorer	27° 30,558'	111° 40,922'	1725	0.4
SO241-15	Multicorer	27° 26,522'	111° 29,925'	1846	0.4
SO241-16	Multicorer	27° 23,827'	111° 25,923'	2047	0.4
SO241-22	Multicorer	27° 28,165'	111° 28,347'	1839	0.4
SO241-23	Multicorer	27° 30,282'	111° 40,770'	1724	0.4
SO241-33	Multicorer	27° 33,301'	111° 32,883'	1843	0.4
SO241-38	HyBis	27° 24,762'	111° 23,225'	1842	HyBis Vent-Transect
SO241-40	Multicorer	27° 24,698'	111° 23,254'	1853,6	0.4
SO241-65	Multicorer	27° 24,342'	111° 22,970'	1846	0.4
SO241-66	Multicorer	27° 24,577'	111° 23,265'	1840	0.4

6.10 HyBis operations

6.10.1 Methods and experimental setup

HyBis is a remotely operated underwater robot manufactured by Hydrolek Ltd., U.K. We ran it on the GEOMAR Hatlapa fibre optic winch supplying 2kV to the instrument. The instrument features two thrusters that allow some maneuverability and two hydraulic pumps that can be used to manipulate various scientific modules underneath the instrument. HyBis also has three cameras and lights that allow online monitoring of the operation. During SO241 we mounted a large hydraulic grab and conducted two dives at the site of the big smoker. The first dive was a reconnaissance dive intended to investigate a potential mud volcano but finding a large active hydrothermal vent system. During the second dive we investigate in detail the along axis of the hydrothermal vent system. For this dive we also mounted a thermometer.

6.10.2 Initial results

The video footage of HyBis unequivocally documents the presence of at least seven vent sites along the ridge of the smoker and that the expelled fluids are injected several hundreds of meters high into the water column. The video footage also suggests the presence of chemosynthetic ecosystem including *beggiatoa* mats and *pogonophora* tube worms.

Temperature measurements conducted above the vent sites are discussed in section 7.9. They show elevated bottom water temperatures in the vicinity of the vent sites. These reach up to 11 degrees C above the ambient bottom water temperature suggesting that hot fluids are expelled at the vents.

We were also able to collect samples of the chimney material. These consist of heavy, black rocks with reflecting minerals presumably predominantly pyrites and pyrotites. These samples are currently being analyzed in the laboratory.

6.11. Biology

6.11.1 Organic Geochemistry

Main Objectives of the organic geochemistry sampling during cruise SO241 was to study microbial abundances and processes in different environmental and depositional settings in the Guaymas basin to describe the microbial community with respect to changes in the organic matter (OM) composition as well as strong temperature gradients which may influence these microbes (Von Damm et al 1985). In this context the main focus was to sample sediments from Multi- and Gravity Corer in high resolution to identify changes within the microbial community at active hydrothermal vent sites. Moreover a transect with differing OM compositions was sampled reaching from the terrestrial dominated upper shelf into the basin. In order to target these objectives different sets of samples were taken in the research area. On one hand solid sediment samples were sampled to analyze the microbial community by analysis of Intact polar lipids (IPLs) for microbes (Sturt et al 2004) and dipolinic acid (DPA) (Lomstein et al 2012) to determine the abundance of spore forming Bacteria. Moreover several samples were sampled to reconstruct the activity of the microbial community with radiotracer experiments. Also porewater was sampled to gain a closer look into changes of the dissolved organic matter (DOM) composition with respect to differing sites and depth in the sediment. Moreover sediment samples were taken to measure the hydrogen concentration in the sediments, which thermodynamically controls the bacterial breakdown of organic matter in anoxic sediments (Hoehler et al,. 1999).

Sampling strategy

Multi corer tubes were immediately transferred to the cold room, where sampling took place. The sampling depths for IPL/DPA (Appendix E Table A), H2-analysis (Appendix E Table B) , as well as pore water sampling for DOM (Appendix E Table C) samples are shown in a table in the appendix . For IPL/DPA- analysis 5 ccm of wet sediment were taken and transferred to sterile 15 mL Falcoon tubes and stored at -20 °C. H2 was detected in the sediments by two different methods the incubation method (H2-INC) and the extraction

method (H2-EXT), (for details see chapter analysis). For the extraction method 3 mL of Sediment were transferred to a 22 mL-Vial and prepared for direct analysis. For the Incubation method 2 mL of sediment were transferred to a 5 mL Vial, followed by an exchange of the headspace with N2 to keep the sample anoxic closed with a thick butyl stopper and crimped. Porewater samples were centrifuged at 2800 rpm and the supernatant was than split for DOM and other analysis. For the DOM measurements two vials were prepared, a precombusted 2 mL vial which was filled with 1.5 mL closed with a cap and then stored at -20 °C for fluorometer analysis and 35 mL precombusted serum bottles for FTICR-MS analysis, which were crimped with seals and stored at 4°C. The later were only taken when more than 10 mL of porewater were available. For some Multi corere sites samples for radiotracer experiments were taken as well, usually in a depth between 0-12 cm below the surface (cmbsf). If a sample was taken sediment was transferred with a cut-off 50 mL syringe to a pre combusted 1L Schott bottle, followed by an exchange of the headspace with N2 and then sealed with an autoclaved black rubber butyl stopper. The samples were stored at 4°C.

The gravity corer sampling was carried out on deck and/or in the hangar. The sampling depths are shown in Tab. 11D. For IPL/DPA analysis 20 ccm sediment were transferred to sterile 50 mL Hungate tube and stored in a portable freezer at 4°C. After sampling the samples were stored in a -20°C freezer. H2 and Porewater sampling were carried out as described for the multicorer tubes. Similarly to the multi corers samples for radiotracer experiments was taken from several sites and depths, by the same method.

Analysis

Samples for IPL-, DPA- and DOM-analysis, as well as the Schott bottles for the radiotracer experiments will be shipped to Bremen at -20 °C and 4 °C respectively. The further processing and analysis of these samples will take part at the MARUM Bremen – AG Organische Geochemie.

The Hydrogen concentrations were determined on board by two different methods as mentioned in the sampling strategy. For the direct extraction (H2-EXT) a method as described by Lin et al 2012 was used. In brief 3 mL sediment were added into a 22 mL vial, filled up with a saturated NaCl solution, sealed with a brom butyl stopper and then crimped. In the following a 5-9 mL headspace was created in the vial by displacing aqueous phase with ultra pure N2 gas. The sample was incubated for 20 minutes and then the H2 in the headspace was measured. 2 blanks containing the solely the NaCl solution were measured as well for every core

The H2-INC method was used as described by Hoehler et al 1998. This protocol is based on an equilibration of H2 in the headspace. For this method 2 mL of sediment were transferred to a 5 mL Vial and degassed with N2 in order to keep it anoxic and to remove H2 remains from the sediment. Afterwards the sample was closed with a thick ruber butyl stopper, crimped and incubated at its ambient temperature for several days. In most cases the samples were measured after 5, 8 and 12 days, where about 60 % of the incubations reached their equilibrium. The equilibrium was defined by change of the hydrogen concentration of less than 0.1 nM in the headspace between two measurements. However the remaining samples were further incubated as long as possible, to gain the equilibrium or a close by value. Moreover a blank for every incubation temperature and core was run, since previous tests had shown that the stoppers produce hydrogen, especially at high temperatures.

Measurements of H2-concentrations were carried out on a Peak Performer 1 gas chromatograph (Peak Laboratories, LLC,USA) run with nitrogen.

6.11.2 Microbiology

The main research questions investigated by the microbiology team can be summarized as follows: (1) How do microbial abundance and community composition (from domain- to operational taxonomic unit-level) shift along thermal gradients, organic matter compositional gradients, and in response to macrofaunal bioturbation? (2) Are there interactions between

temperature, organic matter composition, and bioturbation that are reflected in microbial abundance and community composition? (3) Do patterns in microbial abundances reflect shifts in maintenance power requirements related to temperature?

To address these questions, the Guaymas Basin, with its wide range of temperature gradients, its diverse range of hemipelagic and mixed hemipelagic-terrestrial sediments, and sedimentary sites with and without benthic macrofauna, provides an ideal natural laboratory. A wide array of samples for microbiological, molecular biological, and geochemical analyses was taken to examine patterns in microbial abundance, microbial community composition, and microbial activity. The sampling regime was tightly coordinated with the sampling for 'Organic Geochemistry (section 6.5, Table 6.5.2).

Methods

In addition to sampling, shipboard microbiological work included DNA extractions and quantifications of prokaryotic communities using quantitative polymerase-chain-reaction (qPCR) assays on bacterial and archaeal 16S rRNA genes, following the DNA extraction method and qPCR protocol outlined in Lever et al. (2015). Samples were also taken for shorebased analyses. Planned shorebased analyses include the study of (1) microbial cell abundances by flow cytometry (Morono et al. 2014), (2) microbial community composition based on 16S rRNA gene and catabolic functional gene sequences and possibly gene transcripts (Teske et al. 2014, Lever & Teske 2015), (3) sediment dipicolinic acid content as a proxy for in situ endospore abundances (Lomstein et al. 2012, Langerhuus et al. 2012), (4) methane quantifications and δ13C-isotopic analyses, (5) dissolved and solid-phase concentrations and compositions of microbial hydrolysis and fermentation intermediates, including volatile fatty acids (VFAs), amino acids (AAs), amino sugars (AS), and sugars (S) (Glombitza et al. 2014, Lomstein et al. 2013), (6) depth and rates of macrofaunal sediment reworking based on radioisotope analyses of Pb-210 and Cs-137 (Cochran et al. 1985), and (7) in situ endospore-forming microbial communities based on DNA sequence analyses and pasteurization experiments (de Rezende et al. 2013, Müller et al. 2014). Combined with data on electron acceptor concentrations and in situ temperature gradients this data set will provide insights into links between microbial communities, microbial activity, macroecology, and organic geochemistry.

An overview of the sampling regime is provided Appendix E.

7. Acknowledgements /Danksagung

We thank the Federal Ministry of Education and Science (BMBF)'s SONNE program for funding the expedition. We would also like to thank the master and the ship's crew of R/V Sonne for their relentless support and making our research possible. We thank Dan Lizarralde of WHOI for providing seismic data that was used during cruise planning.

8. References / Literaturverzeichnis

Berner, U., Faber, E., Scheeder, G. und Panten, D., 1995. Primary cracking of algal and landplant kerogens: Kinetic models of isotope variations in methane, ethane, and propane. Chemical Geology, 126: 233-245.

Chan, L.H., Gieskes, J.M., You, C.-F. und Edmond, J.M., 1994. Lithium isotope geochemistry of sediments and hydrothermal fluids of the Guaymas Basin, Gulf of California. Geochemica et Cosmochimica Acta, 58: 4443-4454.

Cochran JK (1985) Particle mixing rates in sediments of the eastern equatorial Pacific: evidence from 210Pb, 239, 240Pu and 137Cs distributions at MANOP sites. Geochim Cosmochim Acta 49: 1195-1210.

Curray, J. R., Moore, D. G. et al., 1982. et al., Init. Repts. DSDP, 64: Washington (U.S. Govt. Printing Office).

de Rezende JR, Kjeldsen KU, Hubert CRJ, Finster K, Loy A, Jørgensen BB. Dispersal of

thermophilic Desulfotomaculum endospores into Baltic Sea sediments over thousands of years. ISME Journal 2013, 7(1), 72-84.

Faber, E., Schmidt, M., Feyzullayev A. (2015) Geochemical Hydrocarbon Exploration – Insights from Stable Isotope Models. Oil Gas European Magazine 41 (2) 93-98.

Fisher, A. T., & Becker, K. (1991). Heat flow, hydrothermal circulation and basalt intrusions in the Guaymas Basin, Gulf of California. Earth and Planetary Science Letters, 103, 84–99.

Galimov, E.M. und Simoneit, B.R.T., 1982. Geochemistry of Interstitial Gases in Sedimentary Deposits of the Gulf of California, Deep Sea Drilling Project Leg 64. In: J.R. Curray and D.G. Moore (Editors), Initial Reports of the Deep Sea Drilling Project. Government Printing Office, Washington, D.C., pp. 781-.

Glombitza C, Pedersen J, Røy H, Jørgensen BB (2014) Direct analysis of volatile fatty acids in marine sediment porewater by two-dimensional ion chromatography-mass spectrometry. Limnol Oceanogr Meth 12:455-468.

Grasshoff, K., Ehrhardt, M., and Kremling, K. (1997) Methods of seawater analysis. Verlag Chemie.

Hansen, J.P.V., Cartwright, J.A., Huuse, M. und Clausen, O.R., 2005. 3D seismic expression of fluid migration and mud remobilization on the Gjallar Ridge, offshore mid-Norway. Basin Research, doi: 10.1111/j.1365-2117.2005.00257.x.

Hoehler T, Alperin MJ, Albert AB, Martens CS (1998) Thermodynamic Control on hydrogen concentrations in anoxic sediments. concentration in subseafloor sediment: A proposal for combined analysis by two distinct approaches. Geochim Cosmochim Acta 62:1745-1756.

Ivanenkov, V.N., Lyakhin, Y.I. (1978) Determination of total alkalinity in seawater. In: Bordovsky, O.K., Ivanenkov, V.N. (Eds.), Methods of Hydrochemical Investigations in the Ocean. Nauka Publ. House, pp. 110–114, in Russian.

Karaca, D., Schleicher, T., Hensen, C., Linke, P., and Wallmann, K. (2014) Quantification of methane emission from bacterial mat sites at Quepos Slide offshore Costa Rica: International Journal of Earth Sciences, v. 103, p. 1817-1829.

Karstens, J., and Berndt, C. (2015). Seismic chimneys in the Southern Viking Graben – Implications for palaeo fluid migration and overpressure evolution. Earth and Planetary Science Letters, *412*(C), 88–100.

Kipfer and Ruedi Ruessel et al., Abstract for the Goldschmidt conference, Prague, August 2015

Langerhuus AT, Røy H, Lever MA, Morono Y, Inagaki F, Jørgensen BB, Lomstein BA (2012) Endospore abundance and D:L amino acid modeling of bacterial turnover in Holocene marine sediment (Aarhus Bay). Geochim Cosmochim Acta 99:87-99.

Lever MA, Teske AP. 2015. Diversity of methane-cycling archaea in hydrothermal sediment investigated by general and group-specific PCR primers. Appl Environ Microbiol 81:1426-1441.

Lever MA, Torti A, Eickenbusch P, Michaud AB, Săntl-Temkiv T, Jørgensen BB. 2015. A modular method for the extraction of DNA and RNA, and the separation of DNA pools from diverse environmental sample types. Frontiers Microbiol 6:476 doi: 10.3389/fmicb.2015.00476.

Liebetrau, V., Augustin, N., Kutterolf, S., Schmidt, M., Eisenhauer, A., Garbe-Schönberg, D., and Weinrebe, W. (2014). Cold-seep-driven carbonate deposits at the Central American forearc: contrasting evolution and timing in escarpment and mound settings. International Journal of Earth Sciences, 103(7), 1845–1872.

Lin Y-S, Heuer VB, Goldhamer T, Kellermann, M Y, Zabel M, Hinrichs K-U (2012) Towards

constraining H2 concentration in subseafloor sediment: A proposal for combined analysis by two distinct approaches. Geochim Cosmochim Acta 77: 186-201.

Linke, P., Schmidt, M., Rohleder, M., Al-Barakati, A., Al-Farawati, R. (2015) Novel online digital video and high-speed data broadcasting via standard coaxial cable onboard marine operating vessels Marine Technology Society Journal, 49 (1) 7-18.

Lizarralde, D., Soule, S.A., Seewald, J.S. und Proskurowski, G., 2010. Carbon release by off-axis magmatism in a young sedimented spreading centre. Nature Geoscience, 4: 50-54.

Lomstein BA, Langerhuus AT, D'Hondt S, Jørgensen BB & Spivack AJ (2012) Endospore abundance, microbial growth and necromass turnover in deep sub-seafloor sediment. Nature 484: 101-104.

Lonsdale, P. und Becker, K., 1985. Hydrothermal plumes, hot springs, and conductive heat flow in the Southern Trough of Guaymas Basin. Earth and Planetary Science Letters, 73: 211-225.

Luff, R., and Wallmann, K. (2003) Fluid flow, methane fluxes, carbonate precipitation and biogeochemical turnover in gas hydrate-bearing sediments at Hydrate Ridge, Cascadia Margin: Numerical modeling and mass balances: Geochimica et Cosmochimica Acta, v. 67, p. 3403–3421.

Mächler, L., Brennwald, M. S., and Kipfer, R. (2012) Membrane inlet mass spectrometer for the quasi-continuous on-site analysis of dissolved gases in groundwater. Environ. Sci. Technol., 46, 8288-8296.

Mächler, L., Brennwald, M. S., Tyroller, L., Livingstone, D. M., Kipfer, R. (2014) Conquering the outdoors with on-site mass spectrometry. Chimia, 68, 155-159.

Morono Y, Terada T, Kallmeyer J, Inagaki F (2013) An improved cell separation technique for marine subsurface sediments: applications for high-throughput analysis using flow cytometry and cell sorting. Environ Microbiol doi:10.1111/1462-2920.12153.

Müller AL, de Rezende JR, Hubert CRJ, Kjeldsen KU, Lagkouvardos I, Berry D, Jørgensen BB, Loy A. Endospores of thermophilic bacteria as tracers of microbial dispersal by ocean currents. ISME Journal 2014,8, 1153-1165.

Paull, C. K., Ussler, W., III, Peltzer, E. T., Brewer, P. G., Keaten, R., Mitts, P. J., et al. (2007). Authigenic carbon entombed in methane-soaked sediments from the northeastern transform margin of the Guaymas Basin, Gulf of California. Deep Sea Research Part II: Topical Studies in Oceanography, 54(11-13), 1240–1267.

Purkl, S., and Eisenhauer, A. (2004). Determination of radium isotopes and 222Rn in a groundwater affected coastal area of the Baltic Sea and the underlying sub-sea floor aquifer. Marine Chemistry, 87(3-4), 137–149.

Schmidt M., Linke P., Esser D. (2013) Recent development in IR-sensor technology for monitoring subsea methane discharge. Marine Technology Society Journal 47 (3), 27-35.

Schmidt, M., Linke, P., Sommer, S., Esser, D. und Cherednichenko, S. (2015) Natural CO2 seeps offshore Panarea – A test site for subsea CO2 leak detection technology Marine Technology Society Journal, 49 (1) 19-30.

Schmitt, M., Thiessen, O. (2003) A new designed sediment degassing system for small sample sizes to analyze free-, total-, and adsorbed-gases. 7th International Conference on Gas Geochemistry (ICGG7). September 2003, Freiberg, Germany.

Scholz, F., Hensen, C., Schmidt, M., and Geersen, J. (2013) Submarine weathering of silicate minerals and the extent of pore water freshening at active continental margins: Geochimica et Cosmochimica Acta, v. 100, p. 200-216.

Schrader, H., 1982. Diatom biostratigraphy and laminated diatomaceous sediments from the Gulf of California DSDP Project Leg 64. In: J.R. Curray and D.G. Moore (Editors), Initial

Reports of the Deep Sea Drilling Project. Government Printing Office, Washington, D.C.

Seewald, J.S., Seyfried, W.E. und Thornton, E.C., 1990. Organic-rich sediment alteration; an experimental and theoretical study at elevated temperatures and pressures. Applied Geochemistry, 5: 193-209.

Simoneit, B.R.T. und Lonsdale, P.F., 1982. Hydrothermal petroleum in mineralized mounds at the seabed of Guaymas Basin. Nature, 295: 198-202.

Stock, J.M. und Lee, J., 1994. Do microplates in subduction zones leave a geological record? Tectonics, 13: 1472-1487.

Sturt HF, Summons RE, Smith KE, Elvert M, Hinrichs K-U (2004) Intact polar membrane lipids in prokaryotes and sediments deciphered by high-performance liquid chromatography/electrospray ionization multistage mass spectrometry—new biomarkers for biogeochemistry and microbial ecology. RCMS 18,617-628

Svensen, H., Planke, S. und Malthe-Sørensen, A., 2004. Release of methane from a volcanic basin as a mechanism for initial Eocene global warming. Nature, 429: 542-545.

Svensen, H., Planke, S., Jamtveit, B. und Pedersen, T., 2003. Seep carbonate formation controlled by hydrothermal vent complexes: a case study from the Vøring volcanic basin, the Norwegian Sea. Geo- Marine Letters, 23: 351-358.

Teske AP, Biddle JF, Lever MA. 2014. Distribution of Subseafloor Life: Biomass, Activity and Genetic Diversity, In “Earth and Life Processes Discovered from Subseafloor Environment – A Decade of Science Achieved by the Integrated Ocean Drilling Program (IODP)”, eds. Stain R, Blackman D, Inagaki F, Larsen HC, Developments in Marine Geology 7, Elsevier.

Von Damm, K.L., Edmond, J.M., Measures, C.I., and Grant, B. (1985) Chemistry of submarine hydrothermal solutions at Guaymas Basin, Gulf of California: Geochimica et Cosmochimica Acta, v. 49, p. 2221-2237.

Wallmann, K., Aloisi, G., Haeckel, M., Tishchenko, P., Pavlova, G., Greinert, J., Kutterolf, S., and Eisenhauer, A. (2008) Silicate weathering in anoxic marine sediments: Geochimica et Cosmochimica Acta, v. 72, p. 363-366.

Zhu, R., Lin, Y.S., Lipp, J.S., Meador, T.B., Hinrichs, K.-U., 2014. Optimizing sample

pretreatment for compound-specific stable carbon isotopic analysis of amino sugars in marine sediment. Biogeosciences Discussion 11, 1-31. doi:10.5194/bgd-11-1-2014.

9. Abbreviations /Abkürzungen

BSR – Bottom Simulating Reflector

DSDP – Deep Sea Drilling Program

OBS – Ocean bottom seismometer

10. Appendices /Anhänge

Appendix A: Participating Institutions /Liste der teilnehmenden Institutionen

GEOMAR Helmholtz-Zentrum für Ozeanforschung Kiel
Kiel
Germany

EAWAG Swiss Federal Institute of Aquatic Sciences
Dübendorf
Switzerland

Eidgenössisch Technische Hochschule
Zürich
Switzerland

Fachbereich Geowissenschaften
Universität Bremen
Germany

Academia Sinica
Taipei
Taiwan

Istituto de Geofisica
UNAM
Coyoacan
Mexico

Appendix B: Station List / Stationsliste

Station	date	time (UTC)	Device	Latitude	Longitude	Action
SO241/1	25.06.2015	12:15:00 PM	CTD	27° 30,781' N	111° 41,062' W	station start
SO241/1	25.06.2015	01:28:00 PM	CTD	27° 30,728' N	111° 40,932' W	Bodenkontakt, Posidonia
SO241/1	25.06.2015	01:28:00 PM	CTD	27° 30,717' N	111° 40,915' W	Bodenkontakt Schiff, SL:1732 m, SZ: 8 kN
SO241/1	25.06.2015	01:30:00 PM	CTD	27° 30,716' N	111° 40,915' W	profile start
SO241/1	25.06.2015	03:15:00 PM	CTD	27° 30,063' N	111° 40,658' W	profile end
SO241/1	25.06.2015	03:52:00 PM	CTD	27° 30,069' N	111° 40,654' W	station end
SO241/2	25.06.2015	06:25:00 PM	Multi Corer	27° 30,599' N	111° 40,517' W	station start
SO241/2	25.06.2015	10:19:00 PM	Multi Corer	27° 30,545' N	111° 40,906' W	Bodenkontakt, Posidonia
SO241/2	25.06.2015	10:19:00 PM	Multi Corer	27° 30,558' N	111° 40,922' W	Bodenkontakt Schiff, SL:1744m
SO241/2	25.06.2015	11:21:00 PM	Multi Corer	27° 30,535' N	111° 40,899' W	station end
SO241/3	25.06.2015	11:22:00 PM	GRAB	27° 30,535' N	111° 40,899' W	station start
SO241/3	26.06.2015	01:27:00 AM	GRAB	27° 30,529' N	111° 40,883' W	Bodenkontakt, Posidonia
SO241/3	26.06.2015	01:27:00 AM	GRAB	27° 30,532' N	111° 40,910' W	Bodenkontakt Schiff, SL: 1745 m
SO241/3	26.06.2015	02:26:00 AM	GRAB	27° 30,538' N	111° 40,907' W	station end
SO241/4	database error					
SO241/5	26.06.2015	02:30:00 AM	Multibeam & Parasound	27° 30,513' N	111° 40,867' W	station start
SO241/5	26.06.2015	05:00:00 AM	Multibeam & Parasound	27° 14,781' N	111° 29,085' W	station end
SO241/6	26.06.2015	05:31:00 AM	2D-Seismik	27° 13,453' N	111° 27,946' W	station start
SO241/6	26.06.2015	09:41:00 AM	2D-Seismik	27° 21,907' N	111° 21,318' W	start of line P2001
SO241/6	26.06.2015	11:12:00 AM	2D-Seismik	27° 25,984' N	111° 18,129' W	end of line P2001
SO241/6	26.06.2015	11:28:00 AM	2D-Seismik	27° 26,929' N	111° 18,842' W	start of line P2002
SO241/6	26.06.2015	04:30:00 PM	2D-Seismik	27° 44,827' N	111° 47,405' W	end of line P2002
SO241/6	26.06.2015	04:37:00 PM	2D-Seismik	27° 44,710' N	111° 47,898' W	start of line P2003
SO241/6	26.06.2015	07:52:00 PM	2D-Seismik	27° 37,069' N	111° 53,919' W	end of line P2003
SO241/6	26.06.2015	08:06:00 PM	2D-Seismik	27° 36,257' N	111° 53,594' W	start of line P2004
SO241/6	27.06.2015	07:18:00 AM	2D-Seismik	27° 11,829' N	111° 14,149' W	end of line P2004
SO241/6	27.06.2015	07:27:00 AM	2D-Seismik	27° 11,961' N	111° 13,492' W	start of line P2005
SO241/6	27.06.2015	08:09:00 AM	2D-Seismik	27° 14,430' N	111° 11,827' W	end of line P2005
SO241/6	27.06.2015	08:20:00 AM	2D-Seismik	27° 15,094' N	111° 11,949' W	start of line P2006
SO241/6	27.06.2015	05:01:00 PM	2D-Seismik	27° 42,073' N	111° 54,562' W	end of line P2006
SO241/6	27.06.2015	05:11:00 PM	2D-Seismik	27° 42,809' N	111° 54,366' W	start of line P2007
SO241/6	27.06.2015	05:22:00 PM	2D-Seismik	27° 43,527' N	111° 53,697' W	end of line P2007
SO241/6	27.06.2015	05:34:00 PM	2D-Seismik	27° 43,659' N	111° 52,963' W	start of line P2008
SO241/6	28.06.2015	07:19:00 AM	2D-Seismik	27° 18,153' N	111° 11,973' W	end of line P2008
SO241/6	28.06.2015	07:25:00 AM	2D-Seismik	27° 18,565' N	111° 11,807' W	start of line P2009
SO241/6	28.06.2015	10:08:00 AM	2D-Seismik	27° 30,844' N	111° 12,202' W	end of line P2009
SO241/6	28.06.2015	10:15:00 AM	2D-Seismik	27° 31,367' N	111° 12,529' W	start of line P2010
SO241/6	28.06.2015	11:56:00 AM	2D-Seismik	27° 36,408' N	111° 21,489' W	end of line P2010
SO241/6	28.06.2015	12:05:00 PM	2D-Seismik	27° 36,386' N	111° 22,143' W	start of line P2011
SO241/6	28.06.2015	02:53:00 PM	2D-Seismik	27° 24,833' N	111° 30,926' W	end of line P2011
SO241/6	28.06.2015	03:05:00 PM	2D-Seismik	27° 23,975' N	111° 31,051' W	start of line P2012
SO241/6	28.06.2015	07:31:00 PM	2D-Seismik	27° 04,282' N	111° 30,294' W	end of line P2012
SO241/6	28.06.2015	08:24:00 PM	2D-Seismik	27° 03,026' N	111° 29,595' W	start of line P2013
SO241/6	29.06.2015	02:48:00 AM	2D-Seismik	27° 25,779' N	111° 41,020' W	end of line P2013

SO241/6	29.06.2015	02:56:00 AM	2D-Seismik	27° 26,256' N	111° 41,029' W	start of line P2014
SO241/6	29.06.2015	07:50:00 AM	2D-Seismik	27° 39,260' N	111° 26,026' W	end of line P2014
SO241/6	29.06.2015	08:08:00 AM	2D-Seismik	27° 40,060' N	111° 26,673' W	start of line P2015
SO241/6	29.06.2015	11:28:00 AM	2D-Seismik	27° 39,599' N	111° 45,830' W	end of line P2015
SO241/6	29.06.2015	12:01:00 PM	2D-Seismik	27° 39,633' N	111° 48,080' W	station end
SO241/7	29.06.2015	01:31:00 PM	Gravity Corer	27° 33,299' N	111° 32,851' W	station start
SO241/7	29.06.2015	02:12:00 PM	Gravity Corer	27° 33,285' N	111° 32,866' W	Bodenkontakt, Posidonia
SO241/7	29.06.2015	02:12:00 PM	Gravity Corer	27° 33,301' N	111° 32,882' W	Bodenkontakt Schiff, SL: 1867 m, SZ: 19 kK
SO241/7	29.06.2015	03:10:00 PM	Gravity Corer	27° 33,300' N	111° 32,887' W	station end
SO241/8	29.06.2015	04:00:00 PM	Gravity Corer	27° 33,298' N	111° 32,878' W	station start
SO241/8	29.06.2015	04:39:00 PM	Gravity Corer	27° 33,301' N	111° 32,884' W	Bodenkontakt Schiff, SL: 1866 m, SZ: 18 kN
SO241/8	29.06.2015	05:23:00 PM	Gravity Corer	27° 33,301' N	111° 32,885' W	station end
SO241/9	29.06.2015	06:35:00 PM	Gravity Corer	27° 28,141' N	111° 28,437' W	station start
SO241/9	29.06.2015	07:15:00 PM	Gravity Corer	27° 28,125' N	111° 28,405' W	Bodenkontakt, Posidonia
SO241/9	29.06.2015	07:15:00 PM	Gravity Corer	27° 28,139' N	111° 28,421' W	Bodenkontakt Schiff, SLmax: 1860m ; Wassertiefe: 1838m
SO241/9	29.06.2015	08:17:00 PM	Gravity Corer	27° 28,140' N	111° 28,419' W	station end
SO241/10	29.06.2015	09:01:00 PM	Gravity Corer	27° 26,530' N	111° 29,929' W	station start
SO241/10	29.06.2015	09:43:00 PM	Gravity Corer	27° 26,549' N	111° 29,922' W	Bodenkontakt, Posidonia
SO241/10	29.06.2015	09:43:00 PM	Gravity Corer	27° 26,531' N	111° 29,928' W	Bodenkontakt Schiff, SL: 1872m
SO241/10	29.06.2015	10:28:00 PM	Gravity Corer	27° 26,532' N	111° 29,927' W	station end
SO241/11	29.06.2015	10:39:00 PM	Releasertest	27° 26,529' N	111° 29,925' W	station start
SO241/11	30.06.2015	12:27:00 AM	Releasertest	27° 26,530' N	111° 29,923' W	station end
SO241/12	30.06.2015	12:48:00 AM	CTD	27° 26,160' N	111° 30,263' W	station start
SO241/12	30.06.2015	02:08:00 AM	CTD	27° 26,133' N	111° 30,268' W	Bodensicht, Posidonia
SO241/12	30.06.2015	02:08:00 AM	CTD	27° 26,151' N	111° 30,280' W	Bodensicht, SL: 1843 m, SZ: 8 kN
SO241/12	30.06.2015	03:19:00 AM	CTD	27° 26,149' N	111° 30,271' W	station end
SO241/13	30.06.2015	04:23:00 AM	CTD	27° 33,344' N	111° 32,871' W	station start
SO241/13	30.06.2015	06:10:00 AM	CTD	27° 33,328' N	111° 32,874' W	Bodensicht, Posidonia
SO241/13	30.06.2015	06:10:00 AM	CTD	27° 33,344' N	111° 32,886' W	Bodensicht, SLmax: 1827m , Wassertiefe: 1846m
SO241/13	30.06.2015	06:24:00 AM	CTD	27° 33,348' N	111° 32,885' W	profile start
SO241/13	30.06.2015	07:20:00 AM	CTD	27° 33,213' N	111° 32,876' W	Bodensicht, SLmax: 1839m
SO241/13	30.06.2015	11:01:00 AM	CTD	27° 33,281' N	111° 32,874' W	station end
SO241/14	30.06.2015	12:10:00 PM	Gravity Corer	27° 23,874' N	111° 25,942' W	station start
SO241/14	30.06.2015	12:56:00 PM	Gravity Corer	27° 23,850' N	111° 25,923' W	Bodenkontakt, Posidonia
SO241/14	30.06.2015	12:56:00 PM	Gravity Corer	27° 23,864' N	111° 25,939' W	Bodenkontakt Schiff, SL: 2056m
SO241/14	30.06.2015	01:52:00 PM	Gravity Corer	27° 23,865' N	111° 25,939' W	station end
SO241/15	30.06.2015	02:50:00 PM	Multi Corer	27° 26,532' N	111° 29,904' W	station start
SO241/15	30.06.2015	06:05:00 PM	Multi Corer	27° 26,522' N	111° 29,925' W	Bodenkontakt Schiff, SLmax: 1856m
SO241/15	30.06.2015	07:03:00 PM	Multi Corer	27° 26,523' N	111° 29,925' W	station end
SO241/16	30.06.2015	07:46:00 PM	Multi Corer	27° 23,953' N	111° 26,032' W	station start
SO241/16	30.06.2015	10:14:00 PM	Multi Corer	27° 23,808' N	111° 25,915' W	Bodenkontakt, Posidonia
SO241/16	30.06.2015	10:14:00 PM	Multi Corer	27° 23,827' N	111° 25,923' W	Bodenkontakt Schiff, SL: 2043m
SO241/16	30.06.2015	11:13:00 PM	Multi Corer	27° 23,827' N	111° 25,919' W	station end
SO241/17	01.07.2015	12:45:00 AM	GRAB	27° 30,412' N	111° 40,760' W	station start
SO241/17	01.07.2015	01:28:00 AM	GRAB	27° 30,447' N	111° 40,776' W	Bodenkontakt, Posidonia
SO241/17	01.07.2015	01:28:00 AM	GRAB	27° 30,467' N	111° 40,778' W	Bodenkontakt Schiff, SL: 1736 m, SZ: 33 kN
SO241/17	01.07.2015	04:02:00 AM	GRAB	27° 30,277' N	111° 40,741' W	station end

SO241/18	01.07.2015	06:21:00 AM	OBS deployment	27° 28,803' N	111° 28,573' W	station start
SO241/18	01.07.2015	12:10:00 PM	OBS deployment	27° 25,929' N	111° 25,919' W	station end
SO241/19	01.07.2015	02:09:00 PM	OBS Seismic	27° 31,428' N	111° 32,104' W	station start
SO241/19	01.07.2015	2:20:00 pm	OBS Seismic	27°31.159' N	111°31.823' W	start of line OBS 2002-01
SO241/19	01.07.2015	7:50:00 pm	OBS Seismic	27° 23.841' N	111°28.469' W	end of line OBS 2002-01
SO241/19	01.07.2015	8:07:00 pm	OBS Seismic	27° 24.544' N	111° 29.168' W	start of line OBS 2002-02
SO241/19	01.07.2015	9:54:00 pm	OBS Seismic	27° 29,329' N	111° 23,288' W	end of line OBS 2002-02
SO241/19	01.07.2015	10:07:00 PM	OBS Seismic	27° 27,635' N	111° 28,640' W	station end
SO241/20	01.07.2015	11:12:00 PM	3D-Seismik	27° 22,090' N	111° 22,432' W	station start
SO241/20	02.07.2015	03:55:00 AM	3D-Seismik	27° 30,653' N	111° 32,212' W	station end
SO241/21	02.07.2015	04:11:00 AM	OBS Seismic	27° 30,907' N	111° 31,816' W	station start
SO241/21	02.07.2015	4:18:00 AM	OBS Seismic	27° 30.900' N	111°31.643' W	start of line OBS 3000-01
SO241/21	02.07.2015	6:11:00 AM	OBS Seismic	27° 30.573' N	111°24.852' W	end of line OBS 3000-01
SO241/21	02.07.2015	6:34:00 AM	OBS Seismic	27° 29.799' N	111° 24.549' W	start of line OBS 3000-02
SO241/21	02.07.2015	7:55:00 AM	OBS Seismic	27° 25.332' N	111° 29.744' W	end of line OBS 3000-02
SO241/21	02.07.2015	8:20:00 AM	OBS Seismic	27° 26.192' N	111° 30.794' W	start of line OBS 3000-03
SO241/21	02.07.2015	10:06:00 AM	OBS Seismic	27° 30.675' N	111° 25.352' W	end of line OBS 3000-03
SO241/21	02.07.2015	10:20:00 AM	OBS Seismic	27° 31.239' N	111° 25.818' W	start of line OBS 3000-04
SO241/21	02.07.2015	11:51:00 AM	OBS Seismic	27° 26.30' N	111° 31.097' W	end of line OBS 3000-04
SO241/21	02.07.2015	12:14:00 PM	OBS Seismic	27° 25.810' N	111° 30.296' W	start of line OBS 3000-05
SO241/21	02.07.2015	2:03:00 PM	OBS Seismic	27° 30.635' N	111° 24.566' W	end of line OBS 3000-05
SO241/21	02.07.2015	2:26:00 PM	OBS Seismic	27° 31.222' N	111° 26.048' W	start of line OBS 3000-06
SO241/21	02.07.2015	3:20:00 PM	OBS Seismic	27° 29.312' N	111° 29.810' W	end of line OBS 3000-06
SO241/21	02.07.2015	3:34:00 PM	OBS Seismic	27° 28.540' N	111° 29.700' W	start of line OBS 3000-07
SO241/21	02.07.2015	4:03:00 PM	OBS Seismic	27° 27.3767' N	111° 28.412' W	end of line OBS 3000-07
SO241/21	02.07.2015	4:17:00 PM	OBS Seismic	27° 27.793' N	111° 28.024' W	start of line OBS 3000-08
SO241/21	02.07.2015	4:31:00 PM	OBS Seismic	27° 28.718' N	111° 29.094' W	end of line OBS 3000-08
SO241/21	02.07.2015	4:43:00 PM	OBS Seismic	27° 28.472' N	111° 29.532' W	start of line OBS 3000-09
SO241/21	02.07.2015	5:00:00 PM	OBS Seismic	27° 27.742' N	111° 28.745' W	end of line OBS 3000-09
SO241/21	02.07.2015	05:08:11 PM	OBS Seismic	27° 27,635' N	111° 28,640' W	station end
SO241/22	02.07.2015	05:46:00 PM	Multi Corer	27° 28,150' N	111° 28,372' W	station start
SO241/22	02.07.2015	08:08:00 PM	Multi Corer	27° 28,150' N	111° 28,331' W	Bodenkontakt, Posidonia
SO241/22	02.07.2015	08:08:00 PM	Multi Corer	27° 28,165' N	111° 28,347' W	Bodenkontakt Schiff, SLmax: 1849m
SO241/22	02.07.2015	09:11:00 PM	Multi Corer	27° 28,167' N	111° 28,342' W	station end
SO241/23	02.07.2015	10:23:00 PM	Multi Corer	27° 30,286' N	111° 40,745' W	station start
SO241/23	02.07.2015	01:02:00 AM	Multi Corer	27° 30,294' N	111° 40,784' W	Bodenkontakt, Posidonia
SO241/23	03.07.2015	01:02:00 AM	Multi Corer	27° 30,282' N	111° 40,770' W	Bodenkontakt Schiff, SL: 1743 m, SZ: 12 kN
SO241/23	03.07.2015	01:59:00 AM	Multi Corer	27° 30,285' N	111° 40,774' W	station end
SO241/24	03.07.2015	03:30:00 AM	OBS Seismic	27° 28,434' N	111° 29,547' W	station start
SO241/24	03.07.2015	3:35:00 AM	OBS Seismic	27° 28.330' N	111°29.423' W	start of line OBS 3000-10
SO241/24	03.07.2015	4:03:00 AM	OBS Seismic	27°27.393' N	111°28.373' W	end of line OBS 3000-10
SO241/24	03.07.2015	4:19:00 AM	OBS Seismic	27°28.012' N	111°28.168' W	start of line OBS 3000-11
SO241/24	03.07.2015	4:31:00 AM	OBS Seismic	27°28.822' N	111°29.179' W	end of line OBS 3000-11
SO241/24	03.07.2015	4:42:00 AM	OBS Seismic	27°28.423' N	111°29.419' W	start of line OBS 3000-12
SO241/24	03.07.2015	5:11:00 AM	OBS Seismic	27°27.432' N	111°28.355' W	end of line OBS 3000-12
SO241/24	03.07.2015	5:28:00 AM	OBS Seismic	27°28.213' N	111°28.326' W	start of line OBS 3000-13
SO241/24	03.07.2015	5:36:00 AM	OBS Seismic	27°28.755' N	111°29.000' W	end of line OBS 3000-13

SO241/24	03.07.2015	5:48:00 AM	OBS Seismic	27°28.531' N	111°29.556' W	start of line OBS 3000-14
SO241/24	03.07.2015	6:22:00 AM	OBS Seismic	27°27.465' N	111°28.349' W	end of line OBS 3000-14
SO241/24	03.07.2015	6:40:00 AM	OBS Seismic	27°28.132' N	111°28.174' W	start of line OBS 3000-15
SO241/24	03.07.2015	6:52:00 AM	OBS Seismic	27°28.737' N	111°28.912' W	end of line OBS 3000-15
SO241/24	03.07.2015	7:08:00 AM	OBS Seismic	27°28.442' N	111°29.476' W	start of line OBS 3000-16
SO241/24	03.07.2015	8:55:00 AM	OBS Seismic	27°24.580' N	111°25.016' W	end of line OBS 3000-16
SO241/24	03.07.2015	9:08:00 AM	OBS Seismic	27°25.120' N	111°24.725' W	start of line OBS 3000-17
SO241/24	03.07.2015	10:06:00 AM	OBS Seismic	27°29.030' N	111°29.197' W	end of line OBS 3000-17
SO241/24	03.07.2015	10:16:00 AM	OBS Seismic	27° 29,680' N	111° 29,888' W	station end
SO241/25	03.07.2015	01:21:00 PM	CTD	27° 55,012' N	111° 1,157' W	station start
SO241/25	03.07.2015	02:09:00 PM	CTD	27° 55,021' N	111° 01,108' W	Bodensicht, Posidonia
SO241/25	03.07.2015	02:09:00 PM	CTD	27° 55,012' N	111° 1,128' W	Bodensicht, SL: 35 m, SZ: 2 kN
SO241/25	03.07.2015	02:22:00 PM	CTD	27° 55,013' N	111° 1,126' W	station end
SO241/26	03.07.2015	02:24:00 PM	Multi Corer	27° 55,013' N	111° 1,126' W	station start
SO241/26	03.07.2015	02:38:00 PM	Multi Corer	27° 55,013' N	111° 1,127' W	Bodenkontakt Schiff, SL: 44 m, SZ: - 3 kN
SO241/26	03.07.2015	02:52:00 PM	Multi Corer	27° 55,014' N	111° 1,129' W	station end
SO241/27	04.07.2015	12:25:00 AM	Multi Corer	27° 42,433' N	111° 13,641' W	station start
SO241/27	04.07.2015	12:51:00 AM	Multi Corer	27° 42,429' N	111° 13,668' W	Bodenkontakt, Posidonia
SO241/27	04.07.2015	12:51:00 AM	Multi Corer	27° 42,415' N	111° 13,654' W	Bodenkontakt Schiff, SL: 675m
SO241/27	04.07.2015	01:12:00 AM	Multi Corer	27° 42,409' N	111° 13,653' W	station end
SO241/28	04.07.2015	01:20:00 AM	Multi Corer	27° 42,410' N	111° 13,655' W	station start
SO241/28	04.07.2015	01:51:00 AM	Multi Corer	27° 42,413' N	111° 13,656' W	Bodenkontakt Schiff, SLmax: 665 m, SZ: 10 kN
SO241/28	04.07.2015	02:12:00 AM	Multi Corer	27° 42,414' N	111° 13,656' W	station end
SO241/29	04.07.2015	02:04:00 AM	Multi Corer	27° 42,413' N	111° 13,652' W	station start
SO241/29	04.07.2015	02:32:00 AM	Multi Corer	27° 42,423' N	111° 13,670'	Bodenkontakt, Posidonia
SO241/29	04.07.2015	02:32:00 AM	Multi Corer	27° 42,410' N	111° 13,656' W	Bodenkontakt Schiff, SL: 667 m, SZ: 8 kN
SO241/29	04.07.2015	02:57:00 AM	Multi Corer	27° 42,396' N	111° 13,691' W	station end
SO241/30	04.07.2015	03:00:00 AM	Multibeam & Parasound	27° 42,356' N	111° 13,713' W	station start
SO241/30	04.07.2015	06:42:00 AM	Multibeam & Parasound	27° 18,223' N	111° 31,383' W	station end
SO241/31	04.07.2015	07:12:00 AM	CTD	27° 18,121' N	111° 31,463' W	station start
SO241/31	04.07.2015	11:25:00 AM	CTD	27° 18,233' N	111° 30,144' W	Bodensicht, SL: 1995m
SO241/31	04.07.2015	12:32:00 PM	CTD	27° 18,233' N	111° 30,148' W	station end
SO241/32	04.07.2015	01:06:00 PM	Multi Corer	27° 18,193' N	111° 30,143' W	station start
SO241/32	04.07.2015	04:31:00 PM	Multi Corer	27° 17,741' N	111° 30,671' W	hieven ohne Bodenkontakt, SL: 2000 m, SZ: 23 kN
SO241/32	04.07.2015	05:21:00 PM	Multi Corer	27° 17,738' N	111° 30,674' W	station end
SO241/33	04.07.2015	07:15:00 PM	Multi Corer	27° 33,312' N	111° 32,914' W	station start
SO241/33	04.07.2015	09:35:00 PM	Multi Corer	27° 33,287' N	111° 32,867' W	Bodenkontakt, Posidonia
SO241/33	04.07.2015	09:35:00 PM	Multi Corer	27° 33,301' N	111° 32,883' W	Bodenkontakt Schiff, SL: 1857m
SO241/33	04.07.2015	10:37:00 PM	Multi Corer	27° 33,298' N	111° 32,884' W	station end
SO241/34	05.07.2015	11:28:00 PM	GRAB	27° 28,159' N	111° 28,430' W	station start
SO241/34	05.07.2015	01:12:47 AM	GRAB	27° 28,165' N	111° 28,374' W	Bodenkontakt, Posidonia
SO241/34	05.07.2015	01:12:47 AM	GRAB	27° 28,180' N	111° 28,389' W	Bodenkontakt Schiff, SLmax: 665 m, SZ: 10 kN
SO241/34	05.07.2015	02:02:43 AM	GRAB	27° 28,179' N	111° 28,384' W	station end
SO241/35	05.07.2015	03:39:00 AM	OBS Seismic	27° 29,467' N	111° 30,467' W	station start
SO241/35	05.07.2015	04:08:00 AM	OBS Seismic	27° 28.621' N	111° 29.497' W	start of line OBS4000-01
SO241/35	05.07.2015	05:39:00 AM	OBS Seismic	27° 24.648' N	111° 24.981' W	end of line OBS4000-01

SO241/35	05.07.2015	05:58:00 AM	OBS Seismic	27° 24.970' N	111° 24.500' W	start of line OBS4000- 02
SO241/35	05.07.2015	07:11:00 AM	OBS Seismic	27° 28.964' N	111° 28.919' W	end of line OBS4000-02
SO241/35	05.07.2015	07:32:00 AM	OBS Seismic	27° 28.727' N	111° 29.460' W	start of line OBS4000-03
SO241/35	05.07.2015	09:06:00 AM	OBS Seismic	27° 24.693' N	111° 24.852' W	end of line OBS4000-03
SO241/35	05.07.2015	09:19:00 AM	OBS Seismic	27° 25.118' N	111° 24.470' W	start of line OBS4000-04
SO241/35	05.07.2015	10:35:00 AM	OBS Seismic	27° 29.117' N	111° 28.878' W	end of line OBS4000-04
SO241/35	05.07.2015	10:45:00 AM	OBS Seismic	27° 28.707' N	111° 29.260' W	start of line OBS4000-05
SO241/35	05.07.2015	12:09:00 PM	OBS Seismic	27° 24.795' N	111° 24.776' W	end of line OBS4000-05
SO241/35	05.07.2015	12:21:00 PM	OBS Seismic	27° 25.265' N	111° 24.405' W	start of line OBS4000-06
SO241/35	05.07.2015	12:56:00 PM	OBS Seismic	27° 27.008' N	111° 26.320' W	end of line OBS4000-06
SO241/35	05.07.2015	01:10:00 PM	OBS Seismic	27° 27,506' N	111° 26,860' W	station end
SO241/36	05.07.2015	02:34:00 PM	Multibeam & Parasound	27° 25,094' N	111° 19,574' W	station start
SO241/36	05.07.2015	06:32:13 PM	Multibeam & Parasound	27° 41,793' N	111° 49,645' W	station end
SO241/37	05.07.2015	10:23:10 PM	Hybis	27° 24,775' N	111° 23,235' W	station start
SO241/37	05.07.2015	12:49:53 AM	Hybis	27° 24,743' N	111° 23,217' W	Bodenkontakt, Posidonia
SO241/37	06.07.2015	12:49:53 AM	Hybis	27° 24,761' N	111° 23,229' W	Bodenkontakt Schiff, SL: 1857m
SO241/37	06.07.2015	02:19:25 AM	Hybis	27° 24,765' N	111° 23,228' W	station end
SO241/38	06.07.2015	02:25:33 AM	Hybis	27° 24,762' N	111° 23,225' W	station start
SO241/38	06.07.2015	08:06:55 AM	Hybis	27° 24,559' N	111° 23,331' W	station end
SO241/39	06.07.2015	08:52:00 AM	CTD	27° 24,763' N	111° 23,232' W	station start
SO241/39	06.07.2015	10:28:20 AM	CTD	27° 24,765' N	111° 23,207' W	Bodensicht, Posidonia
SO241/39	06.07.2015	10:28:20 AM	CTD	27° 24,768' N	111° 23,229' W	Bodensicht, SL: 1768m
SO241/39	06.07.2015	12:14:00 PM	CTD	27° 24,544' N	111° 23,339' W	station end
SO241/40	06.07.2015	01:20:03 PM	Multi Corer	27° 24,691' N	111° 23,249' W	station start
SO241/40	06.07.2015	03:22:34 PM	Multi Corer	27° 24,686' N	111° 23,237' W	Bodenkontakt, Posidonia
SO241/40	06.07.2015	03:22:34 PM	Multi Corer	27° 24,698' N	111° 23,254' W	Bodenkontakt Schiff, SL: 1828 m, SZ: 14 kN
SO241/40	06.07.2015	04:26:32 PM	Multi Corer	27° 24,703' N	111° 23,255' W	station end
SO241/41	06.07.2015	05:53:34 PM	Multi Corer	27° 34,800' N	111° 21,539' W	station start
SO241/41	06.07.2015	06:32:20 PM	Multi Corer	27° 34,800' N	111° 21,537' W	Bodensicht, SL: 1221m
SO241/41	06.07.2015	07:15:47 PM	Multi Corer	27° 34,805' N	111° 21,537' W	station end
SO241/42	06.07.2015	08:36:26 PM	CTD	27° 42,438' N	111° 13,733' W	station start
SO241/42	06.07.2015	09:01:44 PM	CTD	27° 42,411' N	111° 13,663' W	Bodensicht, SLmax: 659m
SO241/42	06.07.2015	09:30:29 PM	CTD	27° 42,409' N	111° 13,655' W	station end
SO241/43	06.07.2015	09:53:14 PM	Multi Corer	27° 42,409' N	111° 13,655' W	station start
SO241/43	06.07.2015	10:23:08 PM	Multi Corer	27° 42,409' N	111° 13,656' W	Bodenkontakt Schiff, SL: 669m
SO241/43	06.07.2015	10:49:18 PM	Multi Corer	27° 42,408' N	111° 13,650' W	station end
SO241/44	07.07.2015	02:18:47 AM	2D-Seismik	27° 17,797' N	111° 44,062' W	station start
SO241/44	07.07.2015	03:02:00 AM	2D-Seismik	27° 17,710' N	111° 42,116' W	start of line P5001
SO241/44	07.07.2015	07:41:00 AM	2D-Seismik	27° 17,215' N	111° 20,655' W	end of line P5001
SO241/44	08.07.2015	07:51:00 AM	2D-Seismik	27° 17,715' N	111° 20,433' W	start of line P5002
SO241/44	08.07.2015	11:08:00 AM	2D-Seismik	27° 30,396' N	111° 25,587' W	end of line P5002
SO241/44	08.07.2015	11:18:00 AM	2D-Seismik	27° 30,400' N	111° 26,348' W	start of line P5003
SO241/44	09.07.2015	12:48:00 PM	2D-Seismik	27° 24,879' N	111° 31,316' W	end of line P5003
SO241/44	07.07.2015	01:30:32 PM	2D-Seismik	27° 24,424' N	111° 29,401' W	station end
SO241/45	07.07.2015	02:15:31 PM	CTD	27° 24,577' N	111° 25,184' W	station start
SO241/45	07.07.2015	03:15:01 PM	CTD	27° 24,580' N	111° 25,164' W	Bodensicht, SL: 2024 m, SZ: 9 kN
SO241/45	07.07.2015	04:25:27 PM	CTD	27° 24,578' N	111° 25,166' W	station end
SO241/46	07.07.2015	06:41:30 PM	Gravity Corer	27° 42,416' N	111° 13,675' W	station start

SO241/46	07.07.2015	07:02:51 PM	Gravity Corer	27° 42,412' N	111° 13,651' W	Bodenkontakt Schiff, SLmax: 680m
SO241/46	07.07.2015	08:00:00 PM	Gravity Corer	27° 42,407' N	111° 13,653' W	station end
SO241/47	07.07.2015	08:00:55 PM	Gravity Corer	27° 42,407' N	111° 13,654' W	station start
SO241/47	07.07.2015	08:40:39 PM	Gravity Corer	27° 42,413' N	111° 13,649' W	Bodenkontakt Schiff, SLmax: 676m
SO241/47	07.07.2015	09:11:34 PM	Gravity Corer	27° 42,416' N	111° 13,646' W	station end
SO241/48	08.07.2015	03:52:23 AM	2D-Seismik	27° 24,110' N	111° 34,760' W	station start
SO241/48	08.07.2015	04:18:00 AM	2D-Seismik	27° 24,200' N	111° 33,215' W	start of line P6001
SO241/48	08.07.2015	10:13:00 AM	2D-Seismik	27° 25,611' N	111° 05,481' W	end of line P6001
SO241/48	08.07.2015	10:30:00 AM	2D-Seismik	27° 24,789' N	111° 05,483' W	start of line P6002
SO241/48	08.07.2015	01:08:00 PM	2D-Seismik	27° 21,116' N	111° 18,130' W	end of line P6002
SO241/48	09.07.2015	01:10:00 PM	2D-Seismik	27° 21,147' N	111° 18,282' W	start of line P6003
SO241/48	09.07.2015	04:05:00 PM	2D-Seismik	27° 29,376' N	111° 30,134' W	end of line P6003
SO241/48	08.07.2015	04:40:00 PM	2D-Seismik	27° 30,335' N	111° 31,507' W	station end
SO241/49	08.07.2015	05:34:21 PM	OBS Recovery	27° 26,645' N	111° 26,016' W	station start
SO241/49	08.07.2015		OBS Recovery			station end
SO241/50	09.07.2015	02:04:06 AM	Gravity Corer	27° 24,786' N	111° 23,249' W	station start
SO241/50	09.07.2015	02:46:57 AM	Gravity Corer	27° 24,695' N	111° 23,220' W	Bodenkontakt, Posidonia
SO241/50	09.07.2015	02:46:57 AM	Gravity Corer	27° 24,715' N	111° 23,228' W	Bodenkontakt Schiff, SL: 1826 m, SZ: 18 kN
SO241/50	09.07.2015	03:48:28 AM	Gravity Corer	27° 24,710' N	111° 23,232' W	station end
SO241/51	09.07.2015	04:08:00 AM	Gravity Corer	27° 24,469' N	111° 23,377' W	station start
SO241/51	09.07.2015	04:49:57 AM	Gravity Corer	27° 24,453' N	111° 23,369' W	Bodenkontakt, Posidonia
SO241/51	09.07.2015	04:49:57 AM	Gravity Corer	27° 24,472' N	111° 23,377' W	Bodenkontakt Schiff, SLmax: 1869 m, SZ: 18 kN
SO241/51	09.07.2015	05:44:51 AM	Gravity Corer	27° 24,467' N	111° 23,380' W	station end
SO241/52	09.07.2015	07:11:03 AM	CTD	27° 24,753' N	111° 23,165' W	station start
SO241/52	09.07.2015	08:30:36 AM	CTD	27° 24,731' N	111° 23,241' W	Bodensicht, Posidonia
SO241/52	09.07.2015	08:30:36 AM	CTD	27° 24,750' N	111° 23,240' W	Bodensicht, SLmax: 1774m
SO241/52	09.07.2015	11:16:31 AM	CTD	27° 24,731' N	111° 23,234' W	station end
SO241/53	09.07.2015	11:25:36 AM	Multibeam & Parasound	27° 24,846' N	111° 23,392' W	station start
SO241/53	09.07.2015	12:53:00 PM	Multibeam & Parasound	27° 24,215' N	111° 23,442' W	station end
SO241/54	09.07.2015	05:35:00 PM	3D-Seismik	27° 22,033' N	111° 17,826' W	station start
SO241/54	10.07.2015	07:21:00 AM	3D-Seismik	27° 21,122' N	111° 21,291' W	station end
SO241/55	10.07.2015	08:44:00 AM	2D-Seismik	27° 18,780' N	111° 34,334' W	station start
SO241/55	10.07.2015	09:18:00 AM	2D-Seismik	27° 18,901' N	111° 35,485' W	start of line P8001
SO241/55	10.07.2015	10:46:00 AM	2D-Seismik	27° 18,515' N	111° 41,101' W	end of line P8001
SO241/55	10.07.2015	11:01:00 AM	2D-Seismik	27° 17,652' N	111° 40,644' W	start of line P8002
SO241/55	10.07.2015	11:26:00 AM	2D-Seismik	27° 17,685' N	111° 38,269' W	end of line P8002
SO241/55	10.07.2015	11:29:00 AM	2D-Seismik	27° 17,799' N	111° 38,110' W	start of line P8003
SO241/55	10.07.2015	12:42:00 PM	2D-Seismik	27° 22,353' N	111° 35,428' W	end of line P8003
SO241/55	10.07.2015	12:47:00 PM	2D-Seismik	27° 22,609' N	111° 35,475' W	start of line P8004
SO241/55	10.07.2015	06:07:00 PM	2D-Seismik	27° 33,005' N	111° 52,045' W	end of line P8004
SO241/55	10.07.2015	06:10:00 PM	2D-Seismik	27° 33,181' N	111° 51,960' W	start of line P8005
SO241/55	10.07.2015	08:41:00 PM	2D-Seismik	27° 41,796' N	111° 46,212' W	end of line P8005
SO241/55	10.07.2015	08:42:00 PM	2D-Seismik	27° 41,856' N	111° 46,117' W	start of line P8006
SO241/55	11.07.2015	01:46:00 AM	2D-Seismik	27° 30,477' N	111° 28,631' W	end of line P8006
SO241/55	11.07.2015	01:50:00 AM	2D-Seismik	27° 30,348' N	111° 28,421' W	start of line P8007
SO241/55	11.07.2015	03:43:00 AM	2D-Seismik	27° 31,489' N	111° 19,778' W	end of line P8007
SO241/55	11.07.2015	03:46:00 AM	2D-Seismik	27° 31,699' N	111° 19,583' W	start of line P8008

SO241/55	11.07.2015	04:37:00 AM	2D-Seismik	27° 35,085' N	111° 17,225' W	end of line P8008
SO241/55	11.07.2015	04:40:00 AM	2D-Seismik	27° 35,136' N	111° 16,962' W	start of line P8009
SO241/55	11.07.2015	05:17:00 AM	2D-Seismik	27° 33,811' N	111° 14,774' W	end of line P8009
SO241/55	11.07.2015	05:21:00 AM	2D-Seismik	27° 33,595' N	111° 14,734' W	start of line P8010
SO241/55	11.07.2015	10:00:00 AM	2D-Seismik	27° 18,026' N	111° 25,339' W	end of line P8010
SO241/55	11.07.2015	10:02:00 AM	2D-Seismik	27° 18,016' N	111° 25,456' W	start of line P8011
SO241/55	11.07.2015	12:41:00 PM	2D-Seismik	27° 22,725' N	111° 35,177' W	end of line P8011
SO241/55	11.07.2015	01:38:00 PM	2D-Seismik	27° 24,725' N	111° 33,182' W	station end
SO241/56	11.07.2015	02:27:00 PM	GRAB	27° 28,179' N	111° 28,422' W	station start
SO241/56	11.07.2015	04:49:00 PM	GRAB	27° 28,179' N	111° 28,362' W	Bodenkontakt, Posidonia
SO241/56	11.07.2015	04:49:00 PM	GRAB	27° 28,181' N	111° 28,387' W	Bodenkontakt Schiff, SL: 1830 m, SZ: 29 kN
SO241/56	11.07.2015	06:05:00 PM	GRAB	27° 28,182' N	111° 28,379' W	station end
SO241/57	11.07.2015	07:25:00 PM	LANDER	27° 24,485' N	111° 23,003' W	station start
SO241/57	11.07.2015	07:42:00 PM	LANDER	27° 24,475' N	111° 22,999' W	station end
SO241/58	11.07.2015	08:01:00 PM	Gravity Corer	27° 24,501' N	111° 23,374' W	station start
SO241/58	11.07.2015	08:45:00 PM	Gravity Corer	27° 24,487' N	111° 23,377' W	Bodenkontakt Schiff, SLmax: 1866m
SO241/58	11.07.2015	09:50:00 PM	Gravity Corer	27° 24,489' N	111° 23,379' W	station end
SO241/59	11.07.2015	10:08:00 PM	Gravity Corer	27° 24,453' N	111° 23,370' W	station start
SO241/59	11.07.2015	11:35:00 PM	Gravity Corer	27° 24,471' N	111° 23,370' W	Bodenkontakt Schiff, SLmax: 1869 m, SZ: 18 kN
SO241/59	12.07.2015	12:20:00 AM	Gravity Corer	27° 24,473' N	111° 23,367' W	station end
SO241/60	12.07.2015	12:51:00 AM	Heat-Flow	27° 24,622' N	111° 23,626' W	station start
SO241/60	12.07.2015	01:48:00 AM	Heat-Flow	27° 24,604' N	111° 23,626' W	Bodenkontakt, Posidonia
SO241/60	12.07.2015	01:48:00 AM	Heat-Flow	27° 24,623' N	111° 23,622' W	1. Bodenkontakt Schiff, SL: 1871 m, SZ: 22 /17 kN
SO241/60	12.07.2015	02:32:00 AM	Heat-Flow	27° 24,527' N	111° 23,514' W	Bodenkontakt, Posidonia
SO241/60	12.07.2015	02:32:00 AM	Heat-Flow	27° 24,546' N	111° 23,509' W	2. Bodenkontakt Schiff, SL: 1863 m, SZ: 21/17 kN
SO241/60	12.07.2015	03:12:00 AM	Heat-Flow	27° 24,446' N	111° 23,392' W	Bodenkontakt, Posidonia
SO241/60	12.07.2015	03:12:00 AM	Heat-Flow	27° 24,465' N	111° 23,386' W	3. Bodenkontakt Schiff, SL: 1863 m, SZ: 22/17 kN
SO241/60	12.07.2015	03:53:00 AM	Heat-Flow	27° 24,379' N	111° 23,285' W	Bodenkontakt, Posidonia
SO241/60	12.07.2015	03:53:00 AM	Heat-Flow	27° 24,397' N	111° 23,280' W	4. Bodenkontakt Schiff, SL: 1874 m, SZ: 22/18 kN
SO241/60	12.07.2015	04:33:00 AM	Heat-Flow	27° 24,313' N	111° 23,171' W	Bodenkontakt, Posidonia
SO241/60	12.07.2015	04:33:00 AM	Heat-Flow	27° 24,335' N	111° 23,171' W	5. Bodenkontakt Schiff, SL: 1884 m, SZ: 21/17 kN
SO241/60	12.07.2015	05:21:00 AM	Heat-Flow	27° 24,240' N	111° 23,075' W	Bodenkontakt, Posidonia
SO241/60	12.07.2015	05:21:00 AM	Heat-Flow	27° 24,260' N	111° 23,075' W	6. Bodenkontakt Schiff, SL: 1881m, SZ: 29,1kN
SO241/60	12.07.2015	05:50:00 AM	Heat-Flow	27° 24,171' N	111° 22,954' W	Bodenkontakt, Posidonia
SO241/60	12.07.2015	05:50:00 AM	Heat-Flow	27° 24,189' N	111° 22,952' W	7. Bodenkontakt Schiff, SLmax: 1867m , SZ: 18,5 kN
SO241/60	12.07.2015	08:09:00 AM	Heat-Flow	27° 24,581' N	111° 23,328' W	Bodenkontakt, Posidonia
SO241/60	12.07.2015	08:09:00 AM	Heat-Flow	27° 24,598' N	111° 23,317' W	8. Bodenkontakt Schiff, SLmax: 1840m
SO241/60	12.07.2015	08:39:00 AM	Heat-Flow	27° 24,552' N	111° 23,346' W	Bodenkontakt, Posidonia
SO241/60	12.07.2015	08:39:00 AM	Heat-Flow	27° 24,568' N	111° 23,336' W	9. Bodenkontakt Schiff, SLmax: 1858m
SO241/60	12.07.2015	09:09:00 AM	Heat-Flow	27° 24,503' N	111° 23,371' W	Bodenkontakt, Posidonia
SO241/60	12.07.2015	09:09:00 AM	Heat-Flow	27° 24,520' N	111° 23,361' W	10. Bodenkontakt Schiff, SL: 1857m
SO241/60	12.07.2015	10:31:00 AM	Heat-Flow	27° 24,787' N	111° 23,221' W	Bodenkontakt, Posidonia
SO241/60	12.07.2015	10:31:00 AM	Heat-Flow	27° 24,804' N	111° 23,210' W	11. Bodenkontakt Schiff, SL: 1833m
SO241/60	12.07.2015	11:37:00 AM	Heat-Flow	27° 24,805' N	111° 23,206' W	station end
SO241/61	12.07.2015	11:47:00 AM	Gravity Corer	27° 24,820' N	111° 23,199' W	station start

SO241/61	12.07.2015	12:31:00 PM	Gravity Corer	27° 24,836' N	111° 23,189' W	Bodenkontakt, Posidonia
SO241/61	12.07.2015	12:31:00 PM	Gravity Corer	27° 24,821' N	111° 23,200' W	Bodenkontakt Schiff, SL: 1869m, SZ: 33,3kN
SO241/61	12.07.2015	01:18:00 PM	Gravity Corer	27° 24,823' N	111° 23,198' W	station end
SO241/62	12.07.2015	02:10:00 PM	Gravity Corer	27° 28,183' N	111° 28,400' W	station start
SO241/62	12.07.2015	03:00:00 PM	Gravity Corer	27° 28,193' N	111° 28,343' W	Bodenkontakt, Posidonia
SO241/62	12.07.2015	03:00:00 PM	Gravity Corer	27° 28,193' N	111° 28,365' W	Bodenkontakt Schiff, SL: 1862 m, SZ: 18 kN
SO241/62	12.07.2015	04:00:00 PM	Gravity Corer	27° 28,191' N	111° 28,364' W	station end
SO241/63	12.07.2015	05:32:00 PM	3D-Seismik	27° 22,237' N	111° 19,866' W	station start
SO241/63	13.07.2015	12:07:00 AM	3D-Seismik	27° 26,838' N	111° 29,107' W	station end
SO241/64	13.07.2015	01:30:00 AM	2D-Seismik	27° 24,725' N	111° 30,396' W	station start
SO241/64	13.07.2015	0:49	2D-Seismik	27° 25,778' N	111° 32,446' W	start of line P10001
SO241/64	13.07.2015	8:59	2D-Seismik	27° 39,013' N	111° 57,849' W	end of line P10001
SO241/64	13.07.2015	8:59	2D-Seismik	27° 39,013' N	111° 57,849' W	start of line P10002
SO241/64	13.07.2015	11:49	2D-Seismik	27° 24,169' N	111° 59,578' W	end of line P10002
SO241/64	13.07.2015	11:49	2D-Seismik	27° 24,169' N	111° 59,578' W	start of line P10003
SO241/64	13.07.2015	18:41	2D-Seismik	27° 06,719' N	111° 28,412' W	end of line P10003
SO241/64	13.07.2015	18:41	2D-Seismik	27° 06,719' N	111° 28,412' W	start of line P10004
SO241/64	13.07.2015	20:20	2D-Seismik	27° 00,870' N	111° 22,952' W	end of line P10004
SO241/64	13.07.2015	20:20	2D-Seismik	27° 00,870' N	111° 22,952' W	start of line P10005
SO241/64	14.07.2015	0:24	2D-Seismik	27° 00,575' N	111° 02,060' W	end of line P1005
SO241/64	14.07.2015	0:24	2D-Seismik	27° 00,575' N	111° 02,060' W	start of line P10006
SO241/64	14.07.2015	4:13	2D-Seismik	27° 15,993' N	111° 00,567' W	end of line P10006
SO241/64	14.07.2015	4:13	2D-Seismik	27° 15,993' N	111° 00,567' W	start of line P10007
SO241/64	14.07.2015	9:13	2D-Seismik	27° 29,024' N	111° 25,833' W	end of line P10007
SO241/64	14.07.2015	9:13	2D-Seismik	27° 29,024' N	111° 25,833' W	start of line P10008
SO241/64	14.07.2015	10:41	2D-Seismik	27° 31,920' N	111° 19,610' W	end of line P10008
SO241/64	14.07.2015	11:07:00 AM	2D-Seismik	27° 32,531' N	111° 18,594' W	station end
SO241/65	14.07.2015	12:08:00 PM	Multi Corer	27° 24,322' N	111° 23,001' W	station start
SO241/65	14.07.2015	12:59:00 PM	Multi Corer	27° 24,342' N	111° 22,970' W	Bodenkontakt Schiff, SL: 1872m
SO241/65	14.07.2015	02:07:00 PM	Multi Corer	27° 24,344' N	111° 22,968' W	station end
SO241/66	14.07.2015	02:40:00 PM	Multi Corer	27° 24,482' N	111° 23,402' W	station start
SO241/66	14.07.2015	05:35:00 PM	Multi Corer	27° 24,566' N	111° 23,245' W	Bodenkontakt, Posidonia
SO241/66	14.07.2015	05:35:00 PM	Multi Corer	27° 24,577' N	111° 23,265' W	Bodenkontakt, SLmax: 1853m
SO241/66	14.07.2015	07:08:00 PM	Multi Corer	27° 24,552' N	111° 23,046' W	station end
SO241/67	14.07.2015	07:30:00 PM	CTD	27° 24,842' N	111° 23,181' W	station start
SO241/67	14.07.2015	11:49:00 PM	CTD	27° 24,439' N	111° 23,381' W	station end
SO241/68	14.07.2015	11:51:00 PM	LANDER	27° 24,439' N	111° 23,381' W	station start
SO241/68	15.07.2015	01:00:00 AM	LANDER	27° 24,649' N	111° 22,472' W	station end
SO241/69	15.07.2015	01:40:00 AM	GRAB	27° 24,772' N	111° 23,227' W	station start
SO241/69	15.07.2015	03:22:00 AM	GRAB	27° 24,730' N	111° 23,223' W	Bodenkontakt, Posidonia
SO241/69	15.07.2015	03:22:00 AM	GRAB	27° 24,749' N	111° 23,224' W	Bodenkontakt Schiff, SL: 1788 m, SZ: 22 kN
SO241/69	15.07.2015	04:54:00 AM	GRAB	27° 24,753' N	111° 23,225' W	station end
SO241/70	15.07.2015	06:24:00 AM	Heat-Flow	27° 25,805' N	111° 25,476' W	station start
SO241/70	15.07.2015	07:11:00 AM	Heat-Flow	27° 25,802' N	111° 25,454' W	Bodenkontakt, Posidonia
SO241/70	15.07.2015	07:11:00 AM	Heat-Flow	27° 25,809' N	111° 25,474' W	1. Bodenkontakt Schiff, SLmax:1905 m
SO241/70	15.07.2015	09:01:00 AM	Heat-Flow	27° 25,471' N	111° 24,923' W	Bodenkontakt, Posidonia
SO241/70	15.07.2015	09:01:00 AM	Heat-Flow	27° 25,476' N	111° 24,945' W	2. Bodenkontakt Schiff, SLmax: 2052m

SO241/70	15.07.2015	10:09:00 AM	Heat-Flow	27° 25,148' N	111° 24,414' W	Bodenkontakt, Posidonia
SO241/70	15.07.2015	10:09:00 AM	Heat-Flow	27° 25,152' N	111° 24,436' W	3. Bodenkontakt Schiff, SL: 2070m
SO241/70	15.07.2015	11:09:00 AM	Heat-Flow	27° 24,841' N	111° 23,932' W	Bodenkontakt, Posidonia
SO241/70	15.07.2015	11:09:00 AM	Heat-Flow	27° 24,847' N	111° 23,954' W	4. Bodenkontakt Schiff, SL: 2046m
SO241/70	15.07.2015	12:09:00 PM	Heat-Flow	27° 24,847' N	111° 23,953' W	station end
SO241/71	15.07.2015	12:51:00 PM	Gravity Corer	27° 28,233' N	111° 28,372' W	station start
SO241/71	15.07.2015	01:31:00 PM	Gravity Corer	27° 28,180' N	111° 28,360' W	Bodenkontakt, Posidonia
SO241/71	15.07.2015	01:31:00 PM	Gravity Corer	27° 28,187' N	111° 28,380' W	Bodenkontakt Schiff, SL: 1859 m, SZ: 17 kN
SO241/71	15.07.2015	02:24:00 PM	Gravity Corer	27° 28,184' N	111° 28,384' W	station end
SO241/72	15.07.2015	02:26:00 PM	Gravity Corer	27° 28,184' N	111° 28,379' W	station start
SO241/72	15.07.2015	03:52:00 PM	Gravity Corer	27° 28,170' N	111° 28,376' W	Bodenkontakt, Posidonia
SO241/72	15.07.2015	03:52:00 PM	Gravity Corer	27° 28,178' N	111° 28,396' W	Bodenkontakt Schiff, SL: 1858 m, SZ: 17 kN
SO241/72	15.07.2015	04:36:00 PM	Gravity Corer	27° 28,178' N	111° 28,396' W	station end

Appendix C: OBS Protocols / OBS Protokolle

Station	Latitude	Longitude	Depth [m]	Deployment	Recovery	Skew [ms]	Recorder
OBS 1	27° 28,806'N	111° 28,571'W	1840	01.07.2015	09.07.2015	-208	OBS 1 MBS
OBS 2	27° 28,536'N	111° 28,849'W	1839	01.07.2015	09.07.2015	-14	OBS 2 MBS
OBS 3	27° 28,237'N	111° 29,172'W	1842	01.07.2015	08.07.2015	36	OBS 3 MBS
OBS 4	27° 27,854'N	111° 28,768'W	1836	01.07.2015	08.07.2015	14	OBS 4 MBS
OBS 5	27° 28,061'N	111° 28,423'W	1838	01.07.2015	08.07.2015	35	OBS 5 MBS
OBS 6	27° 28,404'N	111° 28,111'W	1842	01.07.2015	08.07.2015	-150	OBS 6 MBS
OBS 7	27° 28,000'N	111° 27,628'W	1836	01.07.2015	08.07.2015	-154	OBS 7 MBS
OBS 8	27° 27,735'N	111° 28,037'W	1839	01.07.2015	08.07.2015	-94	OBS 8 MBS
OBS 9	27° 27,439'N	111° 28,390'W	1841	01.07.2015	08.07.2015	-48	OBS 9 MBS
OBS 10	27° 27,277'N	111° 27,478'W	1846	01.07.2015	08.07.2015	10	OBS 10 MBS
OBS 11	27° 25,933'N	111° 25,914'W	1869	01.07.2015	08.07.2015	-77	OBS 11 MBS
Trigger	-	-	-	01.07.2015	09.07.2015	-146	Trigger MBS

Appendix D: HyBis log

SO241-37 Dive at black smoker Guaymas Basin

The objective of the dive was to investigate a mound on the southern edge of the northern rift of Guaymas Basin that we suspected to be a mud volcano. The times recorded in the video are 5 min ahead of UTC. The times recorded in the log are UTC.

05.07.2015

22:25 Deployment at 27°24.773' N 111°23.228' W in 1840 m water depth
23:17 Squids in 400 m
06.07.2015
00:11 Cloudy waters
00:17 After encountering turbid waters approximately 20 m above the seafloor we reached the seafloor. Here we saw large (several meters) white/grayish patches on rugged (20 cm-scale) topography. Some of the elevated rocks were grown over with dark/purple tube worms. There were several brownish crabs. At at least one location we saw approximately 60 cm high and 10-20 cm wide whitish chimneys where were the sources of the cloudy seawater. The water expelled from these chimneys erupted vigorously as known from black smokers on mid ocean ridges. We traversed first 5 m towards the chimneys. When getting right above a chimney we relocated the vessel 10 m towards 160° ending up outside of the cloud again.
00:49 We put down the instrument onto the rough seafloor and grabbed. The seafloor yielded easily to grabbing and hoisted the instrument back on board.
01:30 HyBis back on deck. Upon recovery we found unsorted sediments with large pieces of hard material. At least part of it contained pyrite. A volume loss of the material during ascend suggested that the grab sample originally contained a large fraction of sediments that got washed during recovery.

SO241-38 Dive at black smoker Guaymas Basin

The objective of this dive was to investigate how wide spread seep activity is along the crest of the mounds.

06.07.2015

02:30 Deployment at 27°24.755 N 111°23.232 W in 1842 m water depth
03:15 Observation of first clouds in the water column at 1700 m Posidonia depth
03:17 Sea floor observation at 1775 m rope
03:23 Bacterial mats
03:26 Seep site (bubbles)
03:29 Black smoker – presumably the same as observed in dive SO241-37
03:42 We went down-slope across nodules that become increasingly draped with soft sediments.
03:51 Gas bubbles emitted from the seafloor
03:55 Gas bubbles emitted from the seafloor
03:59 Tube worms
04:00 Black smoker
04:04 We went over the black smoker and pulled up when reaching the plume
04:07 We went back down measuring the difference between rope (1780 m), Posidonia (1730 m) and ship's EM122 (1876). The ship was offset to the southeast away from the mound.
04:11 Ship at WP2
04:18 Bubbles
04:33 Flat area
04:58 Bubbles
05:02 Possible smoker, 1796 m rope, 1745 m Posidonia
05:12 Bubbles, life tube worms, turbid water
05:23 Flat seafloor , 1758 m, potential MUC site
05:57 Two active smokers and 1 extinct smoker
06:01 After a trip up to 1700 m we went back down to the seafloor; on the way up the cloud

was left 57 m above the seafloor, on the down trip the cloud was entered at 59 m above the seafloor.
06:26 Bubbles
06:32 HyBis briefly gets stuck in another dead smoker, after putting out wire and maneuvering away we saw tube worms and turbid waters. Probably there was another smoker in the vicinity but we did not see it.
06:37 Two dead smokers on a rugged edge. Turbid waters and squat lobsters
06:45 Old smoker at the base of the cliff
06:56 Recovery

Appendix E: Biological sampling summary

Overview of samples taken for microbiological and organic geochemical analyses from each gravity core (A) and each of the 4 multicores (B-E) taken per site. All samples were taken by cutoff syringes except sediments used for IPL incubation experiments, which were in some cases taken using a sterile spoon (A, C), as well as samples for Pb-210/Cs-137 analyses, which consisted of leftover sediments from each multicore interval after other samples had been taken (B). Abbreviations: cc=core catcher, AA=amino acids, VFA=volatile fatty acids, AS/S=amino sugars and sugars, IPL=intact polar lipids, X=sample taken on every core of sufficient length; [X]=sample taken on certain cores of sufficient length. Samples for VFA and AS/S analyses were centrifuged in acid-washed 50-cm3 Falcon tubes for 30-60 minutes at 2,800xg to separate dissolved and solid phases. Subsamples of supernatants for VFA analyses were reserved for complementary porewater anion, DOC, and DOM analyses. Samples for IPL and endospore incubations were stored at +4°C. Samples for DNA/RNA, AA, VFA, AS/S, IPL and endospore DNA analyses were frozen (DNA/RNA and endospore-DNA at -80°C, all others at -20°C).

Table A

Depth (cmbsf)	H_2 (2×2 cm^3)	CH_4 (3 cm^3)	Cell counts (0.5 cm^3)	DNA/ RNA (10 cm^3)	AA (5 cm^3)	VFA (100 cm^3)	AS/S (100 cm^3)	IPL (20 cm^3)	IPL In-cubation (500 cm^3)	Endo-spore-DNA (5 cm^3)	Endospore Incubation (50 cm^3)
cc	X	X	X	X	X	X	X	X			
1m above cc	X	X	X	X	X	X	X	X			
2m above cc	X	X	X	X	X	X	X	X			
3m above cc	X	X	X	X	X	X	X	X			
4m above cc	X	X	X	X	X	X	X	X			
5m above cc	X	X	X	X	X	X	X	X			
0.5m above cc	X	X	X	X	X	[X]	[X]	X	[X]	[X]	[X]
1.5m above cc	X	X	X	X	X	[X]	[X]	X	[X]	[X]	[X]
2.5m above cc	X	X	X	X	X	[X]	[X]	X	[X]	[X]	[X]
3.5m above cc	X	X	X	X	X	[X]	[X]	X	[X]	[X]	[X]
4.5m above cc	X	X	X	X	X	[X]	[X]	X	[X]	[X]	[X]

Table B

Depth (cmbsf)	H_2 (2 cm^3)	CH_4 (2 cm^3)	Cell counts (0.5 cm^3)	DNA/RNA (3 cm^3)	Pb-210/Cs-137 (leftovers from each interval)
0-1	X	X	X	X	X
1-2	X	X	X	X	X
2-3	X	X	X	X	X
3-4	X	X	X	X	X
4-6	X	X	X	X	X
6-8	X	X	X	X	X
8-10	X	X	X	X	X
10-12	X	X	X	X	X
12-14	X	X	X	X	X
14-16	X	X	X	X	X
16-18	X	X	X	X	X
18-20	X	X	X	X	X
20-24	X	X	X	X	X
24-28	X	X	X	X	X
28-32	X	X	X	X	X
32-36	X	X	X	X	X
36-40	X	X	X	X	X

Table C

Depth (cmbsf)	VFA (1=50 cm^3, 2=100 cm^3)	AS/S (1=50 cm^3, 2=100 cm^3)	AA (5 cm^3)
0-2	1	1	X
2-4	1	1	X
4-8	1	1	X
12-16	1	1	X
20-24	2	2	X
30-34	2	2	X
40-44	2	2	X

Table D

Depth (cmbsf)	IPL/DPAs (5 cm^3)	Incubation (leftovers)
0-2	X	Sample 1 (leftovers from 0-12 cmbsf)
2-4	X	
4-6	X	
10-12	X	
16-18	X	
24-28	X	